Theses and Dissertations

Spring 2014

Structural and functional assessments of normal vs. asthmatic populations via image registration and CFD techniques

Sanghun Choi
University of Iowa

Recommended Citation

STRUCTURAL AND FUNCTIONAL ASSESSMENTS
OF NORMAL VS. ASTHMATIC POPULATIONS
VIA IMAGE REGISTRATION AND CFD TECHNIQUES

by

Sanghun Choi

A thesis submitted in partial fulfillment
of the requirements for the Doctor of
Philosophy degree in Mechanical Engineering
in the Graduate College of
The University of Iowa

May 2014

Thesis Supervisor: Professor Ching-Long Lin

Graduate College
The University of Iowa
Iowa City, Iowa

CERTIFICATE OF APPROVAL

_____

PH.D. THESIS

_____

This is to certify that the Ph.D. thesis of

Sanghun Choi

has been approved by the Examining Committee
for the thesis requirement for the Doctor of Philosophy
degree in Mechanical Engineering
at the May 2014 graduation.

Thesis Committee: _____
                          Ching-Long Lin, Thesis Supervisor

                          _____
                          Jia Lu

                          _____
                          James H. J. Buchholz

                          _____
                          Eric A. Hoffman

                          _____
                          Kung-Sik Chan

To Eon Ju and Dahye

ACKNOWLEDGMENTS

ABSTRACT

The aim of this study is to investigate the functional and structural differences between normal subjects and asthmatics via image registration and computational fluid dynamics (CFD), together with pulmonary function test's (PFT) and one-image-based variables. We analyzed three populations of CT images: 50 normal, 42 non-severe asthmatic and 52 severe asthmatic subjects at total lung capacity (TLC) and functional residual capacity (FRC). A mass preserving image registration technique was employed to match CT images at TLC and FRC for assessments of regional volume change and anisotropic deformation. Instead of existing threshold-based air-trapping measure, a fraction-based air-trapping measure was proposed to account for inter-site and inter-subject variations of CT density. We also analyzed structural alterations of asthmatic airways, including bifurcation angle, hydraulic diameter, luminal area and wall area. CFD and particle tracking simulations are employed with physiologically-consistent boundary condition. As compared with normal subjects, severe asthmatics exhibit reduced air volume change (consistent with air-trapping) and more isotropic deformation in the basal lung regions, but increased air volume change associated with increased anisotropic deformation in the apical lung regions. In the multi-center study, the traditional air-trapping measure showed the significant site-variability due to the differences of scanners and coaching methods. The proposed fraction-based air-trapping measure is able to overcome the inter-site and inter-subject variations, allowing analysis of large data sets collected from multiple centers. We further demonstrate alterations of bifurcation angle, constriction, wall thickness and non-circularity at local branch level in severe asthmatics. The bifurcation angle, non-circularity and especially reduced hydraulic diameter significantly affect the increase of particle deposition in severe asthmatics. In summary, the two-image registration-based deformation provides a tool for distinguishing differences in lung mechanics among populations. The new fraction-based air-trapping

measure significantly improves the association of air-trapping with the presence and severity of asthma and the correlation with forced expiratory volume in 1 second over forced vital capacity (FEV_1/FVC) than existing approaches. The altered functions and structures such as air-volume change, branching angles, non-circular shapes, wall thickness and hydraulic diameters that found in asthmatics are strongly associated with the flow structures and particle depositions.

TABLE OF CONTENTS

LIST OF TABLES

LIST OF FIGURES

LIST OF ABBREVIATIONS

ADI	Anisotropic Deformation Index
AirT%	Air-Trapping percentage
AirT*	Air-trapping lobar-contribution
ANOVA	Analysis of Variance
AV	Air Volume
β_{air}	Air fraction
BMI	Body Mass Index
BRP	Bioengineering Research Program
BSA	Body Surface Area
β_{tissue}	Tissue fraction
Cc	Cunningham slip correction factor
C_D	Drag coefficient
CFD	Computational Fluid Dynamics
COPD	Chronic Obstructive Pulmonary Disease
Cr	Circularity of airway
D_{ave}	Averaged Diameter of airway
D_h	Hydraulic Diameter of airway
DNS	Direct Numerical Simulation
Δp	Pressure drop
ΔV_{air}	Local air volume change
ΔV_{AirF}	Lobar fraction of air volume change
F	Deformation gradient tensor
f	frictional coefficient
FEV1	Functional Expiratory Volume in 1 second
FRC	Functional Residual Capacity
FVC	Forced Vital Capacity
g	Gravitational acceleration

GE	General Electronics
HU_{air}	Hounsfield Unit of air
HU_{tissue}	Hounsfield Unit of tissue
$I(\mathbf{x})$	CT density at a local position $\mathbf{x}$
IC	Inspiratory Capacity
IRB	Institutional Review Board
J	determinant of Jacobian
K	Minor loss coefficient
LA	Luminal cross-sectional Area of airway
LES	Large Eddy Simulation
λ_i	Eigenvalues
LLL	Left Lower Lobe
LMB	Left Main Bronchus
LUL	Left Upper Lobe
MRI	Magnetic Resonance Image
NS	Normal Subjects
NSA	Non-Severe Asthmatics
p	Pressure
P_e	Perimeter of airway
PET	Positron Emission Tomography
PFT	Pulmonary Function Test
PITT	University of Pittsburgh
QCT	Quantitative Computed Tomography
$\mathbf{R}$	Rotation tensor
ρ_f	fluid density
Re	Reynolds number
RLL	Right Lower Lobe
RMB	Right Main Bronchus
RML	Right Middle Lobe

ROI	Regions of Interests
RUL	Right Upper Lobe
RV	Residual Volume
s	Eigenvector
SA	Severe Asthmatics
SARP	Severe Asthma Research Program
SE or SEM	Standard Error of the Mean
SSTVD	Sum of Squared Tissue Volume Difference
Stk	Stokes number
$\mathbf{T}(\mathbf{x})$	Warping (or Transformation) function of local position $\mathbf{x}$
TA	Total cross-sectional Area of airway
TLC	Total Lung Capacity
TLV	Total Lung Volume including tissue and air
TV	Tissue Volume
U	Stretch tensor
U	mean velocity
u	velocity vector
U/(M+L)|v	Ratio of air-volume change in upper lobes to air-volume change in middle and lower lobes
UI	University of Iowa
v	local volume including tissue and air
v_f	Fluid kinematic viscosity
V_{air}	Local air volume
VC	Vital Capacity
v_T	Turbulent eddy viscosity
V_{tissue}	Local tissue volume
WA	Wall cross-sectional Area of airway
WSL	Washington University in Saint Louis
α	Particle-particle interaction factor

CHAPTER 1

INTRODUCTION

1.1   Backgrounds

1.1.1   Severe Asthma Research Program (SARP)

Asthma is a lung disease that affects more than 25 million people in the United States and 300 million in the world [22, 148]. The asthma can be characterized by symptoms of air flow obstruction, bronchial hyper-responsiveness and airway inflammation [16, 18, 60, 81]. Severe Asthma Research Program (SARP) [21, 46, 79, 104, 105, 143] consisting of several research centers was initiated to better define the genetic, environmental and clinical features that characterize asthma, and subsequently better understand the underlying causes of asthma from multi-disciplinary perspectives of cell biology, physiology, radiology and mechanics.

The SARP studies identified clinical, physiologic, and biologic heterogeneity among asthmatic subjects [79, 105], then introducing five clusters by employing 34 qualitative and quantitative variables, i.e. onset of asthma, asthma duration, gender, lung function, reversibility, atopy, questionnaire data, and so on. The five clusters include 1) mild allergic, 2) mild-moderate allergic, 3) more severe older onset, 4) severe variable allergic asthma and 5) severe fixed airflow asthma, among which clusters 3, 4 and 5 are more likely to be patients with severe disease. However, the cluster analysis was limited to clinical, physiologic, and biologic features. To better understand structural and functional relationship, adding imaging phenotypes to the cluster analysis is essential for developing therapeutic interventions.

With the CT images acquired at SARP studies, Busacker et al. [15] demonstrated that severe asthmatics are characterized by increased air-trapping, as compared with normal and non-severe asthmatics. Furthermore, Aysola et al. [6] demonstrated that

asthmatics are characterized by the increased wall area percentage (WA% = wall area/total area), rather than normal subjects. These studies contributed respectively to either altered function of air-trapping or altered structure of increased wall area percentage. However, establishing lung structure-function relationships and adding imaging phenotypes for differentiating subtypes of asthmatics are yet to be investigated.

Subsequent subsections first describe existing imaging modalities for detection of functional defects and quantitative computed tomography (QCT)-based structural and functional assessments, and then introduce image registration and computational fluid dynamics (CFD) techniques. The registration- and CFD-derived variables are utilized to assess local functional variables as well as flow structure and particle deposition in association with altered structure and function of asthmatics.

1.1.2 Traditional PFT and Functional Defects

The functionally impaired lung functions caused by lung diseases have been evaluated with the aid of Pulmonary Function Test (PFT). This approach is useful to measure and diagnose entire lung functions, but it cannot detect local abnormality. As a result, various imaging techniques, such as Magnetic Resonance Image (MRI) and Positron Emission Tomography (PET) and QCT, have been utilized for more sensitive measures. With the aid of MRI, the region of ventilation defect as well as the movement of diaphragm and chest walls are investigated. Furthermore, the region of ventilation defects measured from hyperpolarized MRI was found to be correlated with that of air-trapping from CT images [45, 116]. Meanwhile, Venegas et al. [135, 136] demonstrated that constricted airways based on tissue abnormality can develop heterogeneity of ventilation by combining an ideal airway model with PET imaging technique. However, both MRI and PET have the drawbacks of low resolution, high cost and long scan time rather than existing static CT images.

1.1.3 Quantitative Computed Tomography

QCT is one of the most popular tools in the lung study because of the high resolution and cost effectiveness. It has been used to study airway wall thickness and air trapping using density of CT image [15, 21, 56, 96, 110]. These studies showed that airway wall area or WA% of asthmatic lungs is bigger than that of normal subjects [6, 57, 59, 60, 139]. However, the CT image is limited to capture airways of low generation (< generation 8) where diameters are smaller than 2 mm. Furthermore, the existing studies on luminal area and wall area in asthmatics are still inclusive among different studies. It is because some studies showed no difference of luminal area and wall area between normal subjects and asthmatics [6, 102]. In addition, cautions must be taken when applying any arbitrary fixed threshold value to determine the air-trapped regions. It is noted that the threshold value is sensitive to experimental conditions such as scanners and breath-hold coaching methods, and air trapping analyzed by the existing approach could misclassify normal subjects into air-trapped subjects [15].

1.1.4 Image Registration Techniques

The non-rigid image registration (matching) technique [35, 73] that matches CT lung volume images of the same human subject is a powerful tool to study lung deformation and regional air volume change in a noninvasive manner. Recently it has been demonstrated that the image registration technique not only can serve as an independent measure of regional volume changes [19, 49, 118, 152], but also can differentiate airway vs. parenchymal phenotypes in a COPD population [51]. In addition, the registration-derived variables via CT images have been compared with different modalities such as MRI, SPECT and Xenon-CT [20, 95, 118], exhibiting fairly significant correlations. Hence, the image registration of two lung volumes can provide an accurate surrogate for regional lung function, allowing evaluation of altered local lung function of asthmatics.

1.1.5   Computational Fluid Dynamics

Computational fluid dynamics (CFD) has become an alternative approach to analyze flow patterns and particle deposition in bronchial airways. A representative though not exhaustive list of such studies can be found in [52, 87, 93, 112, 158]. Tracheal regions of lung airways are in the range of turbulent and transitional area [91, 92], so that direct numerical simulation (DNS) or large eddy simulation (LES) is required to capture the anisotropic nature of turbulent flow. Most of existing CFD studies [157, 158] used Reynolds averaged Navier-Stokes (RANS), k-ε and k-ω models which temporally average the effect of turbulence, but these approaches do not adequately predict transient multi-scale turbulent features. Only a few simulations using CT-resolved-realistic airway models have been performed with LES [27, 28, 32, 101], but most studies were limited to normal subjects. Therefore, the LES along with CT-based airway models could be employed to better understand the relationship between altered structures and altered functions in asthmatics. It also helps to detect hot spots where particles tend to deposit, helping to establish the link between lung mechanics and pathophysiology.

1.2   Thesis Objective and Overview

The main objective of this work is to develop sensitive functional and structural variables and understand their correlations to better differentiate asthmatics from normal population. These variables are summarized in Table 1.1, and are classified into four groups: PFT-based variables, one-image-based variables, registration-based variables, and CFD-based variables. Some are at global (entire lung) scale, and some are at local (segmental) scale. Some are structural variables, whereas some are functional variables. We have established the registration-based variables and have tested their sensitivity in differentiating severe asthmatics from normal subjects in Chapter 2. We have developed a novel fraction-based measure for air trapping that accounts for inter-site and inter-subject variations due to the differences of scanners and coaching methods as described

in Chapter 3. This is a critical step toward population-based analysis that allows analysis of large data sets collected via multi-center studies. The correlations between air-trapping, lung shape and air distribution have also been established. To utilize CFD-based variables, we have identified and quantified local structural variables that affect flow structure and aerosol deposition at a local scale, such as bifurcation angle, circularity, hydraulic diameter and luminal area of airways, in both normal and asthmatic populations as described in Chapter 4. Furthermore, we have established the correlations between PFT-based, one-image-based, registration-based and CFD-based variables at local and global scales. Sensitive structural and functional variables investigated in previous chapters were employed to derive flow-related variables, including wall shear stress, airway resistance and particle deposition in Chapter 5.

In summary, the thesis is organized as follows.

(1) (Chapter 2) Investigate the regional lung function of normal subjects vs. severe asthmatics via image registration techniques. Lobar fraction of air volume change, local air volume change (ΔV_{air}) and J (the determinant of Jacobian representing the ratio of lung volume change) and anisotropic deformation index (ADI) are evaluated to distinguish altered lung functions in asthmatics via image registration technique.

(2) (Chapter 3) Introduce a new fraction-based air-trapping method to account for inter-site and inter-subject variations in a multi-center setting. The proposed fraction-based air-trapping approach is compared with the existing density-based air-trapping method.

(3) (Chapter 4) Investigate the bronchial structural variables of normal subjects vs. non-severe asthmatics vs. severe asthmatics. Airway dimensions such as luminal area (LA*), wall area (WA*) and total area (TA*) normalized by PFT-measured $TLC^{2/3}$ are employed to compare local airway structures among normal, non-severe asthmatic and severe asthmatic populations. Unlike existing normalization

schemes that are based on body surface area (BSA) or BMI, we have proposed a

new normalization scheme based on TLC that exhibits a stronger correlation with

tracheal luminal area. Wall thickness, circularity and hydraulic diameter that are

related to flow pressure drop and airway resistance are compared among the three

populations. Altered bifurcation angle that can potentially affect particle

deposition is also investigated.

(4) (Chapter 5) Investigate airflow and particle transport in selected normal and

severe asthmatic subjects for quantitative analysis of the CFD-related structural

and functional variables in severe asthmatics. We compared the characteristics of

pressure drops and particle depositions between normal subjects and severe

asthmatics, and found that structural and functional heterogeneity of severe

asthmatics that we found in the previous chapters affect flow structure and

particle deposition.

(5) (Chapter 6) Summarize major findings of CHAPTER 2, 3, 4 and 5. Potential

future studies such as multi-center study, cluster analysis and application to

COPD are introduced.

Table 1.1 Classification of structural and functional variables employed in this study

Group	Scale	Structure	Function
PFT-based variables	Global	-	FEV1 % predicted, FVC %predicted, FEV1/FVC, RV % predicted and RV/TLC
One-image-based Variables	Global	Lung shape at TLC	AirT% at FRC (or RV)
	Local	(Airway segmental) WA*, LA*, TA* and WT*	(Lobar) AirT% and AirT*
Registration-based variables	Global	-	U/(M+L)|v
	Local	-	Lobar fraction of air volume change, ΔV_{air}*, J and ADI
CFD-based variables	Local	Bifurcation angle, Circularity and D_h	Flow-rate ratio, Wall shear stress, ΔP, airway resistance, Particle distribution and Particle deposition

The variables in the Table 1.1 are described as follows.

- PFT-based variables:

  They provide global lung functions for air flow obstructions (FEV_1 % predicted, FVC % predicted and FEV1/FVC) and air-trapping (RV % predicted and RV/TLC).

- One-image-based variables:

As global variables, lung shape at TLC is defined as the ratio of apical-to-basal distance to ventral-to-dorsal distance, and AirT% is defined as the number of the air-trapped voxels over the number of total voxels in the whole lung. As local variables, WA*, LA* and TA* are wall area, luminal area and total area normalized by PFT-based $TLC^{2/3}$ respectively. Lobar AirT% is calculated by air-trapped voxels over total voxels in a lobe, and AirT* is the ratio of lobar air-trapped voxels to total air-trapped voxels for evaluating lobar contribution of air-trapping.

- Registration-based variables:

As a global variable, U/(M+L)|v is the ratio of air volume change of upper and middle lobes to air volume change of middle and lower lobes. Lobar fraction of air volume change (ΔV_{airF}) is the ratio of lobar air volume change to total air volume change. In addition, ΔV_{air}, J, ADI obtained from image registration are local air volume change, the determinant of Jacobian and anisotropic deformation index that can evaluate the function of local regions.

- CFD-based variables:

The structural variables of bifurcation angle, circularity and hydraulic diameter (D_h) and the functional variable of air-volume change determine CFD-based functions of wall shear stress, flow pressure drop, airway resistance, particle distribution and particle deposition.

CHAPTER 2

REGISTRATION-BASED ASSESSMENT OF THE REGIONAL LUNG

FUNCTION IN NORMAL SUBJECTS VS. SEVERE ASTHMATICS

2.1   Introduction

Asthma affects more than 25 million people in the United States and can be characterized by different symptoms such as airflow obstruction, bronchial hyper-responsiveness and airway inflammation [16]. Identification of phenotypes serving to separate non-severe asthmatics from severe asthmatics has been the focus of the NIH sponsored multi-center Severe Asthma Research Program (SARP) [21, 79, 104, 105, 143] and the search for phenotypes has included the acquisition of volumetric computed tomography (CT) scans of the lungs at total lung capacity (TLC) and functional residual capacity (FRC).

Imaging techniques such as hyperpolarized Magnetic Resonance Imaging (MRI) [1, 17, 40, 41, 134, 156], Positron Emission Tomography (PET) and Single Photon Emission CT (SPECT) [65, 67, 86, 109, 136] have been utilized for the exploration of functional defects and airway structural changes. Recently, hyperpolarized helium gas MRI has been compared with regional volume changes using paired lung volumes imaged via CT, and regional differences in lung function (expansion) were well matched [62]. CT and MRI as tools for quantitative assessment of the lung have recently been reviewed [141]. While each method provides unique pieces of information regarding lung structure and function, CT has the ability to relate detailed structure together with regional lung function [72]. Over the past 30 years now, CT has been validated in regards to its ability to reflect regional air content of the lung [70], parenchymal destruction in chronic obstructive pulmonary disease (COPD) [34, 54].

Image matching methods as used here have recently demonstrated not only to reflect independent measures of regional volume changes [19, 49, 118, 152], but also to

have shown the utility in differentiating airway vs. parenchymal phenotypes in a COPD population [51]. In addition, the image matching derived variables via CT have been compared with different modalities such as MRI, SPECT and Xenon-CT [20, 95, 118], and they have shown fairly significant correlations. With the demonstration that image registration between two lung volumes provides an accurate surrogate for regional lung function, we utilize CT image matching to assess regional differences in lung function of severe asthmatics, relative to normal subjects.

In this study, we apply a mass-preserving non-rigid registration method [151, 152] with two breath-hold volumes (TLC and FRC) to study alteration of regional air volume change and lung deformation. In the previous studies [151, 152], the method demonstrated the relatively accurate results even in large deformation based on landmarks selected at vessel bifurcations. The registration-derived variables can measure the features of the lung when deforming from one static state to the other, unlike existing air trapping measures [15, 110] that are based on density measures using a single volumetric image at FRC (or in other cases, residual volume, RV).

The purpose of this chapter is to apply a newly emerging tool allowing for the matching of lung volume pairs imaged via CT, and we have selected the normal and severe asthmatic groups to evaluate the utility of such image registration methods in mapping alterations in regional lung mechanics. In addition, we will correlate the registration-derived variables with existing traditional measures, such as PFT's measures and air-trapping, which have been commonly used for the study of asthma, to illustrate the implications of registration-derived measurements.

2.2   Methods

2.2.1   Human Subject Data Sets

Fourteen normal (10F) and thirty severe asthmatic (18F) subjects were chosen for this study. Demographic and pulmonary function data are provided in Table 2.1. Both CT images of normal subjects and severe asthmatics were acquired at the University of Pittsburgh as part of the SARP consortium [21, 46, 104, 143]. The associated human studies along with the imaging protocol were approved by the Institutional Review Board. CT images were gathered during coached breath-holds TLC and FRC in the supine position, and then were processed using the Pulmonary Workstation and Apollo software (VIDA Diagnostics, Coralville, Iowa). Scanning details are provided in Table 2.2. Major criteria used to define severe asthma are provided in [143], and include treatments with oral corticosteroids and high-dose inhaled corticosteroids besides minor criteria such as requirement for daily treatment with a controller medication of long-acting β-agonist, theophylline, or leukotriene antagonist.

2.2.2   Image Registration and Regional Air Volume
    Change

The intensity-based mass preserving image registration method [151, 152] was employed to match two CT lung images. Here, the CT images at TLC and FRC are used for the reference and floating images, respectively. The tissue and air fractions are estimated as follows.

$$\beta_{tissue}(\mathbf{x}) = \frac{I(\mathbf{x}) - HU_{air}}{HU_{tissue} - HU_{air}} \text{ and } \beta_{air}(\mathbf{x}) = \frac{HU_{tissue} - I(\mathbf{x})}{HU_{tissue} - HU_{air}} \tag{2-1}$$

where $\beta_{tissue}(\mathbf{x})$, $\beta_{air}(\mathbf{x})$, $I(\mathbf{x})$, HU_{air} and HU_{tissue} denote tissue fraction, air fraction, Hounsfield unit (HU) of a voxel, HU of air, and HU of tissue, respectively. HU_{air} and

HU_{tissue} are set to -1000 and 55, respectively [151, 152]. The tissue volume $V_{tissue}(\mathbf{x})$ and

air volume $V_{air}(\mathbf{x})$ are calculated by multiplying a local volume $v(\mathbf{x})$ to the tissue and air

fractions, respectively.

The image registration method is to determine a spatial transformation that

matches the two images by minimizing a cost function C, so called the sum of squared

tissue volume difference (SSTVD) as shown below.

$$C = \sum_{\mathbf{x} \in \Omega} \left(V_{tissue}^{ref}(\mathbf{x}) - V_{tissue}^{f}(\mathbf{T}(\mathbf{x})) \right)^2 \tag{2-2}$$

where $V_{tissue}^{ref}(\mathbf{x})$ is the local tissue volume of the reference image, while $V_{tissue}^{f}(\mathbf{T}(\mathbf{x}))$ is the

local tissue volume of the floating image. $\mathbf{T}(\mathbf{x})$, known as the warping function, provides

a transformation that maps a local volume at location $\mathbf{x}$ in the reference image to the

corresponding location in the floating image. A multi-level B-spline transformation

technique is adopted to describe the warping function $\mathbf{T}(\mathbf{x})$. The finest number of control

grids in the entire image domain is selected as $32 \times 32 \times 32$, which has been an optimal

number when considering accuracy and computational cost [26, 152].

Once warping function $\mathbf{T}(\mathbf{x})$ is obtained, the corresponding local volume $v^f(\mathbf{T}(\mathbf{x}))$

at floating image is calculated as $v^f(\mathbf{T}(\mathbf{x})) = v^{ref}(\mathbf{x}) / J$, where J is the determinant of

Jacobian matrix. At the floating image, the air fraction $\beta_{air}^{f}(\mathbf{T}(\mathbf{x}))$ is obtained by CT

intensity value $I(\mathbf{T}(\mathbf{x}))$ (Equation 2-1), so that the air volume $V_{air}^{f}(\mathbf{T}(\mathbf{x}))$ is calculated as

$v^f(\mathbf{T}(\mathbf{x}))\beta_{air}^{f}(\mathbf{T}(\mathbf{x}))$. As a result, the regional air volume change ΔV_{air} is obtained by the air

volume differences between the reference image and the floating image as follows [150].

$$\Delta V_{air}(\mathbf{x}) = V_{air}^{ref}(\mathbf{x}) - V_{air}^{f}(\mathbf{T}(\mathbf{x})) \tag{2-3}$$

2.2.3   Lung Deformation

The volume change (measured by J) and the anisotropic deformation index (ADI) are employed to quantify lung deformation [2]. To obtain J and ADI, the deformation gradient tensor ($\mathbf{F}$) is defined as follows [94].

$$\mathbf{F} = \nabla \mathbf{T} \tag{2-4}$$

where ∇ is the vector gradient operator. $\mathbf{F}$ could be decomposed into a rotation tensor ($\mathbf{R}$) and a stretch tensor ($\mathbf{U}$); $\mathbf{R}$ is orthogonal, whereas $\mathbf{U}$ is symmetric and positive definite.

$$\mathbf{F}^T\mathbf{F} = \left(\mathbf{RU}\right)^T \mathbf{RU} = \mathbf{U}^T\mathbf{R}^T\mathbf{RU} = \mathbf{U}^T\mathbf{U} \tag{2-5}$$

$$\mathbf{F}^T\mathbf{Fs} = \lambda_i^* \mathbf{s} \tag{2-6}$$

$$\mathbf{Us} = \sqrt{\lambda_i^*}\,\mathbf{s} = \frac{1}{\lambda_i}\mathbf{s} \tag{2-7}$$

Cauchy-Green deformation tensor ($\mathbf{F}^T\mathbf{F}$) is symmetric and positive definite due to the orthogonality of $\mathbf{R}$ and the nature of $\mathbf{U}$, and $\mathbf{s}$ denotes the eigenvector, and λ_i^* are the eigenvalues of the ($\mathbf{F}^T\mathbf{F}$) of each local volume from TLC to FRC. In Equation 2-7, both λ_i^* and λ_i are positive, and λ_i represent the principal strains along the principal directions of a deformed lung tissue element from FRC to TLC, where $\lambda_i = 1/\sqrt{\lambda_i^*}$ with $\lambda_1 > \lambda_2 > \lambda_3 > 0$. With the eigenvalues ($\lambda_1$, λ_2, λ_3), J and ADI are calculated as follows.

$$J = \lambda_1 \lambda_2 \lambda_3 \tag{2-8}$$

$$ADI = \sqrt{\left(\frac{\lambda_1 - \lambda_2}{\lambda_2}\right)^2 + \left(\frac{\lambda_2 - \lambda_3}{\lambda_3}\right)^2} \tag{2-9}$$

2.2.4 Physical Interpretation of ΔV_{air}, J and ADI

The three registration-derived variables ΔV_{air}, J and ADI are used to evaluate air volume change and lung deformation. First of all, ΔV_{air} reflects local air volume difference between the reference and floating images, measuring the amount of air entering (or leaving) a local region during inhalation (or exhalation). Second, J is defined as the ratio of $v^{ref}(\mathbf{x})$ at TLC over $v^f(\mathbf{T}(\mathbf{x}))$ at FRC. That is, if $J = 1$ at a local volume, the local volume remains unchanged between the two lung volumes. If $J < 1$, the volume decreases from FRC to TLC (i.e., contracts); while if $J > 1$, it increases (i.e. expands). Because the tissue volume inside a local volume can be assumed unchanged, the change of local volume is primarily due to the change of air volume. Basically, ΔV_{air} and J are measures for air volume change excluding tissue volume and lung volume change including tissue volume, respectively. In fact, both variables exhibit similar characteristics because tissue volumes during lung deformation remain unchanged. However, ΔV_{air} is the volume difference while J is the volume ratio, thus both would not have linear correlations.

The third variable ADI provides information on the preferential deformation of local lung volume [2]. For example, if a local volume is stretched isotropically in all directions, namely $\lambda_1 = \lambda_2 = \lambda_3$, Equation 2-9 gives an ADI value of zero. With increasing anisotropy, ADI increases. An important feature of ADI is its independence from J. That is, even if two local volumes have the same J, their ADI values could be different [2]. Note that ADI measures the degree of anisotropy rather than the direction of anisotropy.

Intrinsically, ΔV_{air} is derived from CT intensity $I(\mathbf{x})$ at each local volume (Equation 2-1), whereas J and ADI are derived from eigenvalues of deformation gradient tensor (Equation 2-4), so that ΔV_{air} could provide a discrete field sensitive to the local CT intensity, while J and ADI could generate more smoothed fields by the 1st order derivative of warping function.

2.2.5 Air Trapping

A voxel is regarded as an air-trapped voxel if the Hounsfield Unit of the voxel at FRC is below -856 (this number varies $\pm$ 6 HU depending upon the studies) [15, 21]. Air trapping percentage "$AirT\%$" is defined as the ratio of the number of air-trapped voxels over the number of voxels in the respective lobes (lobar $AirT\%$) or in the whole lung (total $AirT\%$). Lobar contribution to total air-trapped voxels is denoted by "$AirT^*$", which is defined as the ratio of the number of air-trapped voxels in the lobe over the number of air-trapped voxels in the whole lung. Thus, the summation of $AirT^*$ values in the five lobes is equal to unity.

2.2.6 Data Type and Analysis

The aforementioned air volume change, volume change and anisotropic deformation index (ΔV_{air}, J and ADI) are calculated for each local volume. ΔV_{air}, J and ADI are then normalized by their respective medians of the same subject, denoted by ΔV_{air}^*, J^* and ADI^*. Their spatial distributions are presented by lobe, lung height and depth averaged over all subjects, as well as for the whole lungs of selected individual subjects. Here the normalized lung height Z^* is measured from apical to basal ($Z^* = 0 - 1$), i.e. along the cranio-caudal axis, which is perpendicular to the normalized lung depth Y^* from the non-dependent (ventral) region to the dependent (dorsal) region of the lung ($Y^* = 0 - 1$). When being presented by lobe (or lung height), ΔV_{air}^*, J^* and ADI^* are the medians over all values in lobe (or at a given lung height). In this study, the left upper

lobe, left lower lobe, right upper lobe, right middle lobe, and right lower lobe are denoted by LUL, LLL, RUL, RML and RLL, respectively. To distinguish the features of severe asthmatics from normal subjects, a mixed Analysis of Variance (ANOVA) and independent T-tests are performed for significance check with software R [99]; statistical significance is taken at $P < 0.05$ level.

2.3   Results

2.3.1   Pulmonary Function Test (PFT)

Table 2.1 summarizes the PFT information for the forty-four subjects (14 normal subjects and 30 severe asthmatics) analyzed in this study. The predicted values of TLC, FRC and RV are calculated with the equation of Stocks and Quanjer [129], and the predicted values of FVC and FEV_1 are obtained from the equation of Hankinson [63]. The measured values are then divided by the predicted values, yielding the "% predicted" values in the table. In severe asthmatics, the % predicted values of both TLC and FRC are within the normal range and close to 100%. On the other hand, the % predicted values of FVC, FEV_1, and FEV_1/FVC of severe asthma are significantly smaller than those of normal subjects, as would be expected in severe asthma [104, 105]. In addition, consistent with severe asthma [125], the % predicted values of RV and RV/TLC in the severe asthmatics indicative of air-trapping are higher than those of normal subjects ($P < 0.0005$ and $P < 5.0 \times 10^{-6}$, respectively).

2.3.2   Validation of CT-based Lung Volumes

Figure 2.1 shows the linear correlations of lung volumes between upright PFT and supine CT. CT-based total lung volumes (TLV) including both air volume (AV) and tissue volume (TV) are significantly correlated with PFT-based measures of TLC and FRC (Figure 2.1 A and B). The upright PFT volumes and supine CT-based TLV are in similar

ranges, being adjacent to the identity line. On the other hand, as shown in Figure 2.1 C and D, CT-based *AV* tends to be consistently less than PFT volumes. Table 2.3 compares the ratios of CT-based *TLV, AV* and inspiratory capacity (*IC*) over PFT measurements between normal subjects and severe asthmatics. In normal subjects, the CT-based air volumes at TLC (AV^{TLC}) and FRC (AV^{FRC}) decrease about 24% and 42% respectively, as compared to their corresponding PFT volumes. Similarly, AV^{TLC} and AV^{FRC} in severe asthmatics decrease about 24% and 36% respectively relative to their corresponding PFT volumes. The CT-based *IC* (*CT*) is reduced only 6% and 8% for normal subjects and severe asthmatics, respectively, as compared to PFT measurements. Hence, the ratios of CT supine volumes to PFT upright volumes in severe asthmatics are not statistically different from those of normal subjects as shown in Table 2.3.

Table 2.3 also shows that tissue volume differences between TLC and FRC are about 0.03 liter and 0.04 liter, whereas air volume differences between TLC and FRC are about 2.57 liter and 2.32 liter for normal subjects and severe asthmatics, respectively. The means of tissue volume differences over TLC tissue volume are about 6% in both normal subjects and severe asthmatics. As a result, the difference of tissue volume between TLC and FRC is much smaller than that of air volume, supporting the assumption of SSTVD that tissue volume change is negligible (Table 2.3).

2.3.3 Mixed ANOVA (Analysis of Variance)

A mixed ANOVA test consisting of one between-subject variable and one within-subject variable was performed for two independent groups (normal subjects and severe asthmatics) and five lung regions (LUL, LLL, RUL, RML and RLL), as shown in Table 2.4. The ANOVA test evaluated six dependent variables, including lobar fraction of air volume change, ΔV_{air}^{*}, *J**, *ADI**, *AirT%* and *AirT**. For the between-subject variable "Groups", *AirT%* of severe asthmatics is different from normal subjects ($P < 0.05$) in entire lungs. As a result, a follow-up T-test was conducted to compare total *AirT%*

between normal subjects and severe asthmatics (Table 2.6). On the other hand, the differences of lobar fraction of air volume change, $\Delta V_{air}^{\;\;*}$, J^*, ADI^* and $AirT^*$ between normal subjects and severe asthmatics are not significant. This is because the dependent variables $\Delta V_{air}^{\;\;*}$, J^* and ADI^* were normalized by the respective medians, and the summations of lobar fractions of air volume change and $AirT^*$ values in the five lobes are equal to unity, as described in the Methods section. For within-subject variable "Lung regions", six dependent variables indicate that each lobe has the different characteristics of air volume change, volume change, anisotropic deformation and air trapping. The significant interactions between "Groups" and "Lung regions" of the lobar fraction of air volume change, J^*, ADI^* and $AirT^*$ imply that the effect of severe asthmatic group can affect regional difference of air volume change, deformation and air trappings. Accordingly, the T-tests of these variables in five lobes of both normal subjects and severe asthmatics were performed.

2.3.4 Lobar Fraction of Air Volume Change

Based upon lobar segmentation data, Figure 2.2 shows the means and standard errors (±SE) of lobar fractions of air volume change (lobar air volume change / whole lung air volume change) for normal subjects (black bars) and severe asthmatics (white bars). The T-test indicates that the difference of air volume change fraction in the upper and lower lobes between normal subjects and severe asthmatics is significant ($P < 0.05$), especially in RUL ($P < 0.00005$). Figure 2.3 also displays the ratios of air volume change to the left lung over the right lung $L/R|_v$ for normal subjects (black bars) and severe asthmatics (white bars), and the ratios of air volume change to the upper lobes over the middle and lower lobes $U/(M+L)|_v$ ($P = 0.125$ for $L/R|_v$ and $P < 0.0005$ for $U/(M+L)|_v$). The difference of $U/(M+L)|_v$ is still observed in age-controlled ($P < 0.01$) and BMI-controlled ($P < 0.01$) subgroups, by controlling the sample number of severe asthmatics with age < 50 ($P = 0.33$ for age difference between 14 normal subjects and 17 severe

asthmatics) and BMI < 35 ($P = 0.25$ for BMI difference between 14 normal subjects and 22 severe asthmatics), respectively. Thus, the difference between normal subjects (black bar) and severe asthmatics (white bar) is significant in upper and lower lungs rather than left and right lungs.

2.3.5 Spatial Characteristics of Averaged ΔV_{air}^*, J^* and ADI*

Figure 2.4 shows that lobar air volume changes ΔV_{air}^*, volume changes J^* and anisotropic deformations ADI^* in normal subjects (black bars) and severe asthmatics (white bars) are significantly different except for the RML. In normal subjects, ΔV_{air}^*, J^* and ADI^* of the lower lobes are higher than those of the upper lobes as shown in Figure 2.4, but the difference diminishes in severe asthmatics. The re-distributions of these quantities between upper and lower lobes in asthmatics are particularly evident in Figure 2.5 where the data are presented by lung height along the basal-apical axis. Figure 2.4 also shows that RML has the smallest air volume change (*A*) and volume change (*B*), but the highest anisotropic deformation (*C*) among five lobes in both normal subjects and severe asthmatics.

2.3.6 Subject-Specific Distributions of ΔV_{air}^*, J^* and ADI*

To illustrate and inspect the spatial distributions of ΔV_{air}^*, J^* and ADI^* in individuals, a normal subject with a lobar air volume change ratio of U/(M+L)|$_v$= 0.55 and a severe asthmatic subject with U/(M+L)|$_v$ = 0.81 were chosen because these U/(M+L)|$_v$ values are close to the respective group (normal subjects and severe asthmatics) mean values. Both selected normal and severe asthmatic subjects have normal BMI, same sex and race, but the selected severe asthmatic subject has the characteristics of airflow obstruction (low FEV_1) and air trapping (high RV) (Table 2.5).

In addition, air volumes of two selected subjects, AV^{TLC} and AV^{FRC}, are in the similar range. Figure 2.6 shows the lobar distributions of normalized air volume change (*A, D*), volume change (*B, E*) and anisotropic deformation (*C, F*) for the selected two subjects. The selected normal subject exhibits the overall characteristics found in the normal group, and the selected asthmatic subject shows an obvious shift in the upper- and lower-lobe functions. As further shown in Figure 2.6, the medians of ΔV_{air}^{*}, *J** and *ADI** by lobe are fairly uniform in the severe asthmatic subjects except for the RML.

For the normal subject, Figure 2.7 A and B demonstrate that the apical-basal and ventral-dorsal gradients exist with larger ΔV_{air}^{*} and *J** in the lower (80 %, near base) and dependent (dorsal) regions while smaller ΔV_{air}^{*} and *J** in the upper (20 %, near apex) and non-dependent (ventral) regions. Figure 2.7C shows anisotropic deformation in the lower regions of the normal subject, and relatively isotropic deformation in the upper regions. In contrast, for the severe asthmatic subject, Figure 2.8 A, B, and C show increased heterogeneity of air volume change, volume change, and anisotropic deformation with the lack of regional characteristics. For example, higher air volume change, larger volume change and increased anisotropic deformation are found near the apex.

2.3.7   Air Trapping

Table 2.6 shows the means and standard errors (±SE) of total lung air trapping percentage (*AirT%*) and lobar contribution of the air-trapped voxels (*AirT**) for normal subjects and severe asthmatics. It is noted that the total *AirT%* of severe asthmatics is much higher than that of normal subjects ($P < 0.005$), as observed in the ANOVA test. In addition, lobar contribution of air trapping (*AirT**) is mainly observed in the upper lobes of both normal subjects and severe asthmatics, and *AirT** is the highest in RML irrespective of asthma. Based on the T-test, the most statistically significant differences are mainly found in left lungs: LUL ($P < 0.05$), and LLL ($P < 0.01$). Specifically, *AirT** increases in lower lobes of severe asthmatics relative to normal subjects.

Figure 2.9 shows the spatial distributions of air-trapped clusters (CT intensity < -856) in a normal subject and a severe asthmatic subject. Note that the two subjects are those discussed before in Figure 2.6, 7 and 8. Figure 2.9 shows frontal (*A, B*), left lateral (*C, D*) and right lateral (*E, F*) views of the two subjects with a series of spheres embedded, representing the volume and location of contiguous air-trapped voxels. Air-trapped clusters are color coded by lobes. More air-trapped regions are found in the entire lung of asthmatic subject, as shown in Figure 2.9 B, D and F. The percentages of air-trapped voxels (*AirT%*) in the entire lungs are 0.5 % and 14 %, and lower lobar air-trapping contributions (*AirT**) are 24.7% and 36.8 %, respectively for the normal and severe asthmatic subject.

2.3.8   Tissue Fraction

The tissue fractions (β_{tissue}, Equation 2-1) are averaged with medians of fourteen normal subjects and thirty severe asthmatics along ventral-dorsal and apical-basal axes to observe the differences of tissue fraction between normal subjects and severe asthmatics. Figure 2.10 A and B show that tissue at TLC is almost uniformly distributed, and there seems to be little difference between normal subjects and severe asthmatics at TLC. In contrast, at FRC, tissue fraction of severe asthmatics on both axes decreases at all vertical levels relative to normal subjects. The difference is more evident near the dorsal regions (Y*=0.7-1, Figure 2.10A) and near the basal regions (Z*=0.7-1.0, Figure 2.10B). Since the summation of both air and tissue fractions is equal to unity, the decrease of tissue fraction implies an increase of air fraction.

The distributions of air volume at both TLC and warped FRC for the selected subjects are also displayed in Figure 2.11 for comparison. The FRC image is warped into the TLC image domain by applying the transform for visual comparison. Similar to the distributions of tissue fractions at TLC, the air volumes at TLC for both normal and severe asthmatic subjects are uniformly distributed. Meanwhile, the difference in lung

shape between normal subjects and severe asthmatics is quantified by the ratio of apical-basal to ventral-dorsal lung extent at TLC. The ratios are 1.56 ($\pm$0.05, SE) and 1.36 ($\pm$0.03, SE) for normal and asthmatic subjects, respectively ($P < 0.005$). The morphological difference is still observed in both age-controlled and BMI-controlled asthmatic subjects ($P < 0.005$)

2.4   Discussion

2.4.1   Comparison of CT- and PFT-based Volumes

In both normal subjects and severe asthmatics, the CT-based total lung volume *TLV* (*CT*) and air volume *AV* (*CT*) are significantly correlated with the PFT-based volumes at both TLC and FRC (Figure 2.1). In addition, *TLV* (*CT*) are in similar ranges (~90 %) with PFT volumes (Table 2.3), being consistent with the studies of Brown et al. [13, 14]. For air volume *AV*(*CT*), about 20% and 40% reductions from PFT's are measured at TLC and FRC, respectively, in both normal subjects and severe asthmatics (Table 2.3).

It is known that supine CT-based air volumes are smaller than upright PFT measurements for several reasons. For example, the plethysmographic PFT includes dead space and gas in the abdomen, but CT only includes segmented lung regions. In addition, coaching TLC is difficult and the change of body posture from upright to supine can decrease lung volumes [14, 29, 140]. The effect of body posture from upright to supine is particularly significant at FRC, resulting in about 30% reduction in PFT-based volumes [76, 106]. Therefore, our analysis is consistent with previous studies, and further shows that the effect of body posture on air volume is uniform on both normal and severe asthmatic groups.

2.4.2   Characteristics of $\Delta V_{air}{}^*$, J* and ADI* in Normal

Lungs

Existing studies [70, 71, 144] indicate that ventilation of the dependent region of normal lungs is higher than that of the non-dependent regions in the supine posture (known as vertical gradient) due to the gravity. In addition to this gradient, several researchers [3, 8, 44, 48] have reported an apical-to-basal (horizontal) gradient of ventilation existing in the supine posture. Our quantitative analysis also shows both vertical and horizontal gradients of air volume change ($\Delta V_{air}{}^*$) and volume change (*J*) in the deep breathing of normal lungs. In fact, the gradient of air fraction shall inversely correlate with the gradient of tissue fraction. As shown in Figure 2.10, the gradient of tissue fraction at FRC is greater than at TLC along both dorsal-to-ventral and basal-to-apical axes for normal subjects, consistent with the findings of others [70, 71, 119]. Therefore, air volume change ($\Delta V_{air}{}^*$) and volume change (*J*) could depend on air-volume distribution at FRC as well as lobar size distribution at TLC because air volume at TLC is almost uniformly distributed (Figure 2.11).

Amelon et al. [2] demonstrated that the eigenvector corresponding to the principal eigenvalue (Equation 2-7) mainly orients to the apical-basal axis, being approximately normal to the diaphragm plane. Therefore, the increased anisotropy (*ADI*) near basal regions may reflect the directionality of diaphragm movement as shown in Figure 2.7C. In summary, in the case of normal subjects, relatively large volume change ($\Delta V_{air}{}^*$ and *J*) and anisotropic deformation are observed in the basal and dependent regions, while relatively small volume change and isotropic deformation are observed in apical and non-dependent regions.

2.4.3 Characteristics of ΔV_{air}*, J* and ADI* in Severe Asthmatic Lungs

The air volume change (ΔV_{air}^{*}) in normal lungs increases gradually from the apex to the base (from 20% to 80 %) and from the ventral to dorsal lung regions, whereas it becomes fairly uniformly distributed in severe asthmatic subjects (Figure 2.5, 7 and 8). Quantitatively, the lobar air volume change ratio of U/(M+L)|$_v$ =0.78 in severe asthmatics is much higher than the air volume change ratio of 0.62 in normal subjects, as shown in Figure 2.3B ($P < 0.0005$). Furthermore, the air volume change and volume change (J^*) in severe asthmatics increase in the upper lobes, but decrease in the lower lobes as compared to normal subjects. Accordingly, we demonstrated that reduced air volume change in severe asthma mainly occurs in the lower lobes, which could be substantiated by comparing the contours of air volume change captured near 80 % of the apical to basal distance as demonstrated in Figure 2.7A and 8A. The relatively small anisotropic deformation (ADI^*) of the severe asthmatic subject near the basal region (80 % in Figure 2.8C) might be due to the reduced directionality of diaphragm movement (Table 2.1) in the asthmatic group. The geometric shape of the severe asthmatic lung at TLC exhibits reduced lung height (apical-basal) and increased lung depth (ventral-dorsal), which is also consistent with reduced ADI^* in basal regions.

2.4.4 Relationships between Air Trapping, PFT, ΔV_{air}^{*} and Tissue Fractions

Air-trapping percentage ($AirT\%$) of severe asthmatics significantly increases as compared to normal subjects ($P < 0.005$), being consistent with existing studies [15]. The result is also substantiated with the tissue fractions at FRC in severe asthmatics that are much smaller than in normal subjects on both dorsal-ventral and basal-apical axes as shown in Figure 2.10. In addition to overall $AirT\%$, the lobar distributions of air-trapping fractions ($AirT^*$) at FRC are different between normal and severe asthmatic subjects

(Table 2.6). More specifically, air-trapping fraction in the lower lobes of the severe asthmatic subjects increases as compared to normal subjects (see *AirT** in Table 2.6), being consistent with the finding of Fain et al. [46]. Several imaging studies [1, 66-68, 135] reported that the areas of ventilation defect are observed mostly in the dependent and basal regions. Figure 2.10A and B show that tissue fractions of severe asthmatics are much smaller than those of normal subjects in gravitational dependent and basal regions, thus implying air trapping and reduced air volume change. The results are consistent with existing studies for ventilation defects, qualitatively.

The PFT analysis of the severe asthmatics demonstrated that air trapping (RV/TLC) is correlated with airflow obstruction (FEV_1/FVC). Thus, increased air trapping in the lower lobes of severe asthmatic subjects may be correlated with reduced air volume change. The PFT results shown in Table 2.1 demonstrate that TLC and FRC volumes for both normal and severe asthmatic subjects are close to the predicted values, and CT-based lung volumes are not different between normal subjects and severe asthmatics. Therefore, reduced air volume change in the lower lobes is compensated with increased air volume change from upper lung regions. Figure 2.4A and Figure 2.5A suggest that reduced air volume change in the lower lung may be correlated with relatively increased air volume change of upper lobes, resulting in elevated volume change and anisotropic deformation in the upper lobes. A recent study based on registration of three lung CT images acquired at different inflation levels [154] demonstrated that air volume change depends much more on the lower lobes than the upper lobes at the beginning of expiration from TLC. Since FEV_1 is measured during one second at the beginning of expiration from TLC, the reduced air volume change of lower lobes observed in severe asthmatics may contribute to the reduced FEV_1 measured in PFT.

2.4.5 Characteristics of RML

Among the five lobes, RML has the smallest air volume change, volume change and the highest *ADI* in both normal and severe asthmatic subjects. In addition, significant air trapping is also observed in RML. Intuitively RML has less freedom for deformation because it is bounded with both upper and lower lobes, resulting in smaller air volume change and volume change. The same constraint can also lead to more stretching and shearing, reflecting in a high anisotropic deformation. As noted before, *J* and *ADI* are independent measures.

In conclusion, air volume change and lung deformation of severe asthmatic lungs were studied and compared with those of normal lungs. In the case of normal subjects, air volume change, volume change and anisotropic deformation of lower lobes are higher than those of severe asthmatic subjects. As a result, the dependence of air volume change on lower lobes is greater than upper lobes. In contrast, in the case of severe asthmatic subjects, deformation of lower lobes is limited as suggested by decreased volume change and reduced anisotropic deformation, resulting in increased volume change and enhanced anisotropic deformation in the upper lobes. This study also established some correlations between existing variables, such as PFT and air trapping measure from a single CT image, and registration-based quantities derived from two CT images, such as lobar fraction of air volume change, ΔV_{air}, *J*, and *ADI*. These new variables may potentially serve as sensitive measures for the study of asthmatic lungs.

2.4.6 Limitations and Future Study Directions

This study shall be extended to investigate the effects of age, BMI and the severity of asthma on registration-derived variables in the future. In addition, B-spline cubic interpolation provides the smoothed displacement field, which may result in more smoothed *J** and *ADI**. Therefore, the discontinuous effects of lobar slippage and boundary near diaphragm shall be investigated with the lung physiology [42, 153].

Furthermore, the trends of the ΔV_{air}^{*} and J^{*} in Figure 2.5A and B in the range of $Z^{*}\approx0.85\text{-}1$ are different, and the number of sample points in that region is much smaller than other regions due to TLC lung geometry. Yin et al. [152] reported that the registration errors in the regions near the diaphragm are greater than other regions. Thus, whether the discrepancy in this region is physiological requires further investigation.

Table 2.1 The demographic and PFT information of 14 normal subjects
and 30 severe asthmatics

	Normal	Severe Asthma	P
	Mean ($\pm$SE)	Mean ($\pm$SE)	from T-test
Age, year	34.5 ($\pm$3.9)	47.2 ($\pm$2.2)	< 0.01
BMI	25.6 ($\pm$1.5)	31.1 ($\pm$1.3)	< 0.05
Asthma duration	-	28.2 ($\pm$3.3)	-
Sex, No. (% Female)	10 (71 %)	18 (60 %)	-
Race, No. (White non-hispanic/African American/Other)	10/1/3 (71%/7%/21%)	25/3/2 (83%/10%/7%)	-
TLC, % predicted	96 ($\pm$3)	97 ($\pm$3)	0.75
FRC, % predicted	90 ($\pm$5)	102 ($\pm$5)	0.12
RV, % predicted	90 ($\pm$6)	134 ($\pm$9)	< 0.0005
FVC, % predicted	98 ($\pm$2)	71 ($\pm$3)	$< 1.0 \times 10^{-7}$
FEV_1, % predicted	96 ($\pm$3)	55 ($\pm$4)	$< 1.0 \times 10^{-10}$
$FEV_1/FVC \times 100$	81 ($\pm$1)	60 ($\pm$2)	$< 5.0 \times 10^{-10}$
$RV/TLC \times 100$	27 ($\pm$2)	44 ($\pm$2)	$< 5.0 \times 10^{-6}$

Note: TLC, FRC and RV of 1 normal subject and 1 severe asthmatic subject
were not available.

Table 2.2 The scanner and the scanning protocol used
for both normal subjects and severe asthmatics

	Scanner and protocol
Scanner model	GE VCT 64 slice
Scan type	Helical
Rotation time (s)	0.5
Detector configuration (channel # x mm)	64×0.625 mm
Pitch	0.984
Peak kilovoltage (kVp)	120
miliampere (mA)	S-145 M-180 L-270
Dose modulation	Auto mA OFF
Reconstruction Algorithm	Standard or Detail
Lung Algorithm	None
Additional Image filters	No Selection
Thickness (mm)	0.625
Interval (mm)	0.5
Iterative reconstruction (noise reduction algorithm)	No Selection
Scan Time (s) 30cm length	< 10

Note: mA was varied for SARP protocol based on BMI
size (S: BMI < 20, M: $20 \leq$ BMI ≤ 30, L: BMI > 30).

Table 2.3 The comparison of the ratio of upright PFT volumes to supine CT volumes; air volumes, tissue volumes and tissue volume difference from supine CT between normal subjects and severe asthmatics

	Normal subjects	Severe Asthmatics	P
	Mean ($\pm$SE)	Mean ($\pm$SE)	from T-test
$\text{TLV}^{\text{TLC}}(\text{CT}) / \text{TLC}(\text{PFT}) \times 100$	91 ($\pm$2)	91 ($\pm$2)	0.98
$\text{TLV}^{\text{FRC}}(\text{CT}) / \text{FRC}(\text{PFT}) \times 100$	88 ($\pm$3)	89 ($\pm$3)	0.76
$\text{AV}^{\text{TLC}}(\text{CT}) / \text{TLC}(\text{PFT}) \times 100$	76 ($\pm$2)	76 ($\pm$2)	0.98
$\text{AV}^{\text{FRC}}(\text{CT}) / \text{FRC}(\text{PFT}) \times 100$	58 ($\pm$4)	64 ($\pm$2)	0.23
$\text{IC}(\text{CT}) / \text{IC}(\text{PFT}) \times 100$	94 ($\pm$7)	92 ($\pm$4)	0.85
AV^{TLC} (liters)	4.14 ($\pm$0.2)	4.27 ($\pm$0.2)	0.66
AV^{FRC} (liters)	1.57 ($\pm$0.1)	1.95 ($\pm$0.1)	0.06
TV^{TLC} (liters)	0.79 ($\pm$0.04)	0.79 ($\pm$0.03)	0.96
TV^{FRC} (liters)	0.76 ($\pm$0.04)	0.75 ($\pm$0.02)	0.70
$\dfrac{\left| TV^{TLC} - TV^{FRC} \right|}{TV^{TLC}} \times 100 \; (\%)$	6 ($\pm$1)	6 ($\pm$1)	0.72

Note: PFT volumes (TLC, FRC and IC) of 1 normal subject and 1 severe asthmatic subject were not available. TLV, AV, IC and TV are total lung volume (air + tissue), air volume, inspiratory capacity and tissue volume, respectively.

Table 2.4 A mixed (between group and within group) ANOVA test of normal subjects vs. severe asthmatics (between) and five lobes (repeated measures) as a grouping and a within variable, respectively.

ANOVA (F-test, P value)	Groups (normal vs. asthmatics)	Lung regions (LUL, LLL, RUL, RML and RLL)	Interactions (Groups × Lung regions)
Fraction of Air volume change	0.69	$< 5 \times 10^{-22}$	< 0.005
$\Delta V_{air}{}^{*}$	0.94	$< 5.0 \times 10^{-7}$	0.13
$J*$	0.90	$< 5.0 \times 10^{-15}$	< 0.005
$ADI*$	0.07	$< 1.0 \times 10^{-5}$	< 0.05
$AirT\%$	< 0.05	< 0.05	0.07
$AirT*$	0.49	$< 5 \times 10^{-8}$	< 0.05

Note: Type III sum of squares are employed for F-test, and sphericity is corrected by Greenhouse-Geiser epsilon.

Table 2.5 The demographic, PFT and CT volume information of the selected normal and severe asthmatic subjects

	A selected normal	A selected severe asthmatic
Age, year	57.3	47.7
BMI	19.7	23.9
Asthma duration	-	19.7
Sex	Female	Female
Race	White non-hispanic	White non-hispanic
TLC, % predicted	93	127
FRC, % predicted	92	115
RV, % predicted	88	151
FVC, % predicted	92	80
FEV1, % predicted	95	40
FEV1/FVC $\times$ 100	80	40
RV/TLC $\times$ 100	36	42
AV^{TLC}(CT) / TLC(PFT) $\times$ 100	78	78
AV^{FRC}(CT) / FRC(PFT) $\times$ 100	56	62
IC(CT) / IC(PFT) $\times$ 100	105	95

Table 2.6 Means (±SE) of total lung air-trapping percentage (*AirT%*) and lobar contribution of air-trapped voxels (*AirT**)

		Normal subjects	Severe Asthmatics	*P*
		Mean (±SE)	Mean (±SE)	T-test
Air trapping percentage (Total *AirT%*), %		3.4 (±1.2)	10.9 (±1.9)	< 0.005
Lobar contribution (*AirT**), %	LUL	33.7 (±2.9)	24.8 (±1.8)	< 0.05
	LLL	9.3 (±1.6)	15.7 (±1.6)	< 0.01
	RUL	16.2 (±2.0)	19.2 (±1.6)	0.258
	RML	30.2 (±3.8)	25.9 (±2.2)	0.349
	RLL	10.6 (±1.6)	14.4 (±1.3)	0.075

Note: A voxel at FRC image is treated as an air-trapped region if CT intensity <−856 *HU*. The difference between *AirT%* and *AirT** is described in the section of Method: *Air Trapping*.

Figure 2.1 Comparisons of A: Total lung volume at TLC (TLV^{TLC}), B: Total Lung volume at FRC (TLV^{FRC}), C: Air volume at TLC (AV^{TLC}) and D: Air volume at FRC (AV^{FRC}) from CT scans with the corresponding PFT volumes in normal (black symbols) and severe asthmatic (white symbols) subjects: Solid (normal subjects) and dashed (severe asthmatics) lines indicate linear fitted regression lines.
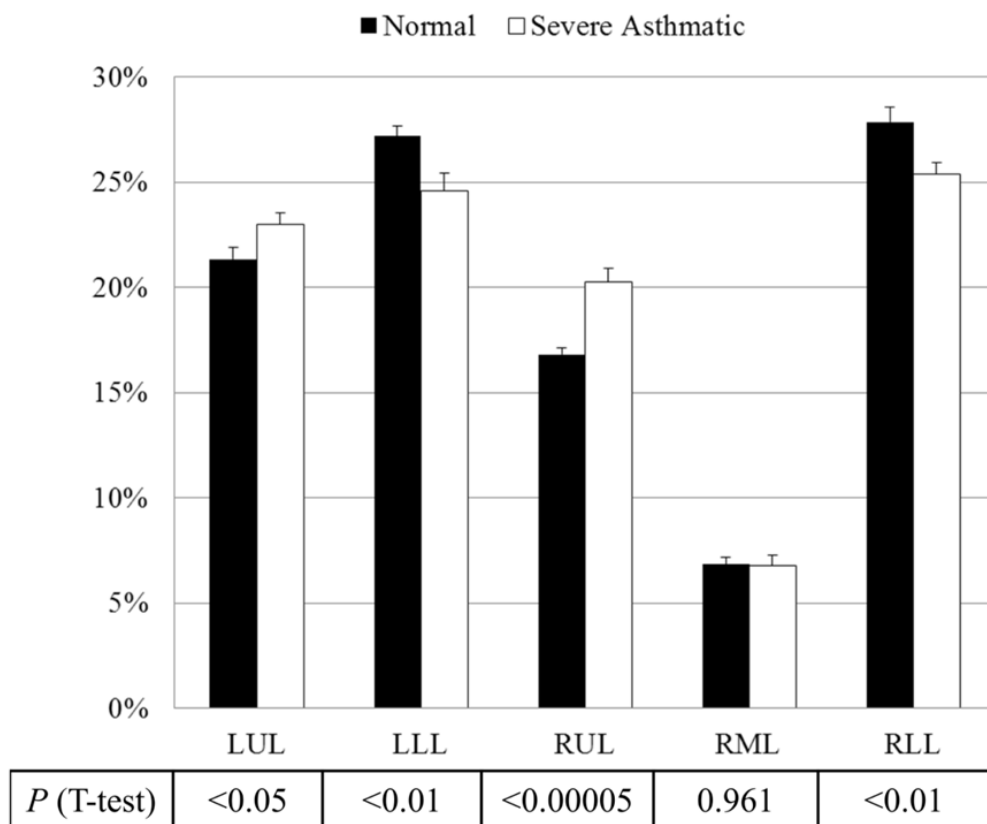
Figure 2.2 Means (±SE) of the fraction of air volume changes in normal subjects (black bars) and severe asthmatics (white bars) by lobe
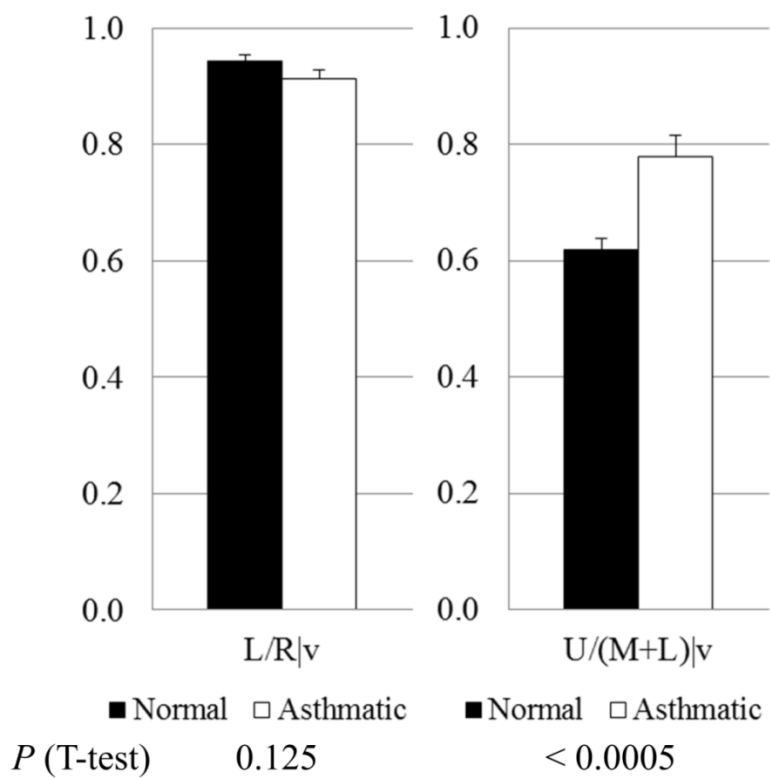
Figure 2.3 Means ($\pm$SE) of A: $L/R|_v$ ratio and B: $U/(M+L)|_v$ ratio of air volume change in normal subjects (black bars) and severe asthmatics (white bars)
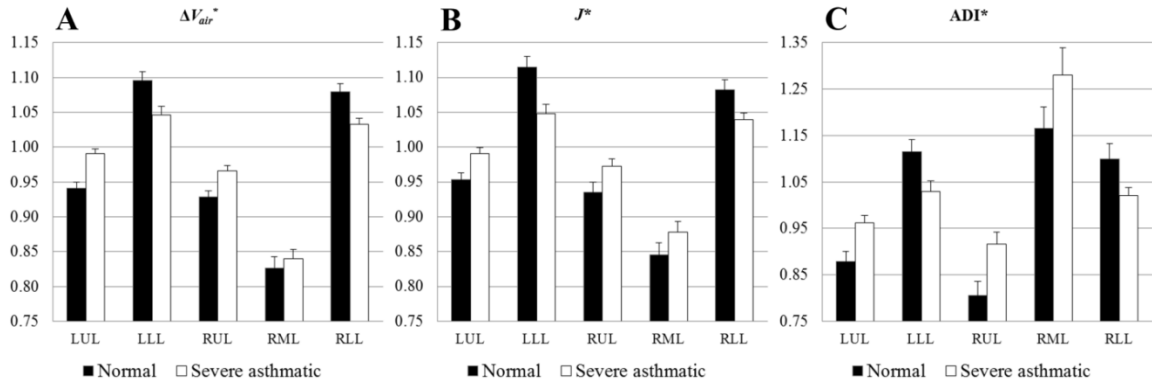
Figure 2.4 Means (±SE) of A: air volume change (ΔV_{air}^{*}; $P<0.05$ in LUL and RLL; $P=0.06$ at LLL; $P=0.07$ at RUL; $P=0.717$ at RML), B: volume change (J^*; $P<0.05$ in upper and lower lobes, and $P=0.183$ in RML) and C: anisotropic deformation (ADI^*; $P<0.05$ in upper and lower lobes, and $P=0.13$ in RML) in normal subjects (black bars) and severe asthmatics (white bars)
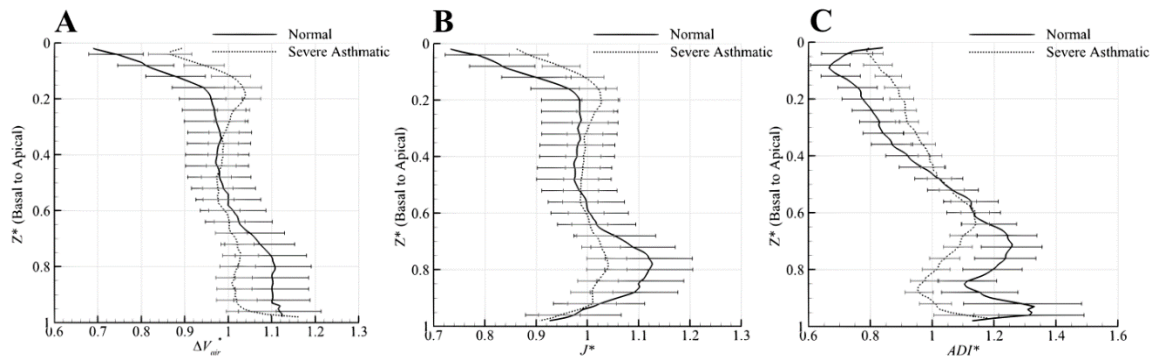
Figure 2.5 A: air volume change (ΔV_{air}^{*}), B: volume change (J^*) and C: anisotropic deformation (ADI^*) between normal subjects (solid) and severe asthmatics (dashed) along lung height (basal-apical axis): Values are normalized by the respective median of entire lung, and presented as means ($\pm$ SE).
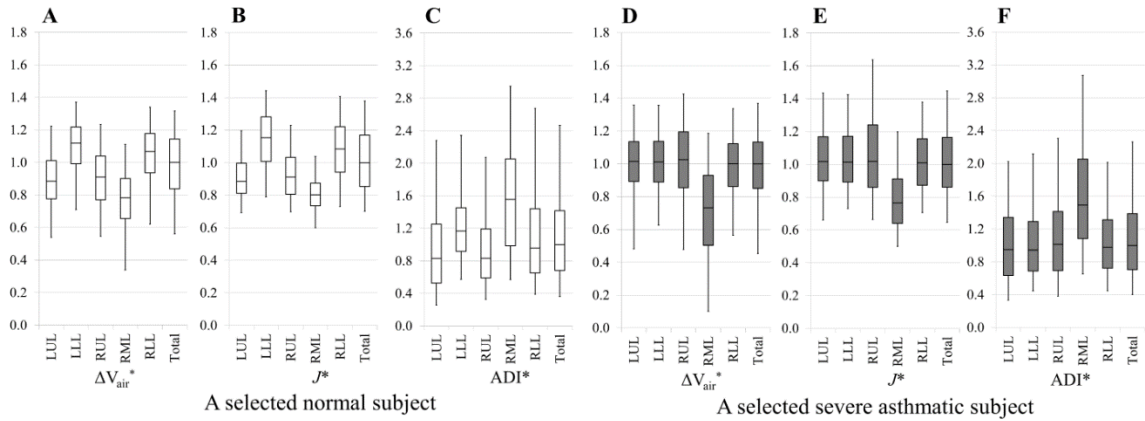
Figure 2.6 Lobar distributions of normalized air volume change (*A, D*), volume change (*B, E*), and anisotropic deformation (*C, F*) for a selected normal subject (left side) and a selected severe asthmatic subject (right side). Normalized values are presented as box (bottom: 25 percentile, middle: median, up: 75 percentile) and whisker plots (bottom: 5 percentile, up: 95 percentiles)
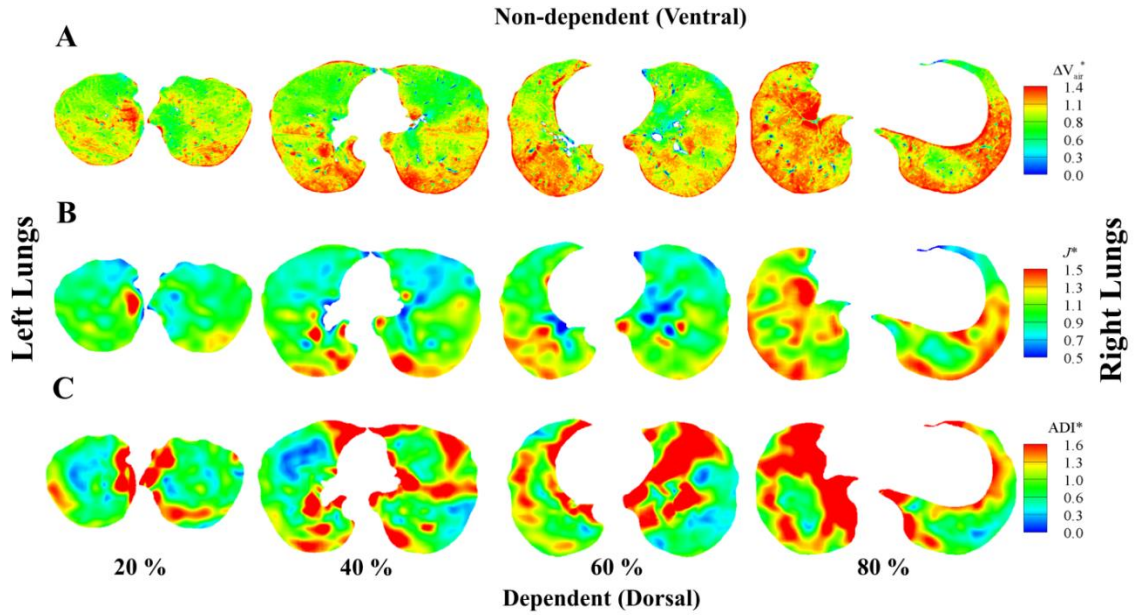
Figure 2.7 Distributions of: A, air volume change (ΔV_{air}^{*}); B, volume change (J^*); C, anisotropic deformation (ADI^*) of a normal subject at 20 % (near apex), 40 %, 60 % and 80 % (near base) from apical to basal: In each slice, the left lungs are on the left and the right lungs are on the right.
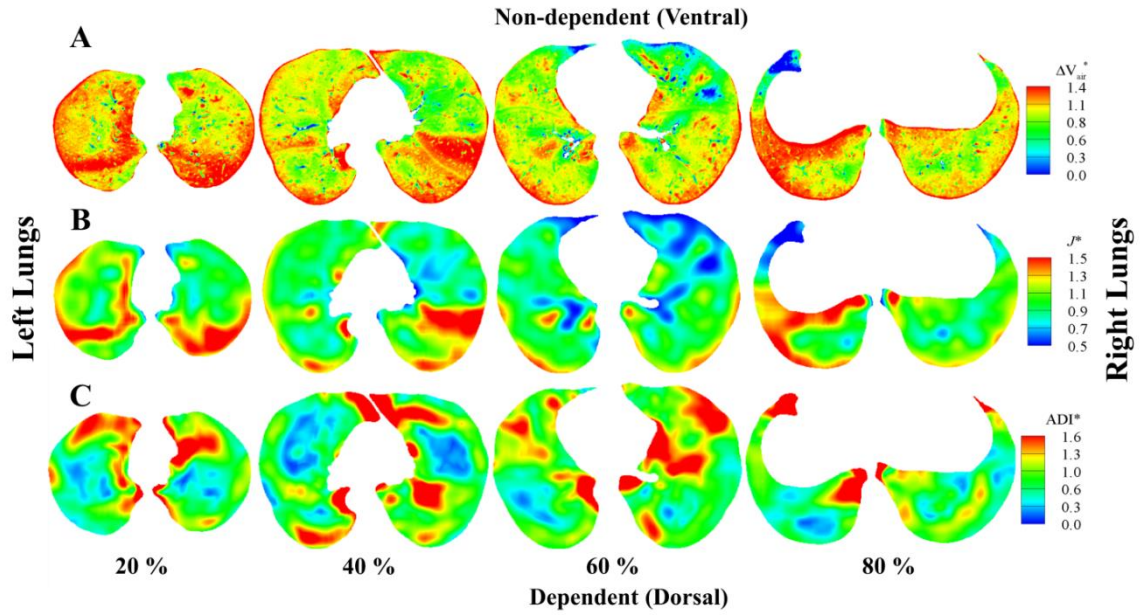
Figure 2.8 Distributions of: A, air volume change (ΔV_{air}^{*}); B, volume change (J^*); C, anisotropic deformation (ADI^*) of a severe asthma subject at 20 % (near apex), 40 %, 60 % and 80 % (near base) from apical to basal. In each slice, the left lungs are on the left and the right lungs are on the right.
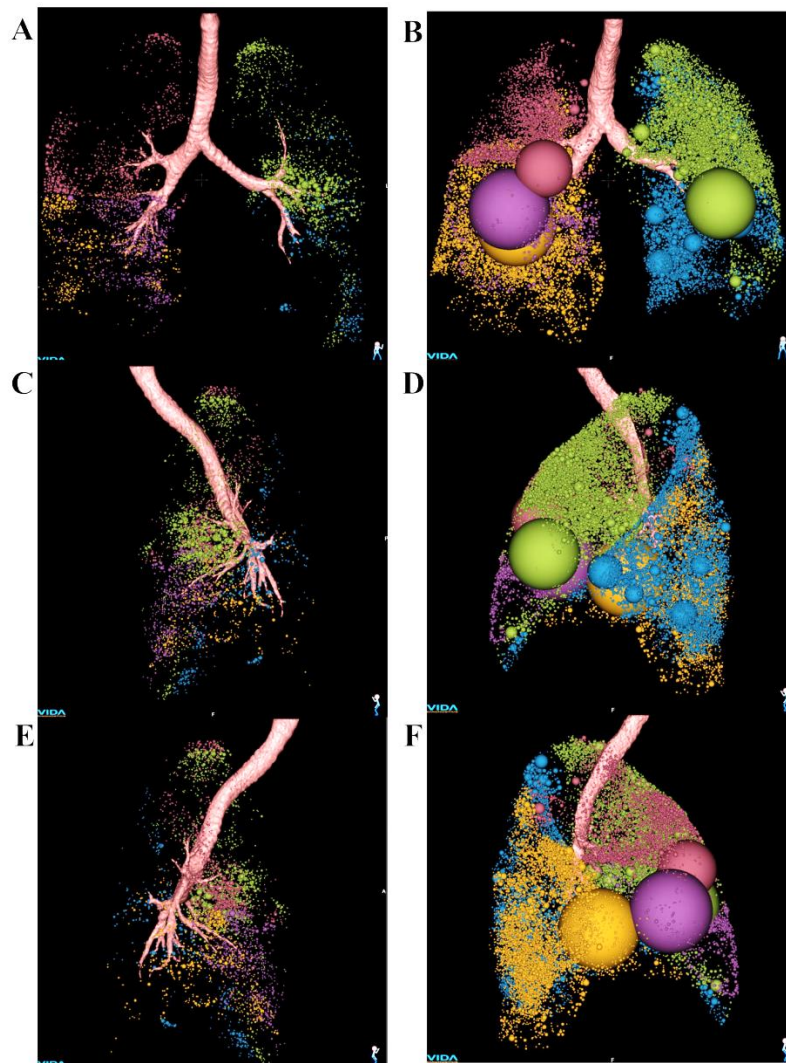
Figure 2.9 Frontal views (A, B), Left lateral views (C, D) and right lateral views (E, F) of air-trapped regions captured by CT intensity at FRC image < -856 HU, from Apollo (Vida Diagnostics). A, C and E: *AirT%* of a normal subject: total, 0.5 %; LUL, 0.9 %; LLL, 0.2 %; RUL, 0.6 %; RML, 1.3 %; RLL, 0.3 % (*AirT**: LUL, 37.6 %; LLL, 7.8 %; RUL, 20.7 %; RML, 17.0 %; RLL, 16.9 %) and B, D and F: *AirT%* of a severe asthmatic subject: total, 14 %; LUL, 14.4 %; LLL, 5.0 %; RUL, 9.3 %; RML, 39.9 %; RLL, 14.9 % (*AirT**: LUL, 24.1 %; LLL, 7.8 %; RUL, 11.6 %; RML, 27.5 %; RLL, 29.0 %). Lobes are color-coded: LUL (green), LLL (blue), RUL (red), RML (purple) and RLL (orange).
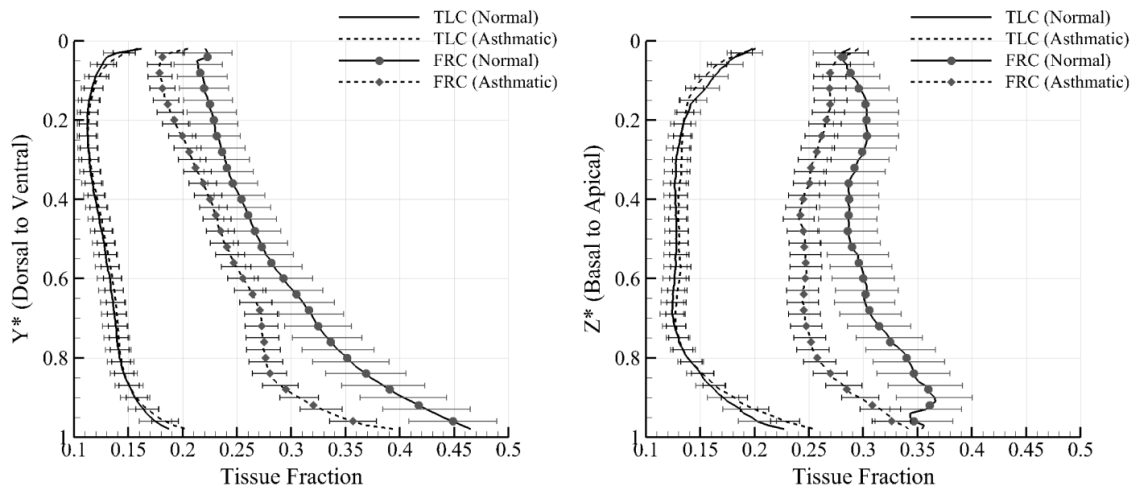
Figure 2.10 Means (± SE) of tissue fraction in TLC and FRC; A: on dorsal-ventral axis, B: on basal-apical axis of both normal subjects and severe asthmatics: The TLC curves for normal subjects and severe asthmatics are difficult to distinguish because they are closely juxtaposed.
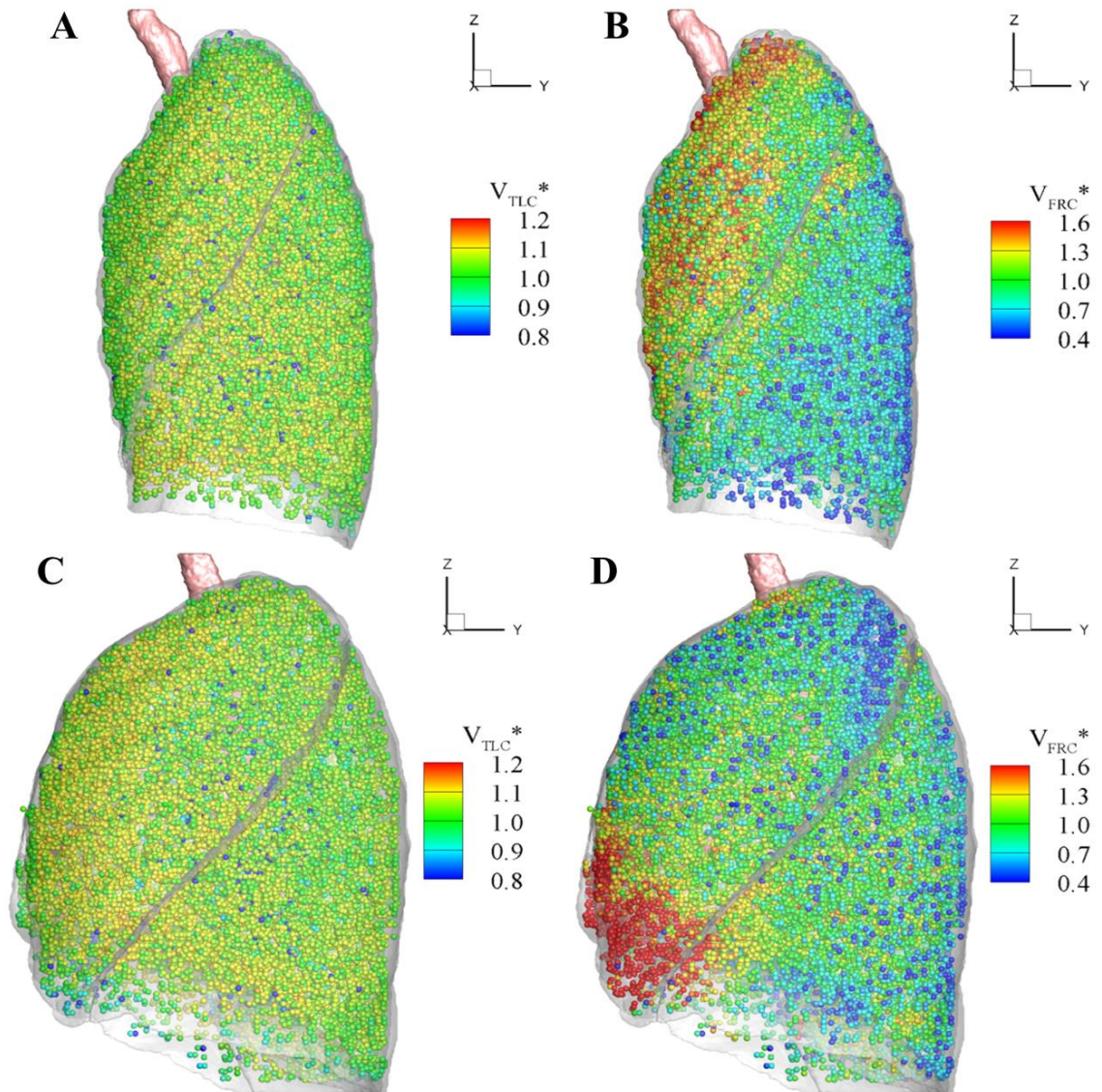
Figure 2.11 Distribution of air volume normalized with the respective mean of: A, TLC; B, warped FRC image of a normal subject and C, TLC; D, warped FRC image of a severe asthmatic subject; For 3D visualization at TLC domains, we define about 30,000 parenchymal cubical units to approximate lumped acini. Each cube consists of about 1,000 voxels given the current image resolutions.

CHAPTER 3

EFFECTS OF PROTOCOL DIFFERENCE ON AIR-TRAPPING AND

REGISTRATION-BASED LUNG ASSESSMENTS

3.1 Introduction

Quantitative computed tomographic (QCT) imaging has received increasing attention as it is used to provide objective phenotypes of lung pathology. In QCT imaging studies, asthmatics on expiratory scans (functional residual capacity (FRC) or residual volume (RV)) have been shown to have more air-trapped voxels than normal subjects [110] and severe asthmatics have more air-trapped voxels than non-severe asthmatics [15]. Air-trapping has not distinguished non-severe asthmatics from normal subjects, but CT-density threshold-based measures of air-trapping have been shown to correlate with pulmonary function tests (PFT) [15, 25, 85, 122, 125]. Air-trapping has also proven to be an important distinguishing characteristic in QCT of chronic obstructive pulmonary (COPD) patients [51, 55, 108, 122]. While air-trapping is typically evaluated in the pulmonary function laboratory at RV because of ease of implementation, image-based air-trapping has been variably studied at either RV or FRC via QCT and shown to be an effective metric in both cases (when scan times for spiral imaging of the lung took 30-40 seconds, it was easier for a subject to hold their breath at FRC than at RV).

Image registration techniques have been used as an alternative to the threshold-based measure for quantification of regional lung mechanics [88, 118, 152] or as a means of linking total lung capacity (TLC) and FRC lung densities [51] through matching of a pair of CT images at different inflation levels. The image-registration derived variables show significant correlations with functional assessment via MRI, SPECT, and Xenon-CT [20, 95, 118]. We have recently demonstrated that volume changes of severe asthmatics decrease preferentially in basal lung regions with compensatory volume elevation and anisotropic deformation in apical regions of the supine posture [25]. These

techniques have proven to be useful in differentiating airway vs. parenchymal phenotypes in a chronic obstructive pulmonary disease (COPD) population [11, 51]. Thus, both CT-density threshold-based measures and two-image registration-based measures have shown strengths in characterizing diseased lungs.

Busacker et al. [15] adopted the CT-density threshold-based method to evaluate air-trapping at FRC CT images of 120 subjects gathered from multiple centers participating in the severe asthma research program (SARP) [21, 46, 79, 104, 105, 143]. However, the issue concerning scanner differences and protocol variability has been identified in various COPD-based studies [9, 98, 123]. To resolve the issues, Kim et al. [85] applied the density correction to control inter-subject variability with densities of tracheal air and aorta to improve quantification of emphysema at TLC. In addition, acquisition and standardization of lung volumes remain a challenging issue, and the repeatability and reproducibility in obtaining lung volumes at the same inflation level could be important for quantitative analysis of CT images [30, 50, 140].

With the goal of utilizing both density-based and two-image metrics to improve the differentiation among normal, non-severe and severe asthmatic populations in the context of image data gathered from multiple centers, we have utilized data acquired via two centers of the NIH-sponsored multi-center severe asthma research program (SARP: the University of Pittsburgh (PITT) and the Washington university in Saint Louis (WSL)) [21, 46, 79, 104, 105, 143] and normal data acquired at the University of Iowa (UI) via a NIH bioengineering research partnership (BRP) grant (HL-064368). Both General Electric and Siemens scanners were employed, and coached (SARP) as well as pneumotach-controlled (BRP) methods were used to achieve TLC and FRC lung volumes. We have sought to employ corrections for the differences of Hounsfield Unit of air (HU_{air}) and lung volumes, by introducing a new fraction-based method. Furthermore, we utilized the fraction-based measure of air-trapping together with two-image-based measure of air

volume change and chest wall configuration, to provide a combined metric serving to better differentiate among three populations.

3.2   Methods

3.2.1   Human Subject Data Sets

This imaging study and protocols for acquiring CT images at both TLC and FRC were approved by the Institutional Review Boards of respective institutions. We utilized data acquired at the UI (Center 1), and at two centers of the SARP at the PITT (Center 2) and the WSL (Center 3) [21, 46, 79, 104, 105, 143]. 25 normal subjects were from Center 1; 70 subjects including "14 normal subjects, 26 non-severe and 30 severe asthmatics" were from Center 2; 49 subjects including "11 normal subjects, 16 non-severe asthmatics and 22 severe asthmatics" were from Center 3. Thus 50 normal subjects, 42 non-severe and 52 severe asthmatics were used for this study (see Table 3.1). Major criteria used to define severe asthma include treatments with oral corticosteroids and high-dose inhaled corticosteroids, besides several minor criteria [104, 143]. All asthmatic subjects who did not meet criteria for severe asthma were classified as non-severe asthmatics. All CT images were acquired in the supine postures, and airway and lobar segmentations were processed using the Pulmonary Workstation and Apollo software (VIDA Diagnostics, Coralville, Iowa) [75, 133].

3.2.2   Protocol Differences

The major differences in the protocols included the use of different scanners and breath-hold coaching methods. Center 1, Center 2 and Center 3 used Siemens-Sensation 64 slice, GE-VCT 64 slice, and Siemens-Sensation 16 slice, respectively (Table 3.2). Center 1 employed pneumotach-monitored coaching, whereas Center 2 and Center 3 employed verbal coaching. To evaluate the sensitivity of scanner difference, tracheal CT

densities for voxel air values were measured as follows: The airway masks were first obtained via the Pulmonary Workstation or Apollo pulmonary analysis software (VIDA Diagnostics, Coralville, Iowa) [72]. They were then eroded using binary filters to exclude partial volume contaminated (higher) CT densities near the boundaries. The binary erosion was carried out with a ball-shaped element of radius of 6 voxels to all images (see Figure 3.1). The median of CT densities in the remaining voxels was used as the HU_{air} for each subject.

As for the coaching methods, the subjects at Center 2 and Center 3 were coached to take three deep inspirations and then to hold their breath at TLC for the inspiratory scan. For the expiratory scan (FRC), they were coached to take three deep breaths in and out and then take deep breath in and release breath out normally and then hold breath. In contrast, the breathing volumes of the normal subjects at Center 1 were studied with nose plugs in place along with a pneumotachometer. The pneumotachometer was monitored using custom-built Lab View software which logged both TLC and RV efforts for defining vital capacity (VC) and then was set to close a balloon valve after three deep inspirations at ~95% VC and ~20% VC to approximate TLC and FRC, respectively [50]. To evaluate the reliability of pneumotach controlled method, we calculated inspiratory capacity (IC) from supine pneumotachometer-based measurements acquired in the pulmonary function laboratory on the same day as scanning. The pneumotachometer-measured IC from Center 1 was calculated as follows:

$$IC = VC \times [\%VC \text{ (at TLC) - } \%VC \text{ (at FRC)}] \qquad (3\text{-}1)$$

The calculated IC from Equation (3-1) was then compared with the difference in lung air volume calculated from the inspiratory and expiratory CT scans.

3.2.3   Traditional threshold-based and new fraction-based

Air-Trapping Measures

Air-trapping percentage (AirT%) is defined as the ratio of the number of air-trapped voxels to the number of voxels in the whole lung (total AirT%). With the existing density-threshold-based method (Table 3.3), a voxel was regarded as an air-trapped voxel if the CT density (I) is below -856 (or -850) at FRC [15, 110], but the approach can be sensitive to scanner differences in air calibrations and approaches to handling beam hardening and scatter correction. Accordingly, we propose a fraction-threshold-based method using fixed air fraction (β_{air}) to calculate adjusted thresholds ($I_{threshold}$). First, air fraction is defined as follows:

$$\beta_{air}(x) = \frac{HU_{tissue} - I}{HU_{tissue} - HU_{air}} \qquad (3\text{-}2)$$

β_{air} is a dimensionless parameter, representing normalized (or relative) air content that ranges between 0 and 1. Thus, it is expected to be less sensitive to the scanner difference as compared with the existing density threshold-based method that relies on the absolute value of CT density.

$$I_{threshold} = \beta_{air,threshold} HU_{air} + (1 - \beta_{air,threshold}) HU_{tissue} \qquad (3\text{-}3)$$

Given the fraction threshold $\beta_{air,threshold}$ for air-trapping, HU_{tissue} of 55 and subject-specific HU_{air} obtained from the CT density at trachea, Equation (3-3) rearranged from Equation (3-2) can be used to obtain subject-specific threshold $I_{threshold}$ to quantify air-trapping. This new measure is referred to as the "fraction-based" air-trapping metric (see Table 3.3).

3.2.4 Structural and Functional Metrics

Previously we applied an image registration technique to study local distributions of air volume change between TLC and FRC in severe asthmatics against those of normal subjects [25]. The study has shown that more air is delivered to the upper lobes than the lower lobes when asthmatic lungs are expanded from FRC to TLC as compared with normal subjects. The shift of air volume change is not only due to increased air-trapping in basal and dependent regions at FRC, but also due to the reduced diaphragm movement along the apical to basal axis. Hence, we employed two more sensitive variables from the previous study. One is the ratio of "the air volume change in the upper lobes" to "the air volume change in the lower and middle lobes" (hereafter referred to as the "U/(M+L)|v"). This value can be obtained either by image registration between TLC and FRC or by the difference of segmented lung volumes at TLC and FRC (see Figure 3.2). While the registration can derive the U/(M+L)|v metric at organ scales, it can further provide more sensitive variables at local voxel scales [25]. The other is the ratio of "the apical-basal distance" to "ventral-dorsal distance" at TLC (hereafter referred to as the "lung shape") by measuring the extreme positions on each axis (Figure 3.2). Thus, we combined the U/(M+L)|v and lung shape along with the above-discussed fraction-based metric (Table 3.3) for differentiating populations of normal subjects, non-severe and severe asthmatics.

3.2.5 Statistical Analysis

To evaluate the performance of the proposed fraction-threshold-based method vs. the traditional density-threshold-based method for differentiating subject populations and the enhanced performance obtained by the additions of U/(M+L)|v and the lung shape, analysis of variance (ANOVA) tests with post-hoc Tukey's tests were performed. χ^2 tests were also performed to evaluate association between air-trapping and the severity of asthma. Furthermore, Pearson linear correlations and linear regressions were employed.

The software R [5, 74, 117] was used for the statistical analysis and statistical significance is taken at $P < 0.05$ level.

3.3   Results

3.3.1   Pulmonary Function Test

Table 3.1 shows demographic and PFT information for 50 normal, 42 non-severe asthmatic and 52 severe asthmatic subjects under investigation. The predicted values of TLC, FRC and RV are calculated with the equations of Stocks and Quanjer [129], and the predicted values of FVC and FEV_1 are obtained from the equations of Hankinson [63]. RV % predicted values and RV/TLC indicating air-trapping increase in severe asthmatics, as compared with normal and non-severe asthmatic subjects, whereas there are no differences between normal subjects and non-severe asthmatics. In severe asthmatics, both FVC % predicted, FEV_1 % predicted values and FEV1/FVC indicating air flow obstruction are much smaller than normal and non-severe asthmatic subjects ($P < 0.001$), and those values of non-severe asthmatics are smaller than normal subjects ($P < 0.01$). These characteristics of severe asthmatics are consistent with existing studies [25, 125].

3.3.2   Tracheal HU_{air} in Different Scanners

HU_{air} measured inside trachea is generally expected to be close to -1000 HU. Table 3.4 shows that the HU_{air} for each scanner is the mean of the medians for each subject in the same imaging center. The HU_{air} in Center 3 images (Siemens-Sensation-16 scanner) is the closest to the ideal HU_{air} of -1000. Although Center 1 also used a Siemens scanner, this was a Sensation-64 and the tracheal HU_{air} was significantly different from that of Center 3. The HU_{air} in Center 2 images measured with GE-VCT-64 shows a greater deviation from the ideal HU_{air}. The standard errors of the means ($\pm$SEM) of HU_{air}

in Table 3.4 further indicate that inter-site variability is much more significant than inter-subject variability.

3.3.3 CT-based Lung Volumes

CT images were acquired in the supine position, whereas PFT volumes were acquired in the upright position (except for the additional supine measurements acquired in Center 1). To compare CT-based lung volumes among different centers, the supine CT-based air volumes (AV) at TLC and FRC were normalized by their corresponding PFT volumes. Table 3.5 shows that the normalized AV^{TLC} and AV^{FRC} are different among three imaging centers, whereas the difference of the normalized IC among centers is negligible. The AV^{TLC} of Center 3 images is smaller than those of Center 1 and Center 2 images at TLC ($P<0.01$), and the AV^{FRC} of Center 1 images is much larger than those of Center 2 and Center 3 images at FRC ($P<0.001$).

Employing a pneumotachometer-based volume controller, the Center 1 protocol yielded the elevated lung volumes at both TLC and FRC, as compared with those of Center 2 and Center 3. The Pearson correlation of Center 1 ($r = 0.92$) between TLC (PFT) and air volume at TLC (AV^{TLC} (CT)) is stronger than those of Center 2 ($r = 0.76$) and Center 3 ($r = 0.74$); the correlation of Center 1 ($r = 0.91$) between FRC (PFT) and air volume at FRC (AV^{FRC} (CT)) is also stronger than those of Center 2 ($r = 0.82$) and Center 3 ($r = 0.59$). In addition, pneumotachometer-measured IC could be calculated with %VC for TLC and %VC for FRC measured in the supine position (Equation (3-1)). The pneumotachometer-measured IC is significantly correlated with the segmented IC, as shown in Figure 3.3 ($r = 0.94$), supporting the reliability of volume controllers in obtaining CT images. Furthermore, although Center 2 and Center 3 used the same coaching method, AV^{TLC} between them are different.

3.3.4   Air-Trapping Percentage (AirT%)

PFT results (see Table 3.1) indicate that non-severe asthmatics did not have air-trapping because RV% predicted values and RV/TLC are in the normal range. Hence, we first analyzed the two extreme populations: normal subjects vs. severe asthmatics for air-trapping using the traditional density-threshold-based approach (Table 3.3). Figure 3.4 shows linear regressions between AV^{FRC} and AirT% for Center 2 and Center 3 groups, respectively. The increases in air-trapping of severe asthmatics are prominent in both Center 2 and Center 3 groups as compared with the normal subjects. AirT% in both Center 2 and Center 3 show two distinct slopes for normal subjects and severe asthmatics, being significantly correlated with AV^{FRC} measured in CT. However, if Center 1, Center 2 and Center 3 data are plotted altogether as in Figure 3.5A, the two populations are not distinguishable because of inter-site variability. For example, the slope of Center 3 normal subjects is much steeper than that of Center 2 severe asthmatics, and the means of AirT% between Center 3 normal subjects and Center 2 severe asthmatics are not different (Figure 3.5).

Next, we examined the proposed fraction-based method. The optimal $\beta_{air, threshold}$ was determined empirically by applying seven values of $\beta_{air}=(86,87,88,89,90,91,92)\%$ to the normal subjects from Center 1, Center 2 and Center 3. The above range of β_{air} was estimated with the CT density of I$=-856$ HU (Table 3.4). The adjusted thresholds ($I_{threshold}$) for each subject were calculated using Equation (3-2) with the tracheal HU_{air} of each subject. Figure 3.6 shows linear regressions between AV^{FRC} and adjusted AirT% for three different β_{air} values of 88%, 90% and 92% in normal subjects. The results show that with fixed air fraction β_{air}, data acquired from different sites almost collapse into a single regression line. The Spearman correlation between FEV_1/FVC and AirT% in normal subjects is the best ($r=-0.303$) with $\beta_{air}=90\%$, although the difference among the correlations obtained with these β_{air} values is marginal. Thus, we adopted a threshold of

$\beta_{air,\,threshold}$=90% for the following analysis. The β_{air} of 90% is equivalent to the density threshold of -895 HU when HU_{air} and HU_{tissue} are set to -1000 and 55.

When applying the fraction-based method to Center 2 and Center 3 severe asthmatics, the correlations exhibit consistent slopes (Figure 3.7A). The mean of air-trapping in Center 2 severe asthmatics is greater than that in Center 3 severe asthmatics (P<0.05, Figure 3.7B). In PFT results, FEV_1/FVC of Center 2 severe asthmatics (0.60 ± 0.02) was smaller than that of Center 3 severe asthmatics (0.68 ± 0.03) (P<0.05), which may be associated with the elevated AirT% in Center 2 severe asthmatics. Meanwhile, the slopes of air-trapping for non-severe asthmatics are close to those of normal subjects as expected from the PFT analysis.

Adjusted AirT% calculated with the fraction-based approach is significantly correlated with AV^{FRC} (Figure 3.8). Therefore, we introduced a slope-based scheme using two representative regression lines for classification of subjects into three phenotypes: no air-trapping, non-severe air-trapping and severe air-trapping. The association test for this new classification scheme shows much stronger association of air-trapping with the presence and severity of asthma than that of the existing classification scheme [15] based upon a constant threshold of 5.31% (Table 3.6). The threshold used in the existing scheme is the median of existing AirT% (calculated with the threshold-based approach) of the entire samples, depending on the number and distribution of samples. For example, a threshold of 9.66% was obtained in the reference [15] due in part to the fewer normal subjects in their study. In addition, adjusted AirT% shows stronger correlation (r=-0.453 with P<1×10^{-7}) with FEV_1/FVC than existing AirT% (r=-0.416 with P<1×10^{-6}).

3.3.5 Structural and Functional Metrics Added to Phenotype

The lung shape metric (Figure 3.2), measured as the apical-basal vs. ventral-dorsal distance ratio at TLC, of normal subjects, non-severe asthmatics and severe

asthmatics shows clear differences among populations: $P<0.01$ for normal vs. non-severe asthmatic, $P<0.05$ for non-severe asthmatic vs. severe asthmatic, and $P<1\times10^{-4}$ for normal vs. severe asthmatic (Table 3.6). The lung shape is also significantly correlated with the decrease of FEV_1/FVC ($r=0.36$, $P<1\times10^{-5}$). Furthermore, the χ^2 association test with a threshold of 1.4 for the lung shape indicates the association of lung shape with the presence and severity of asthma (Table 3.7). The U/(M+L)|v also shows the clear distinction among populations: $P<0.05$ for normal vs. non-severe asthmatic, $P<1\times10^{-4}$ for non-severe asthmatic vs. severe asthmatic, and $P<1\times10^{-4}$ for normal vs. severe asthmatic (Table 3.6). The U/(M+L)|v is significantly correlated with air flow obstruction with FEV_1% predicted ($r=-0.47$ with $P<1\times10^{-8}$) and FVC% predicted values ($r=-0.48$, $P<1\times10^{-9}$). χ^2 association test with a threshold of 0.7 shows the significant association of U/(M+L)|v with the presence and severity of asthma (Table 3.6). The distinctive characteristics of lung shape and U/(M+L)|v among populations are still observed in BMI controlled sub-group tests (Table 3.7).

3.4   Discussions

Several publications [85, 98, 123] have reported the difference of CT density caused by scanner differences, but there remain uncertainties regarding how to account for these differences. CT density is used for determining air-trapping and emphysema, as well as for calculating air fraction and tissue fraction. Therefore, it is important to assess the sensitivity of density-based approach to variation of CT density caused by scanner difference. This study shows that HU_{air} at trachea is different even using the scanners of the same company but different model, and that HU_{air} of GE scanner exhibits greater divergence from -1000 HU than those of the two Siemens scanners (see Table 3.4). CT density measured in the aorta can be used as HU_{tissue} [85], but this study assumes HU_{tissue} as a constant value because the difference was negligible in determining adjusted

threshold $I_{threshold}$. This is based on the estimation that with $\beta_{air}=0.9$, correction of HU_{air} is 9 times more significant than that of HU_{tissue} according to Equation (3-3).

Generally, supine CT-based lung volumes are smaller than upright PFT lung volumes because of body posture, dead space, and gas in abdomen [142]. While coaching subjects helps, there remains variability amongst subject efforts. Compared with Center 2 and Center 3, Center 1 normal subjects have larger TLC, and more reliable volumes with small standard deviation and stronger correlation with PFT-based TLC. Pneumotachometer-based volume controllers employed in Center 1 normal subjects can monitor lung volumes and enable immediate feedback to the technician during coaching subjects to reach the targeted 95% VC. The accuracy of the pneumotach-controlled lung volume approach used in Center 1 is further demonstrated by the similarity between the IC measured in the supine posture in the pulmonary function laboratory vs. IC calculated based upon the CT metrics (Figure 3.3). The effects of body posture and protocol differences are more significant in FRC lung volumes (Table 3.5). Relative to Center 1, the reduced correlations of AV^{FRC} with FRC (PFT) in Center 2 and Center 3 may reflect the difficulty of coaching patients to FRC without the aid of a pneumotachometer [39].

Air-trapping is reflected in an increase of RV. However, historically, expiratory lung scans have been acquired at FRC because of the difficulty in holding lung volumes at RV during, what used to be a 30-40 second breath hold. While current spiral scanning is accomplished in well under 10 seconds, many studies have continued to use FRC. This is in the process of changing, such that the NIH sponsored SPIROMICS [33] study has shifted to RV. For the purposes of this study, seeking to harmonize data across sites, the choice of RV or FRC is inconsequential. In fact, CT density can decrease not only due to air-trapping, but also due to the increase of air content from RV to FRC. FRC predicted values are also calculated based upon age, gender and height. Thus, air-trapping assessed at FRC becomes significantly correlated with the volume of the lung during the FRC breath-hold, which has been shown to be variable among sites. Thus, imposing a single

AirT% threshold (e.g., 5.31%) to determine air-trapped lungs has the risk of misclassifying normal lungs as air-trapped lungs. For example, 44% of normal subjects in this study (Table 3.6) and 35% of normal subjects in the previous study [15] were considered as air-trapped when the previous classification scheme based on a single AirT% threshold [15] was employed. Some normal subjects might be indeed air-trapped, but the percentages of air-trapped subjects are unreasonably high given that their PFT-based RV/TLC values fall in the normal range.

Accordingly we introduced a new classification scheme for assessing air-trapping based on two representative slopes (Figure 3.8). We made an allowance of 2.5% air-trapping for the normal group to account for the CT-unresolved airways in the lobar masks that may be treated as air-trapped voxels. This approach enables analysis of CT images collected across multi-center studies, because it accounts for FRC levels of Center 1 which are quite different from those of Center 2 and Center 3 (Table 3.5). Relative to the existing density-threshold based approach, the strength of the proposed fraction-based approach has been demonstrated through the association test with the presence and severity of asthma (Table 3.6) as well as the correlation test with FEV_1/FVC.

The lung shape at TLC and the U/(M+L)|v of severe asthmatics are significantly smaller and greater than those of normal subjects, respectively (Table 3.7), being consistent with an existing study [25]. The lung shape at TLC and U/(M+L)|v for non-severe asthmatics fall between those of normal and severe asthmatic groups. This result suggests the necessity of studying TLC images as well as FRC images to differentiate non-severe asthmatic subjects from normal and several asthmatic subjects. Relative to the air-trapping measure, the variables of the lung shape and U/(M+L)|v are more sensitive than the air-trapping variable of AirT% in terms of differentiating non-severe asthmatics from normal subjects (Table 3.6).

In conclusion, this study showed the difference of HU_{air} caused by the scanners as well as the difference of lung volumes caused by the coaching methods in a multi-center

trial setting. We then demonstrated improved correlation with PFT measurements vs. those derived from CT imaging when lung volumes are pneumotachometer-controlled. When such protocol or coaching differences exist, the existing threshold-based air-trapping method is required to be adjusted for these multi-center image differences. Hence, we proposed a new fraction-based air-trapping measure and a new slope-based classification scheme for air-trapping. These approaches substantially improved association with the presence and severity of asthma and the correlation with FEV_1/FVC. Furthermore, this study suggested that lung shape and air volume change (U/(M+L)|v) in conjunction with the above new methods provide an improved metric serving to differentiate severe from non-severe and non-severe from normal populations.

Table 3.1 Demographic and PFT information for 50 normal subjects, 42 non-severe and 52 severe asthmatics

	Normal Subjects	Non-severe asthmatics	Severe asthmatics	ANOVA (*F*-test, *P* value)
Subjects, No.	50	42	52	-
Age, year	38.6 (±2.0)	33.7 (±1.5)	43.6 (±1.7)	< 0.001 ¥
BMI	26.3 (±0.8)	29.5 (±1.2)	32.9 (±1.3)	< 0.001 *
Asthma duration	-	19.2 (±1.9)	26.1 (±2.2)	< 0.05 ¥
Gender, No. (% Female)	31 (62%)	27 (64%)	36 (69%)	= 0.74
Race, No. (White non-hispanic/ African American/Other)	42/3/5 (84/6/10%)	28/9/5 (67/21/12%)	32/14/6 (62/27/12%)	-
TLC % predicted	102 (±2)	94 (±2)	104 (±3)	< 0.05 ¥
FRC % predicted	96 (±3)	89 (±3)	107 (±5)	< 0.05 ¥
RV % predicted	105 (±3)	101 (±4)	145 (±8)	$< 1 \times 10^{-7}$ ¥*
RV/TLC × 100	31 (±1)	31 (±1)	44 (±1)	$< 1 \times 10^{-13}$ ¥*
FVC % predicted	99 (±2)	89 (±2)	72 (±2)	$< 1 \times 10^{-13}$ §¥*
FEV$_1$ % predicted	101 (±2)	80 (±3)	57 (±3)	$< 1 \times 10^{-15}$ §¥*
FEV$_1$/FVC × 100	83 (±1)	74 (±2)	63 (±2)	$< 1 \times 10^{-15}$ §¥*

Note: The values are presented as means (±SEM). TLC, FRC and RV of 2 normal, 1 non-severe asthmatic and 1 severe asthmatic subjects were not available and only FRC of 1 non-severe asthmatic was not available. ANOVA tests with Tukey's post-hoc tests were performed for "populations: normal subjects vs. non-severe asthmatics vs. severe asthmatics". § indicates $P<0.05$ for normal subjects vs. non-severe asthmatics; ¥ indicates $P<0.05$ for non-severe asthmatics vs. severe asthmatics; * indicates $P<0.05$ for normal subjects vs. severe asthmatics.

Table 3.2 Scanners and the scanning protocols used for normal, non-severe asthmatic and severe asthmatic subjects in different institutions: Center1 (UI), Center2 (PITT), and Center3 (WSL).

Imaging center	UI	PITT	WSL
Project	BRP	SARP	SARP
Scanner model	Siemens Sensation 64 slice	GE VCT 64 slice	Siemens Sensation 16 Slice
Scan type	Spiral	Helical	Spiral
Rotation time (s)	0.5	0.5	0.5
Detector configuration (channel # x mm)	64 × 0.6 mm	64 × 0.625 mm	16 × 0.75 mm
Pitch	1.0	0.984	1.5
Peak kilovoltage (kVp)	120	120	120
a) Siemens = Eff. mAs* b) GE = mA*	Effective mAs 100	mA S-145; M-180; L-270	Effective mAs 33
Dose modulation	Care Dose OFF	Auto mA OFF	Care Dose OFF
Reconstruction Algorithm	B35	Standard or Detail	B30
Lung Algorithm	None	None	None
Additional Image filters	No Selection	No Selection	No Selection
Thickness (mm)	0.75	0.625	1.0
Interval (mm)	0.5	0.5 – 0.625	0.5 – 1.0
Iterative reconstruction (noise reduction algorithm)	No Selection	No Selection	No Selection
Scan Time (s) 30cm length	< 10	< 10	< 15

Note: mA was varied for PITT protocol based on BMI size (small: BMI < 20, medium: $20 \leq BMI \leq 30$, large: BMI > 30).

Table 3.3 Terminologies and the corresponding definitions of imaging phenotypes employed in this study

Terminology	Definition
Density-threshold-based air-trapping	Air-trapping estimation with a fixed CT density (I) of empirical threshold (e.g. $I < -856$)
Fraction-threshold-based air-trapping	Air-trapping estimation with a fixed air-fraction (β_{air}): an adjusted threshold ($I_{threshold}$) for tracheal air attenuation is obtained by Equation (3-2) (e.g. $\beta_{air} > 0.9$).
U/(M+L)|v	The ratio of "air volume change in upper lobes" to "air volume change in lower and middle lobes" between TLC and FRC (Figure 3-2)
Lung shape (chest wall configuration)	The ratio of "apical-basal distance" to "ventral-dorsal distance" (i.e. the ratio of "craniocaudal distance" to "anteroposterior distance") (Figure 3-2)

Table 3.4 The means (±SEM) of HU_{air} in each center, air fractions (β_{air}) calculated with the fixed density threshold (I=-856) and tracheal HU_{air} (Equation 3-1), and adjusted thresholds by the suggested β_{air} (90%) (Equation 3-2).

	Center 1	Center 2	Center 3	ANOVA (F-test, P value)
HU_{air} (measured in trachea)	-952 (±2.0)	-934 (±2.1)	-994 (±1.3)	$< 1 \times 10^{-15}$ ΠΣΘ
β_{air} (Fixed density I=-856)	90.5%	92.1%	86.8%	-
Adjusted $I_{threshold}$ (Fixed β_{air} = 90%)	-851	-835	-889	-

Note: This table only shows the estimated difference from scanner difference. The actually adjusted threshold of each subject is determined by the respective median, not from the value listed in the table. Π indicates $P<0.05$ for Center 1 vs. Center 2; Σ indicates $P<0.05$ for Center 2 vs. Center 3; Θ indicates $P<0.05$ for Center 1 vs. Center 3.

Table 3.5 The comparison of the ratio of supine air volumes (AV) to upright PFT volumes and the ratio of supine inspiratory capacity (IC) to upright PFT in normal, non-severe asthmatic and severe asthmatic subjects

	Center1	Center2	Center3	ANOVA (F-test, P)
$AV^{TLC}(CT)$ / TLC(PFT)	83 ($\pm$1)	77 ($\pm$2)	70 ($\pm$2)	$< 1 \times 10^{-4}\,\Sigma\Theta$
$AV^{FRC}(CT)$ / FRC(PFT)	78 ($\pm$2)	63 ($\pm$2)	58 ($\pm$3)	$< 1 \times 10^{-5}\,\Pi\Theta$
IC(CT) / IC(PFT)	87 ($\pm$3)	93 ($\pm$4)	84 ($\pm$3)	$= 0.152$

Note: The values are presented as means ($\pm$SEM). In two-way ANOVA tests, HU_{air}, AV^{TLC}/TLC (PFT), AV^{FRC}/FRC (PFT) and IC/IC(PFT) were not different in between-populations, so that we performed the follow-up one-way ANOVA tests as shown in above. PFT volumes (TLC, FRC and IC) of one Center1, two Center2 and one Center3 subjects were not available, and only FRC of one Center3 subject was not available. AV and IC are air volume and inspiratory capacity, respectively. Π indicates $P<0.05$ for Center1 vs. Center2; Σ indicates $P<0.05$ for Center2 vs. Center3; Θ indicates $P<0.05$ for Center1 vs. Center3.

Table 3.6 χ^2 association tests of existing threshold-based AirT% (threshold = median of 5.31%), adjusted fraction-based AirT%, lung shape at TLC and functional ratio of air volume change U/(M+L)|v with the presence and severity of asthma

		Normal Subjects	Non-severe asthmatics	Severe asthmatics	χ^2 test (*P* value)
Existing AirT%	No air-trapping	28 (0)	24 (0)	20 (0)	0.114
	Air-trapping	22 (0)	18 (0)	32 (0)	
Adjusted AirT%	No air-trapping	33 (0)	32 (0)	14 (-)	$< 1 \times 10^{-5}$
	Non-severe air-trapping	13 (0)	4 (0)	16 (0)	
	Severe air-trapping	4 (0)	6 (0)	22 (+)	
Lung shape at TLC	Lung shape ≥ 1.4	45 (+)	30 (0)	19 (-)	$< 1 \times 10^{-7}$
	Lung shape < 1.4	5 (-)	12 (0)	33 (+)	
Ratio of air volume change	U/(M+L)|v ≤ 0.7	47 (+)	32 (0)	18 (-)	$< 1 \times 10^{-9}$
	U/(M+L)|v > 0.7	3 (-)	10 (0)	34 (+)	

Note: The values are presented as the number of subjects (sign of standardized Pearson residual). The thresholds of standardized Pearson residual are set to absolute values of 3 and 4 for 2×3 and 3×3 tables, respectively. Lung shape is defined as the apical-basal vs. ventral-dorsal distance ratio.

Table 3.7 One-way ANOVA tests with Tukey's tests for lung shape at TLC (the apical-basal vs. ventral-dorsal distance ratio), U/(M+L)|v (the air volume change in upper lobes vs. middle and lower lobes ratio)

	Normal Subjects	Non-severe asthmatics	Severe asthmatics	ANOVA (F-test, *P* value)
Lung shape at TLC	1.56 (±0.02)	1.45 (±0.02)	1.37 (±0.02)	$< 1 \times 10^{-7}$§¥*
U/(M+L)|v	0.57 (±0.01)	0.66 (±0.02)	0.80 (±0.03)	$< 1 \times 10^{-11}$ §¥*
BMI-controlled sub-group tests below				
Lung shape at TLC	1.57 (±0.02)	1.45 (±0.02)	1.42 (±0.03)	$< 1 \times 10^{-4}$ §*
U/(M+L)|v	0.56 (±0.01)	0.67 (±0.02)	0.77 (±0.03)	$< 1 \times 10^{-8}$ §¥*

Note: The values are presented as mean (±SEM). One-way ANOVA tests are performed with three populations: normal subjects, non-severe asthmatics, and severe asthmatics. § indicates $P < 0.05$ for normal subjects vs. non-severe asthmatics; ¥ indicates $P < 0.05$ for non-severe asthmatics vs. severe asthmatics; * indicates $P<0.05$ for normal subjects vs. severe asthmatics. In the BMI-controlled sub-group tests (BMI < 32, $P = 0.45$ for BMI among sub-groups), means (±SEM) of BMI in 46 normal subjects, 30 non-severe asthmatics and 27 severe asthmatics are 25.2 (±0.5), 25.6 (±0.5) and 26.3 (±0.7), respectively.
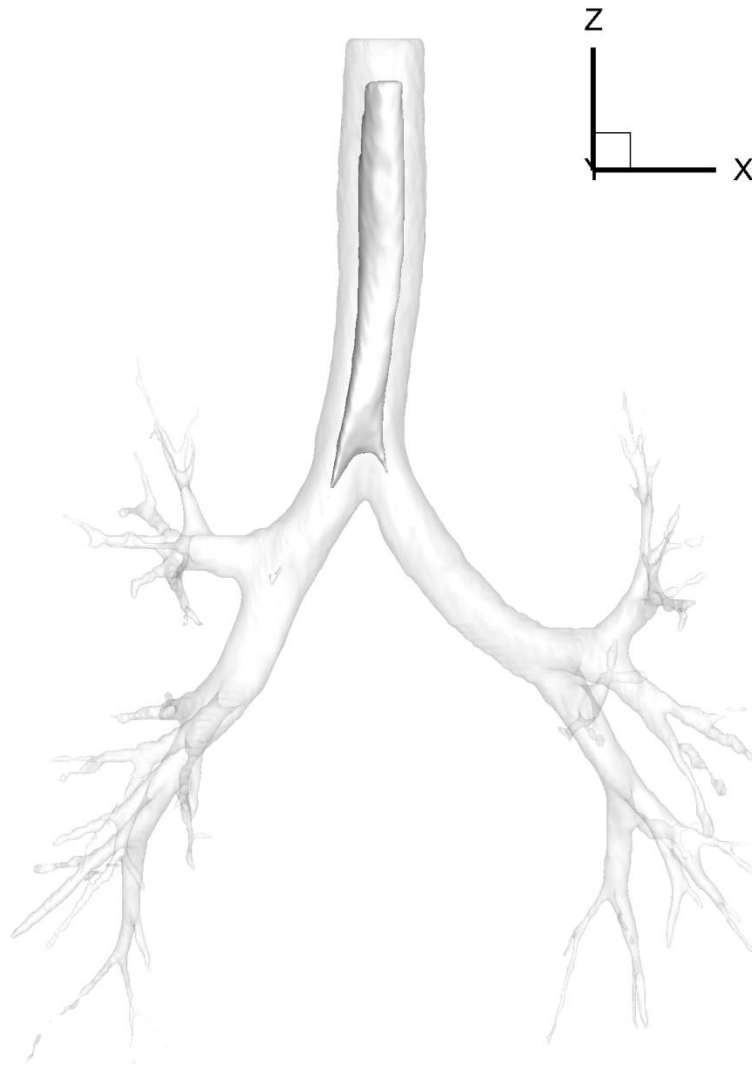
Figure 3.1 The segmented airway mask (Transparent) and eroded airway mask (Opaque). Binary filters of 6 radius are applied for the erosion.
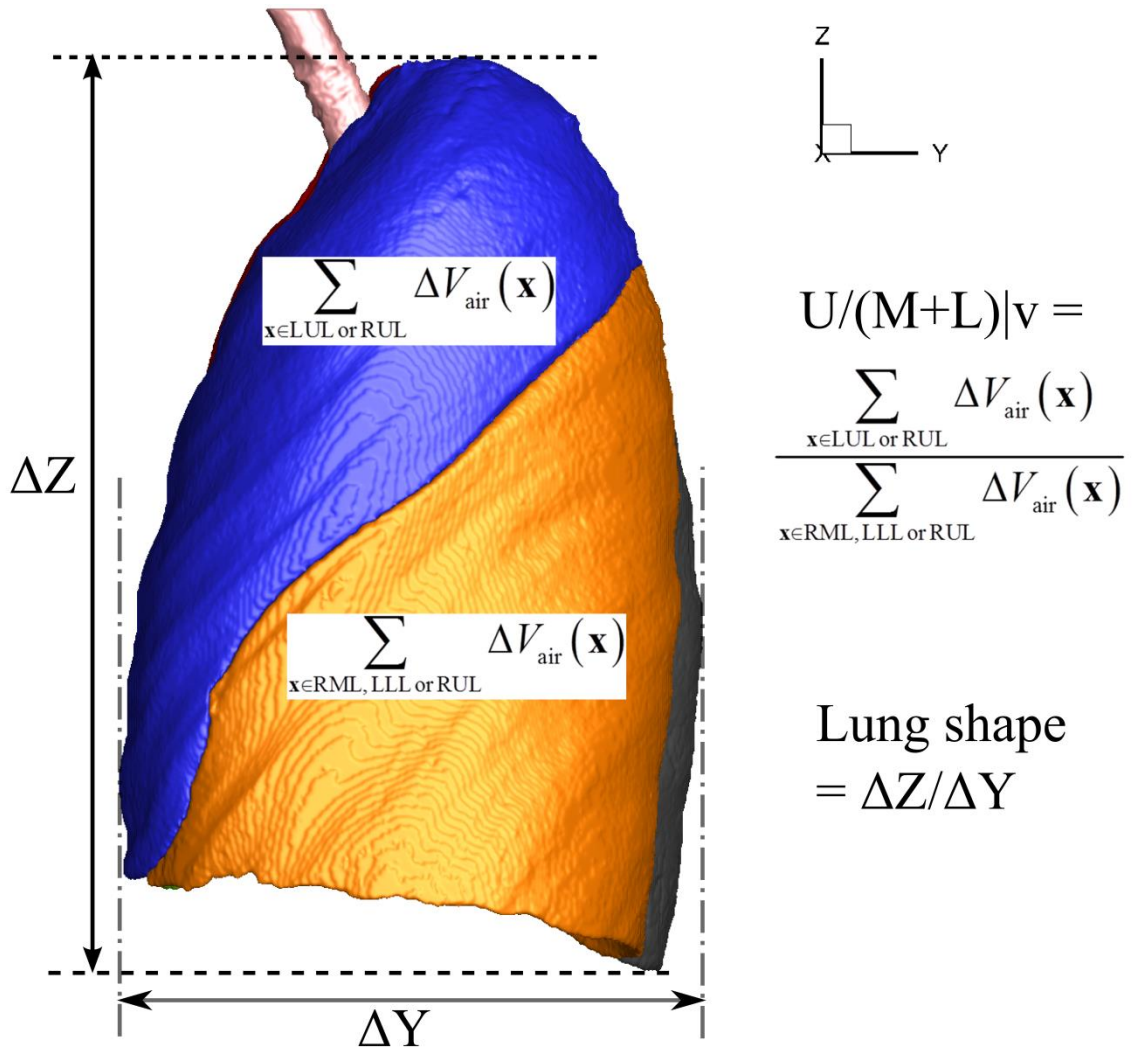
Figure 3.2 Schematics of "U/(M+L)|v" (the ratio of air-volume change in upper lobes to air-volume change in lower lobes) and "lung shape" (the ratio of apical-basal distance to ventral-dorsal distance). LUL, LLL, RUL, RML and RLL indicate left-upper-lobe, left-lower-lobe, right-upper-lobe, right-middle-lobe and right-lower-lobe, respectively.

Spirometrically-measured IC vs. CT-segmented IC
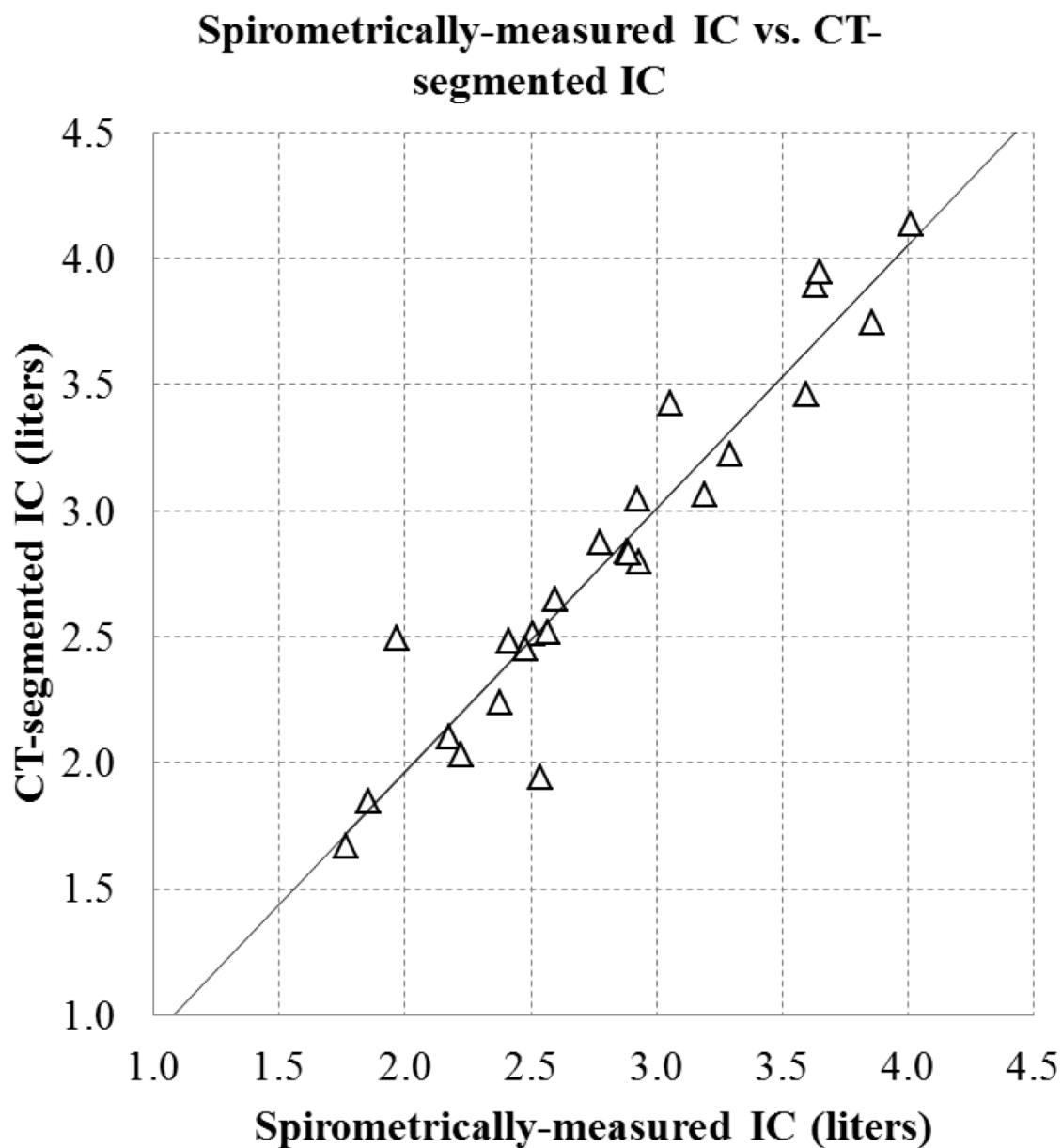
Figure 3.3 Linear regressions (Pearson $r = 0.949$, P $< 1 \times 10^{-12}$) of supine pneumotachometer-measured inspiratory capacity (IC) acquired in the pulmonary function laboratory vs. CT segmented IC. Pneumotachometer-measured IC is calculated with Equation 3-1. This data is from the Center 1.

A AV^FRC (CT) vs. Existing AirT% (Center2)

B AV^FRC (CT) vs. Existing AirT% (Center3)
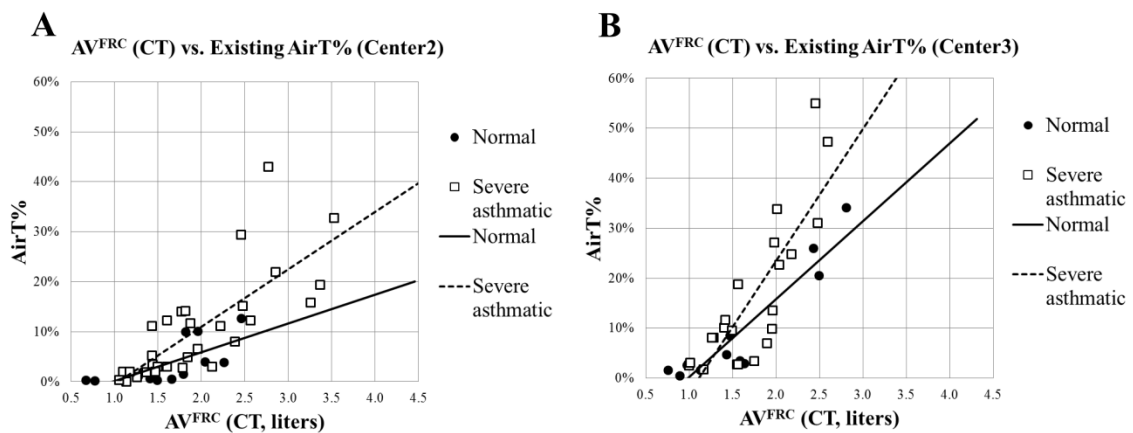
Figure 3.4 Existing density-threshold-based AirT% of A: Center 2 normal subjects vs. severe asthmatics and B: Center 3 normal subjects vs. severe asthmatics when the threshold -856 is applied.
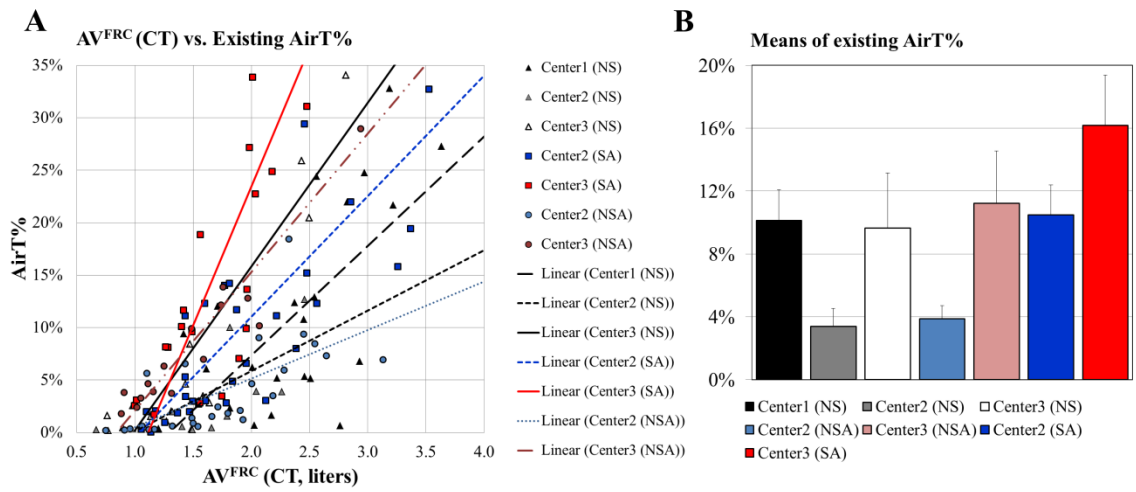
Figure 3.5 A: Linear Regressions between AV^{FRC} and existing threshold-based AirT%, B: means (±SEM) of existing AirT% on seven groups. Center 1 (NS), Center 2 (NS) and Center 3 (NS) denote normal subjects; Center 2 (NSA) and Center 3 (NSA) denote non-severe asthmatics; Center 2 (SA) and Center 3 (SA) denote severe asthmatics from respective imaging centers.
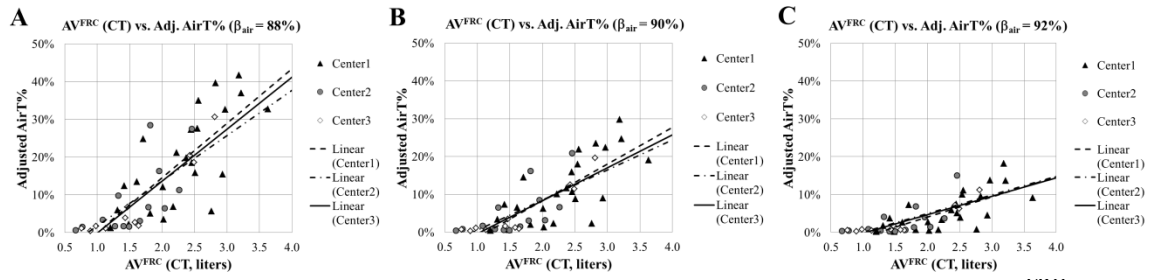
Figure 3.6 Normal subjects from the three sites: Linear regressions between AV^{FRC} and adjusted fraction-based AirT% are based on different air fractions: A, 88%; B, 90%; C, 92%.

A AV^{FRC} (CT) vs. Adjusted AirT% (β_{air} = 90%)

B Means of adjusted AirT% (β_{air} = 90%)
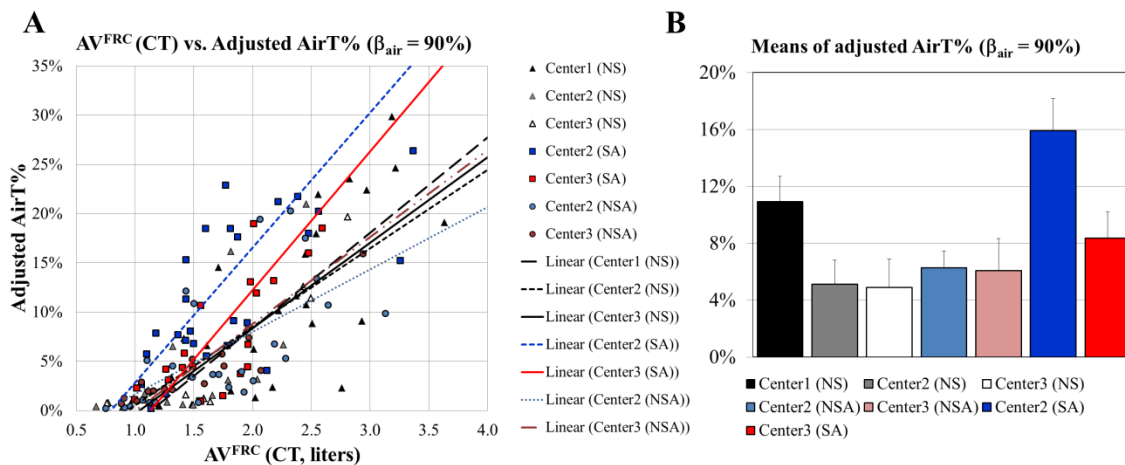
Figure 3.7 A: Linear Regressions between AV^{FRC} and adjusted fraction-based AirT%, B: means (±SEM) of adjusted AirT% on seven groups. Center 1 (NS), Center 2 (NS) and Center 3 (NS) denote normal subjects; Center 2 (NSA) and Center 3 (NSA) denote non-severe asthmatics; Center 2 (SA) and Center 3 (SA) denote severe asthmatics from respective imaging centers. Note that the severe asthmatics significantly differentiate from the non-severe asthmatics and normal subjects, but the normal subjects and non-severe asthmatics have statistically the same slopes.

AV^{FRC} (CT) vs. Adj. AirT% (β_{air} = 90%)
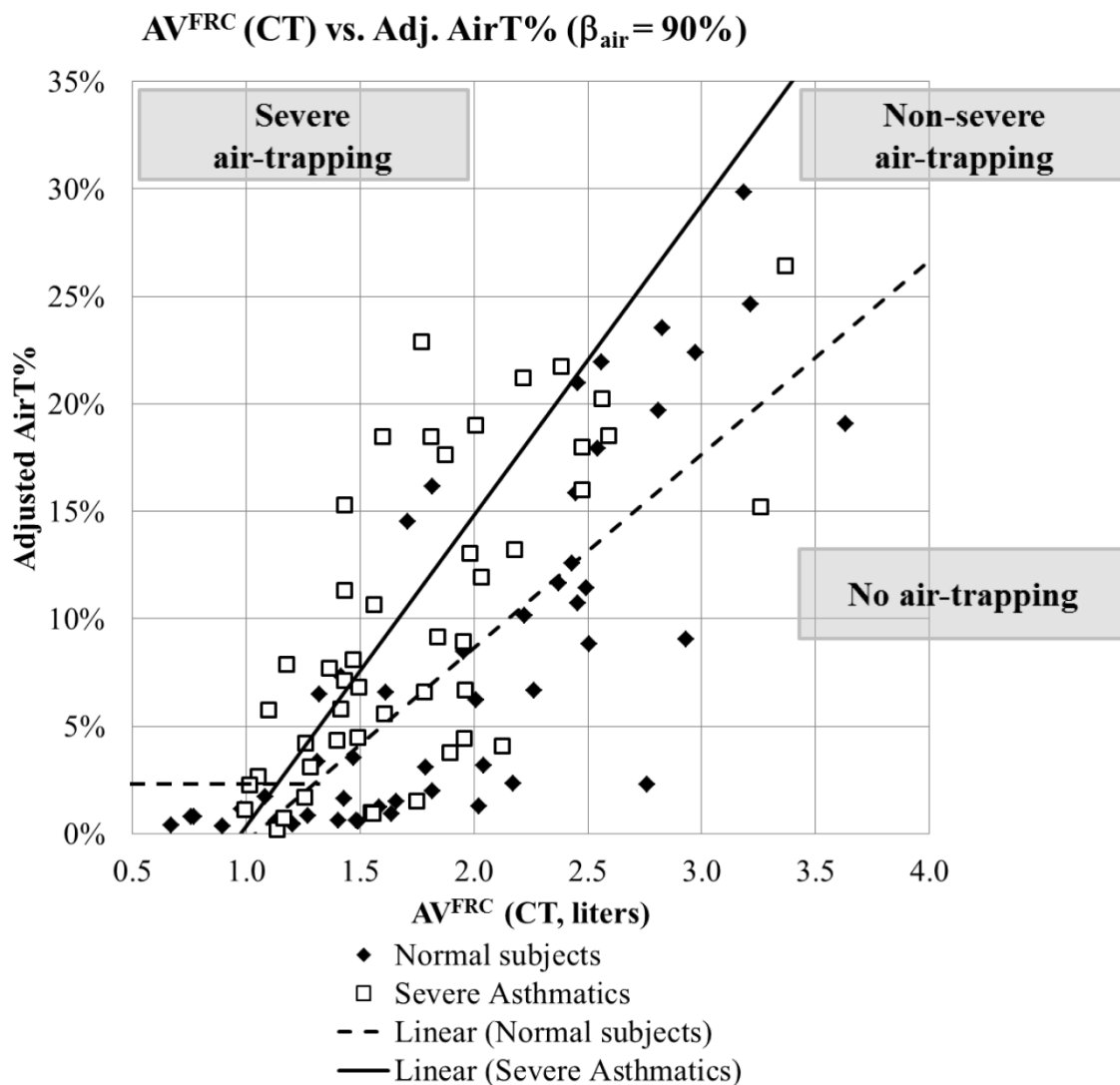
	Pearson correlation	The equations of fitted lines
Normal subjects	$r=0.792$ (P< 1×10^{-11})	AirT% (dashed) = $0.145 \times$ AV^{FRC} - 0.141
Severe asthmatics	$r=0.768$ (P< 1×10^{-10})	AirT% (Solid) = $0.09 \times$ AV^{FRC} - 0.094
T-test for 2 slopes	$P < 0.01$	

Figure 3.8 The slope-based regimes of adjusted fraction-based AirT%, obtained from linear regressions of normal subjects and severe asthmatics.

CHAPTER 4

STRUCTURAL ASSESSMENT OF AIRWAYS IN ASTHMATIC

POPULATIONS

4.1   Introduction

Asthma can be characterized by several phenotypes of airflow obstruction, bronchial hyper-responsiveness and airway inflammation [16]. The hyper-responsiveness and chronic inflammation of airways lead to the infiltration of inflammatory cells to smooth muscles and the increase of smooth muscle mass. The airway remodeling results in the increase of wall area (WA) and the decrease of luminal area (LA), associated with acute or chronic airway obstruction [7, 18, 43, 78, 80, 127, 128]. NIH-sponsored multi-center Severe Asthma Research Program (SARP) [21, 46, 79, 104, 105, 143] has acquired CT images at total lung capacity (TLC) and functional residual capacity (FRC), enabling the quantitative comparisons of bronchial dimensions among populations via large datasets.

Quantitative computed tomography (CT) has been used to evaluate WA and LA of the airways with the advantages of high resolution and noninvasiveness. Some of the imaging studies [6, 83] demonstrated significant correlations of CT-measured WA with epithelial thickness measures on the biopsy samples. However, the altered morphology of airway dimensions in the asthmatic studies remains still controversial. An early study [111] investigated the apical bronchus of right upper lobe, and reported that WA increases in asthmatics, but LA remains the same as compared with normal subjects. A large multi-center study [6] of 123 subjects sponsored by SARP demonstrated the increased WA% (WA/total area (TA)) in severe asthmatics, relative to normal and non-severe asthmatics. However, they also concluded that there is no difference in LA between normal subjects and asthmatics. In contrast, the other study [102] argued that LA

in asthmatics is smaller than that of normal subjects, but WA in asthmatics is also smaller than that of normal subjects.

Meanwhile, air-trapping is also known to be a physiological characteristic in asthmatic patients, which can be assessed by CT image at FRC level (or residual volume (RV)). Existing studies found that the air-trapping increases in asthmatics [110], and the increase of air-trapping is only prominent in severe asthmatics [15, 24] rather than normal subjects and non-severe asthmatics. A recent study [61] clustered asthmatic populations with the local changes of luminal volume (LV), wall volume (WV) of right apical bronchus and global changes of air-trapping. The study assumed that local changes of right apical bronchus are consistent with the alterations of airways in entire regions. Meanwhile, we improved existing air-trapping method with a fraction-based approach that accounts for the inter-site protocol variation [24], enabling quantitative analysis of large data sets acquired via multiple imaging centers. Furthermore, we demonstrated that reduced air volume changes of asthmatic patients are observed in mainly lower lobes, and the reduced volume changes are compensated with the increased volume change in upper lobes with the aid of image registration techniques [24, 25].

The alterations of structural and functional variables in asthmatics have been reported independently in the existing studies. Nonetheless, the link between these variables at both global and local levels [39, 45] is yet to be established to better understand their interplays that may shed light on lung pathophysiology. Accordingly, we seek to connect structural variables with PFT-based, density-based air-trapping and two image-based functional variables. This is because airflow obstruction can be potentially correlated with the morphological changes of LA, WA, circularity and bifurcation angles [82, 103, 147, 149]. In this study, we examine local structural variables of circularity and bifurcation angles as well as LA and WA that have been commonly analyzed. All of airway structural variables are normalized by $TLC^{2/3}$ or $TLC^{1/3}$ measured in PFT instead of BSA. The hydraulic diameter (D_h) representing the combined effect of non-circularity

and reduced LA is compared among normal subjects, non-severe and severe asthmatics. The D_h is further correlated with the functional quantities of PFT-based and density-based and two image-based measures.

4.2   Methods

4.2.1   Human Subject Data Sets

50 normal subjects, 42 non-severe asthmatic and 52 severe asthmatics were used for this study. Among the subjects, 25 normal subjects were acquired from a NIH bioengineering research partnership (BRP) at the University of Iowa (UI); 14 normal subjects, 26 non-severe asthmatics and 30 severe asthmatics were from SARP at the University of Pittsburgh (PITT); 11 normal subjects, 16 non-severe asthmatics and 22 severe asthmatics were from SARP at Washington University in St. Louis (WSL) [21, 46, 79, 143]. All of the subjects were used to develop a new air trapping measure in a previous study [24]. The imaging protocols for acquiring CT images at both TLC and FRC were approved by the Institutional Review Boards of respective institution. Table 4.1 shows the information regarding demography and PFTs, and Table 4.2 summarizes the scanners and protocols of respective institution. Major criteria used to define severe asthma include treatments with oral corticosteroids and high-dose inhaled corticosteroids, besides several minor criteria [104, 143].

4.2.2   Structural Variables

For the geometric analysis, we extracted averaged LA, averaged TA, averaged perimeter of LA (P_e) and 1D skeleton from airway masks (Figure 4.1) using the VIDA pulmonary software. All of the averaged values were extracted from the middle region (30% - 70%) of an airway segment by excluding the first 30% of the proximal region and

the last 30% of the distal region. The 1D airway skeleton was used to calculate bifurcation angle as follows.

$$\text{Bifurcation angle} = \cos^{-1}\left(\frac{\mathbf{d1}\cdot\mathbf{d2}}{|\mathbf{d1}||\mathbf{d2}|}\right), \tag{4-1}$$

where $\mathbf{d1}$ and $\mathbf{d2}$, $\cdot$(dot) and $||$ denote directional vectors of daughter branches, inner product of two vectors, and magnitude of the vector, respectively. In this study, the angle of a named segment (Figure 4.1) represents bifurcation angle between daughter branches of the corresponding segment. The branch of trifurcation angle is excluded in this analysis.

WA is calculated by WA=TA–LA (Figure 4.2A), and averaged luminal diameter (D_{ave}) and outer diameter (D_{outer}) are calculated by $D_{ave}=\sqrt{4\times LA/\pi}$ and $D_{outer}=\sqrt{4\times TA/\pi}$, respectively. Wall thickness (WT) is calculated by the subtraction of D_{ave} from D_{outer}. WT can have different characteristics against WA if airways are constricted (Figure 4.2B). LA (or D_{ave}) and WT are mainly employed for evaluating luminal constriction (Figure 4.3A and B) and wall thickening, respectively. In addition, circularity Cr [138] is employed to assess the degree of non-circularity because some of the asthmatic airways have elliptical cross sections (Figure 4.3C and D):

$$Cr = \frac{\text{Perimeter of an area equivalent circle}}{\text{Perimeter of a luminal area}} = \frac{\pi D_{ave}}{P_e}. \tag{4-2}$$

Figure 4.2C shows that the circularity is equal to one if luminal shape is exactly circular, whereas it decreases with increasing non-circularity.

4.2.3   Flow Parameters

Two important parameters related to pulmonary airflow and airway resistance are hydraulic diameter (D_h) and flow-driven pressure drop (Δp) as follows:

$$D_h = \frac{4 \times LA}{P_e} = \frac{Cr^2}{\pi} P_e,$$ (4-3)

$$\Delta p = \underbrace{f \frac{L}{D_h} \frac{\rho U^2}{2}}_{\text{major loss}} + \underbrace{K \frac{\rho U^2}{2}}_{\text{minor loss}},$$ (4-4)

where f, L, ρ, U and K denote frictional coefficient, length of the segment, fluid density of air, mean velocity and coefficient of minor loss, respectively. The D_h is associated with either "LA and P_e" or "Cr and P_e" (Equation 4-3). The first term on the right hand side of Equation 4-4 is major loss due to flow-driven pressure drop. It is noted that the major loss depends on D_h depending on Cr, rather than D_{ave}. In fully developed laminar flow, f is equal to $64/\text{Re}_{D_h}$, where $\text{Re}_{D_h} = UD_h/v$ and v is kinematic viscosity of the fluid [145]. Therefore, given airway length L and mean velocity U in a segment, Δp due to major loss is inversely proportional to D_h^2 in laminar flow conditions, implying the importance of D_h. Meanwhile, the second term on the right-hand side of Equation 4-4 is known as minor loss due to flow obstructions caused by airway branching structures and heterogeneous airway geometrical shapes.

4.2.4   Density and Functional Assessment

To evaluate the correlations of structural variables with functional assessment, we obtained air-trapping percentage (AirT%) with CT image at FRC level [15, 24, 110]. The AirT% is defined as the ratio of the number of air-trapped voxels to the number of voxels in the whole lung (or respective lobes). Instead of existing threshold-based method (CT

density < -856) [15, 110], we used a fraction-based method [24] employing air fraction ($\beta_{air,threshold} = 0.9$) to calculate adjusted thresholds ($I_{threshold}$) as follows:

$$I_{threshold} = \beta_{air,threshold} HU_{air} + \left(1 - \beta_{air,threshold}\right) HU_{tissue}. \tag{4-5}$$

A voxel is regarded as an air-trapped voxel if the CT density (I) is below $I_{threshold}$, and HU_{air} is extracted form tracheal density, and HU_{tissue} is set to 55.

In the previous study [24, 25], we found that air volume changes in lower lobes are reduced and those in upper lobes are elevated in severe asthmatics, as compared with normal subjects. Therefore, we employed two more variables: lobar fraction of air volume change (ΔV_{airF}) and apical-to-basal distance over ventral-to-dorsal distance (hereafter referred to as "lung shape") to correlate with structural variables such as D_h and bifurcation angle.

4.2.5 Regions of Interests (ROIs)

Based on anatomical labeling, we have chosen 36 segmental regions of interest (ROIs), as shown in Figure 4.1. The aforementioned structural variables can be classified into two types: orientation independence vs. orientation dependence. The orientation-independent variables include WA, LA, TA, WT, Cr, D_{ave} and D_h. Analysis of the orientation-independent variables allows grouping of ROIs in proximity to facilitate data analysis. Instead of analyzing six major branches as in [113, 155], we grouped relatively small segments into six subgroups to study the correlation of average "local" structural variables with "global" PFT-based and "lobar" image-based functional variables. Here, among 36 segmental ROIs, 25 relatively small segments are grouped into six subgroups of right upper lobe (sRUL), right middle lobe (sRML), right lower lobe (sRLL), left upper lobe (sLUL), left middle lobe (sLML or lingual) and left lower lobe (sLLL). They are sRUL=(RB1, RB2, RB3), sRML=(RB4+5, RB4, RB5), sRLL=(RB6, RB7, RB8,

RB9+10, RB9, RB10), sLUL=(LB1+2+3, LB1+2, LB1, LB2, LB3), sLML=(LB4+5, LB4, LB5), and sLLL=(LB6, LB8, LB9+10, LB9, LB10). Those grouped branches belong to the respective lobes as illustrated in Figure 4.1. The anatomical left upper lobe is split into sLML (lingual) and sLUL subgroups because sLML can be branched out upwards toward the upper lobe or downwards toward the lower lobe. Thus, for the analysis of orientation-independent variables, we used 17 ROIs: 11 large-segmental ROIs + 6 grouped ROIs.

On the other hand, bifurcation angle is an orientation-dependent variable, depending on the alignment of child branches, e.g. with the apical-to-basal axis, the ventral-to-dorsal axis, or the left-to-right axis. Thus, grouping of these variables is not feasible. For the analysis of orientation-dependent variables, we analyzed only 22 branches up to generation number 4 (upper lobes) or 5 (lower lobes), i.e. Trachea, RMB, TriRUL, RB1, RB2, RB3, BronInt, RLL6, RLL7, TriRLL, RB8, RB9+10, LMB, TriLUL, LB1+2+3, LB1+2, LB3, LB4+5, LLB6, TriLLB, LB8 and LB9+10.

4.2.6 Normalization

In many studies [59, 102, 130], BSA or body mass index (BMI) have been used to normalize LA and WA. However, lung volumes at TLC level are not affected by weight, but rather by gender and height based on predicted values of lung volumes [129]. CT-based TLC would not be a good parameter to normalize LA and WA because we found that protocol difference due to different centers affects measurement of lung volume [24]. Therefore, we tested the normalization schemes based on BSA and TLC (PFT) for all of the dimensional variables. Areas (LA, TA and WA) and lengths (WT, D_{ave} and D_h) are normalized by $TLC^{2/3}$ and $TLC^{1/3}$, respectively. Hereafter, the normalized quantities are denoted as LA*, TA*, WA*, WT*, D_{ave}^* and D_h^*.

The percentage of airway wall area defined as follows (see also Figure 4.2A):

$$WA\% = \frac{WA}{TA} = \frac{TA - LA}{TA} \qquad (4\text{-}6)$$

Several existing studies [6, 102] analyzed WA% instead of WA normalized by BSA or WA (not normalized), because the WA normalized by BSA or WA of asthmatics were similar or smaller. However, WA% is dependent on both LA and TA (Equation 4-6), so that an increase of WA% does not guarantee the increase of WA. Thus, caution must be taken in using WA% when evaluating airway wall thickness.

4.2.7   Statistical Analysis

Analysis-of-Variance (ANOVA) tests along with Tukey's post-hoc tests were performed for significance check. Furthermore, linear regressions and Pearson linear correlations were employed. The software R [5, 74, 117] was used for statistical analysis with significance taken at $P < 0.05$ level.

4.3   Results

4.3.1   Comparison of Normalization Schemes

In existing studies [59, 102, 130], BSA was used to normalize LA and WA because there exist some relationships between BSA and lung volume at FRC [120, 121]. However, PFT-based TLC lung volume [24] would be more appropriate for normalization of bronchial dimension than BSA [12, 58] because it depends on gender and height. We compared linear correlations of tracheal LA with BSA and $TLC^{2/3}$ in normal subjects. Figure 4.4 shows that PFT-based TLC lung volume ($r = 0.671$) is more correlated with the tracheal LA than BSA ($r = 0.489$). Therefore, in this study, we normalized all of the areas and lengths by $TLC^{2/3}$ and $TLC^{1/3}$, respectively, rather than BSA.

4.3.2   Bifurcation Angle

The overall bifurcation angles in three populations were close to ~67° (Table 4.3), exhibiting no statistical difference at global organ scale. However, ANOVA with Tukey's post-hoc tests on individual bifurcating segments reveals significant difference at local segmental level. Figure 4.5 shows that bifurcation angle of RB3 in severe asthmatics is smaller than that of normal subjects ($P < 0.05$), and the bifurcation angle of non-severe asthmatics falls between normal subjects and severe asthmatics. In addition, the bifurcation angle of LMB in non-severe asthmatics is smaller than normal subjects ($P < 0.05$) and the bifurcation angle of severe asthmatics is close to significant level ($P = 0.069$) as compared with that of normal subjects. We found that the decrease of the bifurcation angle in LMB is correlated with the decrease of lung shape (apical-basal distance to ventral-dorsal distance ratio, $r=0.26$ with $P<0.005$). Furthermore, the bifurcation angles of LB1+2 and RB1 (i.e. the most apical bronchus in respective left and right lungs) in severe asthmatics are greater than those of normal subjects, and those in non-severe asthmatics fall between normal and severe asthmatics (Figure 4.5). The greater angles of both apical bronchi of LB1+2 and RB1 are also correlated with the increase of lobar air volume change ΔV_{AirF} as $r=0.258$ ($P < 0.01$) and $r=0.353$ ($P < 1\times10^{-4}$), respectively.

4.3.3   Normalized Luminal Area, Total Area, Wall Area
         and Wall Thickness

The averaged LA*, TA* and WA* at the global organ level are not statistically different among three populations (Table 4.3), but these variables are significantly different at some ROIs (Table 4.4 and Table 4.5). Specifically, LA* of severe asthmatics decreases in the sRML, sRLL, TriLLB and sLLL as compared with normal and non-severe asthmatics, whereas it is in the similar ranges for other ROIs. Most of the regions of reduced LA* are consistent with the regions of reduced TA* (including the sRML,

sRLL, TriLLB and sLLL). In addition, we compared the existing WA% (WA/TA) with LA*. As shown in Figure 4.6, the increase of WA% is significantly correlated with the reduction of LA*. Thus, it is difficult to conclude that WA% only reflects airway wall thickening in an absolute sense, because the increase of WA% may merely reflect the decrease of LA* without changing WA (Figure 4.6). WA* of non-severe asthmatics is larger in Trachea and LMB than that of normal subjects, and that in sRLL and sLLL of non-severe asthmatics is larger than severe asthmatics. Although WT* might be equivalent to WA*, WT* can be different from WA* if airway is constricted or enlarged (Figure 4.2B). Therefore, in this study, we focused on analysis of WT* to assess wall thickening (Table 4.5) rather than WA* and WA%. Specifically, WT* of BronInt and RLL6 in severe asthmatics are larger than that of normal subjects, and WT* of sRUL and LMB in both non-severe asthmatic and severe asthmatics also increase.

4.3.4 Circularity, Normalized Averaged Diameter and Hydraulic Diameter

The overall Cr of severe asthmatics is smaller than that of normal subjects (Table 4.3), indicating that airways of severe asthmatics are likely to exhibit the shapes of Figure 4.3C and D. The decrease of circularity (i.e. increase of non-circularity) in severe asthmatics is most prominent in the ROIs of RMB, LMB, TriLLB (see Table 4.6), as compared with normal subjects. In addition, $D_{ave}*$ calculated from LA* shows clear distinction not only between normal subjects and severe asthmatics, but also between non-severe asthmatics and severe asthmatics in the RLL7, sRML, sRLL, TriLLB and sLLL, especially in the sRLL and sLLL (Table 4.7). Because D_h* depends on both circularity and $D_{ave}*$ (Equation 4-3), the difference of D_h* between normal subjects and severe asthmatics is augmented especially in the TriRLL, sRLL and sLLL, as compared with $D_{ave}*$. Furthermore, D_h plays a more important role in airway resistance than D_{ave} as expressed in Equation 4-4.

4.3.5   Correlation of Geometric Variables with Functional

Quantities

D_h is one of the major variables that determine flow-driven pressure drop

(Equation 4-4). Therefore, we performed correlation tests of D_h* with PFT-based, air-

trapping and two image-based lobar air volume changes. In severe asthmatics, FEV1 %

predicted and FEV1/FVC (measuring airflow obstruction) and RV % predicted and

RV/TLC (measuring air-trapping) show significant correlations with D_h* (Figure 4.7A).

AirT% is inversely correlated with the D_h* in the LLL, RML and RLL, suggesting that

constricted airways might be associated with the increase of air-trapping in the same

regions (Figure 4.7B). In addition, the decrease of ΔV_{airF} in the lower and middle lobes of

LLL, RLL and RML is correlated with the decrease of D_h* (Figure 4.7B), indicating that

constricted airways reduce air volume change in peripheral regions.

4.3.6   Six Subgroups vs. Six Major Branches

We grouped CT-resolved small branches belonging to each lobe into sLUL,

sLML, sLLL, sRUL, sRML and sRLL, in order to correlate structural variables with

functional variables such as PFT measurements, lobar air-volume change or AirT%. On

the other hand, existing studies [113, 155] focused on major paths such as RB1, RB4,

RB10, LB1, LB4 and LB10, so that we compared the results of current groupings with

those of five major paths. Table 4.8 shows that D_h* of major branches is consistent with

that of grouped lobes (Table 4.7), but the selected five paths could not represent other

branches in the same lobe. For instance, D_h* of RB4 and RB10 is not significantly

different between normal and severe asthmatics (Table 4.8), but the other branches in the

same lobes such as RB5, RB7 and RB9 show the significant difference between normal

subjects and severe asthmatics (Table 4.9). Thus, the selected major branches would not

reflect overall alterations of the corresponding lobes. In addition, we performed

correlation tests with PFT- and image-based functional variables (Figure 4.8). The D_h

averaged in each lobe shows much stronger correlations with PFT-based FEV1/FVC and RV % predicted values, lobar AirT% and ΔV_{airF}. The results imply that grouped variables would be more representative lobar-variables than six-major branches.

4.4   Discussions

In this study, we adopted the normalization scheme that normalizes airway structural variables of LA, TA, WA, D_{ave} and D_h by $TLC^{2/3}$ (liter$^{2/3}$) or $TLC^{1/3}$ (liter$^{1/3}$) measured in PFTs. In contrast, many existing studies used BSA or BMI for normalization to control inter-subject variability [59, 102, 130]. However, the relationships between BSA or BMI (determined by height and weight) and airway dimensions (or TLC volumes) are unclear [120, 121, 129]. Instead, it is reported that tracheal diameters are correlated with gender and height [12, 38, 58]. Since TLC predicted values are determined by gender and height [129], we employed lung volume at TLC to normalize bronchial dimensions instead of BSA. The correlations with tracheal LA in normal subjects show that PFT-based TLC volume is more appropriate than BSA to control inter-subject variability of airway dimension (Figure 4.4). It is noted that CT-based TLC lung volume is not a good normalization parameter because it is sensitive to inter-site protocol differences [24].

There exist controversies concerning the increase or decrease of LA and WA in asthmatics. Some studies [10, 102] reported the decrease of LA in asthmatics, whereas some [6, 111] reported no statistical difference between normal subjects and asthmatics. In addition, most of the studies [6, 59, 102] employed WA% for analysis, because WA or WA normalized by BSA of asthmatics are similar or decreased relative to normal subjects. However, WA% measures the net effect of alterations in LA and WA. That is, WA% could be increased with only LA reduction regardless of the increase of WA (Figure 4.6). If TA* also decrease along with LA*, it is hard to conclude that WA% reflects the mere change of WA. In addition, WA* can also behave differently with WT*

if airway size is different (Figure 4.2B). Therefore, it would be better to use WT* than WA* and WA% in assessing airway wall thickness.

WT* increases in the ROIs of BronInt, RLL6, sRUL and LMB in severe asthmatics, and it increases in the sRUL, sRLL, sLUL and sLLL of non-severe asthmatics. Both non-severe asthmatic and severe asthmatics show the increase of WT* in the sRUL including right apical bronchus (RB1). Most of the existing endobronchial biopsies were extracted from RB1, and they were compared with CT-measured WT in the same region, because it is easily identified on CT scans [56, 59, 111]. In addition, wall volume and luminal volume of RB1 were recently used to cluster asthmatic populations into luminal constriction and wall thickening [61]. However, our analysis demonstrates that alterations of wall thickness and luminal constriction are different, exhibiting heterogeneous nature. For instance, the D_{ave}* (or LA*) decreases mostly in lower-lobar regions of severe asthmatics, whereas it remains the same in other regions (Table 4.4 and Table 4.7).

In addition, we analyzed bifurcation angle because of its associations with flow structure and local air-volume change. As shown in Figure 4.5, alteration of bifurcation angle is locally observed such that the angles of LMB, RB1, RB3 and LB1+2 in asthmatics are greater or smaller than those of normal subjects. The decrease of the LMB angle in both non-severe and severe asthmatics is distinguishable from that of normal subjects. Intuitively, the spatial correlation with the "global" variable of lung shape may indicate that reduced deformation on apical-basal axis affect the decreased angle of LMB at local segmental level. In addition, only the angles in RB1 and LB1+2 in severe asthmatics are significantly greater than those of normal subjects. In fact, the branches of RB1 and LB1+2 are the most apical branches in the CT-resolved airways (Figure 4.1). Hence, the result implies that relative increase of angle in RB1 and LB1+2 would be associated with the increase of air volume change in the corresponding upper-lobar regions ($r > 0.25$ with $P < 0.01$) [25].

Furthermore, we introduced the new structural variable of circularity. In existing studies, this variable was overlooked, although a study mentioned that neglecting the effect would underestimate total resistance [147]. The circularity significantly decreases in severe asthmatics, as compared with normal subjects (Table 4.3). The non-circular shape may reflect distributions of the heterogeneous tissue or smooth muscle mass in circumference. In addition, D_h reflects the combined effect of airway constriction and non-circularity (Equation 4-3), serving as a sensitive variable in differentiating normal subjects from severe asthmatics in the ROIs of sRUL, sRLL and sLLL as compared with D_{ave}. It is noted that D_h is a key parameter in evaluating flow-driven pressure drop, because the D_h^2 is inversely proportional to the major loss (Equation 4-4). Although LA*, D_{ave}* and D_h* show similar characteristics, utilizing D_h* is more appropriate than utilizing LA* and D_{ave}* in quantitative assessment of airway narrowing, because it is directly associated with pressure drop.

We tested correlations of D_h* with different PFT-measurements, one image-based AirT% (measuring air trappings), and two image-based assessment. FEV1 % predicted values are the most strongly correlated with D_h^* in the lower-lobar regions of LLL and RLL (Figure 4.7A). Furthermore, RV % predicted values and AirT% are also significantly correlated with D_h*, especially in the middle- and lower-lobar regions (Figure 4.7). Therefore, the constricted airway geometries detected at TLC image might be associated with the residual air at lung volume close to RV level. Furthermore, the decrease of air volume change in lower lobes is associated with the decrease of D_h^*, implying that constricted airways reduce air volume change in the peripheral regions (Figure 4.7B).

Non-severe and severe asthmatics are statistically characterized by wall thickness without luminal constriction and wall thickness with luminal constriction, respectively, but not all subjects exhibit the same tendency inside the respective groups. A recent study [61] with 30 normal, 17 non-severe and 48 severe asthmatics performed imaging-

phenotype-based cluster analysis. They grouped asthmatics into three clusters, i.e. 1) severe air-trapping with wall thickening and luminal dilation (11 asthmatics), 2) moderate air-trapping (34 asthmatics), and 3) severe air-trapping and luminal constriction (17 asthmatics). Their severe asthmatics were mostly grouped into cluster 1 and cluster 3, and non-severe asthmatics were largely grouped into cluster 2. However, they only focused on luminal volume and wall volume of RB1 and global air-trapping, but we found that constriction is locally observed in lower-lobar regions of severe asthmatics, and wall thickness locally increases in both non-severe and severe asthmatics, indicating regional heterogeneous nature of variable alterations. Therefore, it is desirable to perform more comprehensive cluster analysis including air-trapping, lobar distribution of air-volume change, lung shape at TLC, regional wall thickness and hydraulic diameter and the representative bifurcation angles, e.g. at LMB, RB1, LB1+2. The imaging cluster analysis can be further associated with clinical phenotypes such as allergy, onset of asthma and FEV1 [79].

In conclusion, we demonstrated that LA* is smaller in severe asthmatics and that the reduction of LA is mainly observed in the lower-lobar segment. In addition, only WT* increases in some local regions of both non-severe and severe asthmatics. With regard to three different populations (i.e. normal subjects, non-severe and severe asthmatics), severe asthmatics are characterized by chronic luminal constriction (reduced D_h*), whereas both non-severe asthmatics and severe asthmatics are characterized by the elevated wall thickness (increased WT*) (Table 4.3). In addition, we found that bifurcation angles in asthmatics are locally different from those of normal subjects, and local alterations of bifurcation angle at TLC are associated with the lung shape at TLC and lobar air-volume change between TLC and FRC. The circularity is also significantly decreased in severe asthmatics as compared with normal subjects. The reduced D_h^* would contribute to the increase of airflow pressure drop, resulting in airway resistance. It is

also found that the D_h^* observed at TLC level are correlated with PFT-based FEV1 and RV, and CT-based AirT% at FRC and two-image based functional variables (ΔV_{airF}).

Table 4.1 Demographic and PFT information for 50 normal, 42 non-severe asthmatic and 52 severe asthmatic subjects

	Normal Subjects	Non-severe asthmatics	Severe asthmatics	ANOVA (*F*-test, *P* value)
Subjects, No.	50	42	52	-
Age, year	38.6 (±2.0)	33.7 (±1.5)	43.6 (±1.7)	< 0.001 ¥
BMI	26.3 (±0.8)	29.5 (±1.2)	32.9 (±1.3)	< 0.001 *
Asthma duration	-	19.2 (±1.9)	26.1 (±2.2)	< 0.05 ¥
Gender, No. (% Female)	31 (62%)	27 (64%)	36 (69%)	= 0.74
Race, No. (White non-hispanic/ African American/Other)	42/3/5 (84/6/10%)	28/9/5 (67/21/12%)	32/14/6 (62/27/12%)	-
TLC % predicted	102 (±2)	94 (±2)	104 (±3)	< 0.05 ¥
FRC % predicted	96 (±3)	89 (±3)	107 (±5)	< 0.05 ¥
RV % predicted	105 (±3)	101 (±4)	145 (±8)	$< 1 \times 10^{-7}$ ¥*
RV/TLC × 100	31 (±1)	31 (±1)	44 (±1)	$< 1 \times 10^{-13}$ ¥*
FVC % predicted	99 (±2)	89 (±2)	72 (±2)	$< 1 \times 10^{-13}$ §¥*
FEV$_1$ % predicted	101 (±2)	80 (±3)	57 (±3)	$< 1 \times 10^{-15}$ §¥*
FEV$_1$/FVC × 100	83 (±1)	74 (±2)	63 (±2)	$< 1 \times 10^{-15}$ §¥*

Note: The values are presented as means (±SEM). TLC, FRC and RV of 2 normal, 1 non-severe asthmatic and 1 severe asthmatic subjects were not available and only FRC of 1 non-severe asthmatic was not available. ANOVA tests with Tukey's post-hoc tests were performed for "populations: normal subjects vs. non-severe asthmatics vs. severe asthmatics". § indicates *P*<0.05 for normal subjects vs. non-severe asthmatics; ¥ indicates *P*<0.05 for non-severe asthmatics vs. severe asthmatics; * indicates *P*<0.05 for normal subjects vs. severe asthmatics.

Table 4.2 Scanners and the scanning protocols used for normal and severe asthmatic subjects in different institutions: UI, PITT, and WSL

Imaging center	UI	PITT	WSL
Project	BRP	SARP	SARP
Scanner model	Siemens Sensation 64 slice	GE VCT 64 slice	Siemens Sensation 16 Slice
Scan type	Spiral	Helical	Spiral
Rotation time (s)	0.5	0.5	0.5
Detector configuration (channel # x mm)	64 × 0.6 mm	64 × 0.625 mm	16 x 0.75 mm
Pitch	1.0	0.984	1.5
Peak kilovoltage (kVp)	120	120	120
a) Siemens = Eff. mAs* b) GE = mA*	Effective mAs 100	mA S-145; M-180; L-270	Effective mAs 33
Dose modulation	Care Dose OFF	Auto mA OFF	Care Dose OFF
Reconstruction Algorithm	B35	Standard or Detail	B30
Lung Algorithm	None	None	None
Additional Image filters	No Selection	No Selection	No Selection
Thickness (mm)	0.75	0.625	1.0
Interval (mm)	0.5	0.5 – 0.625	0.5 – 1.0
Iterative reconstruction (noise reduction algorithm)	No Selection	No Selection	No Selection
Scan Time (s) 30cm length	< 10	< 10	< 15

Note: mA was varied for PITT protocol based on BMI size (small: BMI < 20, medium: $20 \leq BMI \leq 30$, large: BMI > 30).

Table 4.3 ANOVA with Tukey's post-hoc tests of structural variables among normal subjects, non-severe and severe asthmatics in entire regions

	Normal subjects	Non-severe asthmatics	Severe asthmatics	ANOVA (*F*-test, *P* value)
Bifurcation angle	66.7 ($\pm$0.55)	66.7 ($\pm$0.58)	67.7 ($\pm$0.53)	0.379
Circularity	0.962 ($\pm$0.001)	0.961 ($\pm$0.001)	0.958 ($\pm$0.001)	< 0.01 *
LA* ($\times 10^4$)	15.03 ($\pm$0.35)	15.20 ($\pm$0.41)	14.25 ($\pm$0.37)	0.1713
TA* $\times 10^4$)	29.87 ($\pm$0.57)	30.67 ($\pm$0.66)	29.08 ($\pm$0.59)	0.1836
WA* ($\times 10^4$)	14.85 ($\pm$0.22)	15.50 ($\pm$0.26)	14.83 ($\pm$0.23)	0.0781
WT* ($\times 100$)	1.810 ($\pm$0.008)	1.876 ($\pm$0.009)	1.857 ($\pm$0.008)	$< 1 \times 10^{-6}$ §*
D_{ave}* ($\times 100$)	4.020 ($\pm$0.042)	4.000 ($\pm$0.048)	3.833 ($\pm$0.044)	< 0.005 ¥*
D_h* ($\times 100$)	3.857 ($\pm$0.040)	3.841 ($\pm$0.046)	3.674 ($\pm$0.042)	< 0.005 ¥*

Note: The values are presented as means ($\pm$SEM). § indicates *P*<0.05 for normal subjects vs. non-severe asthmatics; ¥ indicates *P*<0.05 for non-severe asthmatics vs. severe asthmatics; * indicates *P*<0.05 for normal subjects vs. severe asthmatics.

Table 4.4 ANOVA with Tukey's post-hoc tests of luminal area (LA*), total area (TA*) normalized by $TLC^{2/3}$ ($liter^{2/3}$) among normal subjects, non-severe and severe asthmatics in each ROI

17 ROI	LA* ($\times 10^4$)				TA* ($\times 10^4$)			
	Normal subjects	Non-severe asthmatics	Severe asthmatics	ANOVA (F-test, P value)	Normal subjects	Non-severe asthmatics	Severe asthmatics	ANOVA (F-test, P value)
Trachea	69.1 (±1.7)	76.0 (±2.5)	74.8 (±2.3)	0.066	116.2 (±2.5)	127.3 (±3.5)	124.7 (±3.3)	< 0.05 §
RMB	50.1 (±1.3)	53.2 (±1.6)	50.1 (±1.6)	0.254	86.4 (±2.3)	93.2 (±2.9)	86.1 (±2.6)	0.110
TriRUL	22.9 (±0.9)	23.7 (±1.7)	20.9 (±1.1)	0.236	43.2 (±1.6)	44.7 (±2.7)	41.0 (±1.7)	0.412
BronInt	29.8 (±0.8)	31.6 (±1.0)	31.3 (±0.9)	0.349	52.7 (±1.3)	55.8 (±1.5)	55.8 (±1.4)	0.187
RLL6	26.4 (±1.5)	26.5 (±1.4)	26.9 (±2.1)	0.978	46.5 (±2.2)	47.4 (±2.0)	48.9 (±3.0)	0.782
RLL7	18.2 (±0.7)	18.3 (±0.7)	16.0 (±0.8)	0.050	35.5 (±1.1)	36.5 (±1.3)	32.5 (±1.2)	< 0.05 ¥
TriRLL	14.5 (±0.6)	14.9 (±0.9)	12.7 (±0.6)	0.069	29.5 (±1.0)	30.7 (±1.4)	27.4 (±1.0)	0.100
sRUL	7.8 (±0.3)	7.5 (±0.3)	7.0 (±0.3)	0.178	18.3 (±0.5)	18.3 (±0.6)	17.6 (±0.5)	0.510
sRML	7.8 (±0.3)	7.8 (±0.4)	6.5 (±0.3)	< 0.01 ¥*	18.3 (±0.6)	18.7 (±0.7)	16.6 (±0.5)	< 0.05 ¥
sRLL	8.0 (±0.3)	7.6 (±0.3)	6.8 (±0.2)	< 0.01 *	18.5 (±0.4)	18.2 (±0.5)	16.7 (±0.4)	< 0.01 *
LMB	31.6 (±1.0)	34.1 (±1.2)	33.5 (±1.0)	0.235	55.3 (±1.7)	61.6 (±2.1)	60.0 (±1.7)	< 0.05
TriLUL	25.8 (±1.8)	24.1 (±1.4)	23.8 (±1.1)	0.581	49.1 (±3.1)	46.9 (±2.2)	46.2 (±1.8)	0.680
LLB6	24.0 (±1.0)	25.3 (±1.4)	23.9 (±1.6)	0.732	45.6 (±1.9)	48.4 (±2.2)	45.5 (±2.6)	0.612
TriLLB	17.0 (±0.5)	16.7 (±0.6)	14.5 (±0.7)	< 0.01 ¥*	33.7 (±0.9)	33.6 (±1.0)	30.4 (±1.1)	<0.05
sLUL	7.7 (±0.3)	8.1 (±0.4)	7.3 (±0.3)	0.268	17.9 (±0.6)	19.0 (±0.7)	17.7 (±0.6)	0.301
sLML	8.4 (±0.6)	6.8 (±0.3)	7.2 (±0.5)	0.074	18.8 (±1.0)	16.7 (±0.7)	17.3 (±0.8)	0.203
sLLL	10.3 (±0.4)	9.8 (±0.3)	8.2 (±0.3)	$< 1 \times 10^{-5}$ ¥*	22.5 (±0.6)	22.3 (±0.5)	19.6 (±0.5)	$< 1 \times 10^{-4}$ ¥*

Note: The values are presented as means (±SEM). § indicates $P<0.05$ for normal subjects vs. non-severe asthmatics; ¥ indicates $P<0.05$ for non-severe asthmatics vs. severe asthmatics; * indicates $P<0.05$ for normal subjects vs. severe asthmatics.

Table 4.5 ANOVA with Tukey's post-hoc tests of wall area (WA*) normalized by $TLC^{2/3}$ ($liter^{2/3}$) and wall thickness (WT*) normalized by $TLC^{1/3}$ ($liter^{1/3}$) among normal subjects, non-severe and severe asthmatics in each ROI

17 ROI	WA* ($\times 10^4$)				WT* ($\times 10^4$)			
	Normal subjects	Non-severe asthmatics	Severe asthmatics	ANOVA (F-test, P value)	Normal subjects	Non-severe asthmatics	Severe asthmatics	ANOVA (F-test, P value)
Trachea	47.0 (±0.9)	51.3 (±1.1)	49.9 (±1.2)	< 0.05 §	2.78 (±0.03)	2.90 (±0.03)	2.84 (±0.04)	0.092
RMB	36.3 (±1.1)	40.0 (±1.4)	36.0 (±1.1)	0.052	2.49 (±0.05)	2.64 (±0.06)	2.48 (±0.04)	0.053
TriRUL	20.3 (±0.7)	21.0 (±1.1)	20.1 (±0.7)	0.712	2.01 (±0.04)	2.05 (±0.04)	2.07 (±0.03)	0.496
BronInt	22.8 (±0.5)	24.3 (±0.6)	24.6 (±0.6)	0.073	2.02 (±0.03)	2.09 (±0.03)	2.12 (±0.03)	< 0.05 *
RLL 6	20.0 (±0.8)	20.9 (±0.7)	22.0 (±1.0)	0.240	1.91 (±0.04)	1.97 (±0.03)	2.06 (±0.03)	< 0.01 *
RLL7	17.3 (±0.5)	18.3 (±0.6)	16.5 (±0.5)	0.050	1.92 (±0.03)	1.99 (±0.03)	1.93 (±0.02)	0.154
TriRLL	15.0 (±0.4)	15.8 (±0.5)	14.7 (±0.4)	0.174	1.83 (±0.03)	1.91 (±0.02)	1.89 (±0.02)	0.107
sRUL	10.6 (±0.2)	10.8 (±0.3)	10.6 (±0.2)	0.711	1.69 (±0.01)	1.75 (±0.02)	1.75 (±0.02)	< 0.01 §*
sRML	10.5 (±0.3)	10.9 (±0.3)	10.1 (±0.3)	0.113	1.68 (±0.02)	1.74 (±0.02)	1.72 (±0.02)	0.101
sRLL	10.5 (±0.2)	10.6 (±0.2)	10.0 (±0.2)	< 0.05 ¥	1.67 (±0.01)	1.72 (±0.01)	1.69 (±0.01)	< 0.05 §
LMB	23.7 (±0.8)	27.5 (±1.0)	26.5 (±0.8)	< 0.01 §	2.04 (±0.04)	2.26 (±0.05)	2.20 (±0.04)	< 0.001 §*
TriLUL	23.3 (±1.4)	22.8 (±1.0)	22.3 (±0.8)	0.829	2.15 (±0.07)	2.18 (±0.05)	2.16 (±0.04)	0.903
LLB6	21.5 (±0.9)	23.0 (±0.9)	21.6 (±1.0)	0.476	2.07 (±0.05)	2.17 (±0.04)	2.10 (±0.04)	0.294
TriLLB	16.7 (±0.4)	16.9 (±0.4)	15.9 (±0.5)	0.242	1.90 (±0.03)	1.94 (±0.02)	1.93 (±0.03)	0.513
sLUL	10.2 (±0.3)	10.9 (±0.3)	10.4 (±0.3)	0.246	1.65 (±0.02)	1.72 (±0.02)	1.70 (±0.02)	< 0.05 §
sLML	10.4 (±0.4)	9.9 (±0.3)	10.1 (±0.3)	0.581	1.64 (±0.02)	1.67 (±0.02)	1.68 (±0.02)	0.380
sLLL	12.2 (±0.2)	12.6 (±0.2)	11.4 (±0.2)	< 0.001 ¥*	1.75 (±0.01)	1.82 (±0.01)	1.78 (±0.01)	< 0.001 §

Note: The values are presented as means (±SEM). § indicates $P<0.05$ for normal subjects vs. non-severe asthmatics; ¥ indicates $P<0.05$ for non-severe asthmatics vs. severe asthmatics; * indicates $P<0.05$ for normal subjects vs. severe asthmatics.

Table 4.6 ANOVA with Tukey's post-hoc tests of circularity among normal subjects, non-severe asthmatics and severe asthmatics in each ROI

17 ROI	Circularity			
	Normal subjects	Non-severe asthmatics	Severe asthmatics	ANOVA (F-test, P value)
Trachea	0.985 (±0.001)	0.985 (±0.001)	0.982 (±0.001)	0.101
RMB	0.971 (±0.002)	0.967 (±0.002)	0.958 (±0.003)	< 0.001 ¥*
TriRUL	0.940 (±0.004)	0.942 (±0.006)	0.943 (±0.004)	0.852
BronInt	0.956 (±0.002)	0.961 (±0.002)	0.958 (±0.002)	0.326
RLL 6	0.916 (±0.010)	0.931 (±0.009)	0.929 (±0.009)	0.462
RLL7	0.968 (±0.006)	0.973 (±0.005)	0.966 (±0.006)	0.717
TriRLL	0.968 (±0.005)	0.959 (±0.009)	0.965 (±0.003)	0.586
sRUL	0.970 (±0.002)	0.962 (±0.003)	0.964 (±0.002)	0.086
sRML	0.968 (±0.002)	0.966 (±0.002)	0.962 (±0.002)	0.065
sRLL	0.963 (±0.002)	0.962 (±0.002)	0.957 (±0.002)	0.059
LMB	0.977 (±0.001)	0.974 (±0.001)	0.973 (±0.001)	< 0.05 *
TriLUL	0.933 (±0.009)	0.954 (±0.006)	0.954 (±0.007)	0.069
LLB6	0.960 (±0.005)	0.943 (±0.007)	0.950 (±0.006)	0.178
TriLLB	0.982 (±0.001)	0.978 (±0.003)	0.973 (±0.003)	< 0.05 *
sLUL	0.960 (±0.002)	0.955 (±0.003)	0.957 (±0.002)	0.394
sLML	0.957 (±0.003)	0.962 (±0.002)	0.954 (±0.003)	0.227
sLLL	0.959 (±0.002)	0.961 (±0.002)	0.954 (±0.002)	0.066

Note: The values are presented as means (±SEM). § indicates $P<0.05$ for normal subjects vs. non-severe asthmatics; ¥ indicates $P<0.05$ for non-severe asthmatics vs. severe asthmatics; * indicates $P<0.05$ for normal subjects vs. severe asthmatics.

Table 4.7 ANOVA with Tukey's post-hoc tests of averaged diameter (D_{ave}*) and hydraulic diameter (D_h*) normalized by $TLC^{1/3}$ ($liter^{1/3}$) between normal subjects, non-severe and severe asthmatics in each ROI

17 ROI	D_{ave}* ($\times$ 100)				D_h* ($\times$ 100)			
	Normal subjects	Non-severe asthmatics	Severe asthmatics	ANOVA (*F*-test, *P* value)	Normal subjects	Non-severe asthmatics	Severe asthmatics	ANOVA (*F*-test, *P* value)
Trachea	9.35 (±0.12)	9.79 (±0.16)	9.70 (±0.15)	0.078	9.21 (±0.12)	9.64 (±0.16)	9.53 (±0.15)	0.096
RMB	7.96 (±0.10)	8.20 (±0.12)	7.94 (±0.13)	0.239	7.73 (±0.10)	7.92 (±0.11)	7.60 (±0.12)	0.144
TriRUL	5.36 (±0.11)	5.41 (±0.16)	5.08 (±0.12)	0.157	5.03 (±0.10)	5.08 (±0.12)	4.79 (±0.12)	0.150
BronInt	6.14 (±0.08)	6.31 (±0.09)	6.27 (±0.09)	0.371	5.87 (±0.08)	6.07 (±0.09)	6.01 (±0.09)	0.268
RLL 6	5.70 (±0.16)	5.73 (±0.15)	5.68 (±0.20)	0.982	5.15 (±0.11)	5.31 (±0.12)	5.21 (±0.15)	0.681
RLL7	4.77 (±0.09)	4.79 (±0.09)	4.44 (±0.11)	< 0.05 ¥*	4.60 (±0.08)	4.65 (±0.08)	4.29 (±0.11)	< 0.05 ¥*
TriRLL	4.26 (±0.09)	4.29 (±0.11)	3.97 (±0.09)	< 0.05	4.11 (±0.07)	4.08 (±0.07)	3.83 (±0.08)	< 0.05 *
sRUL	3.10 (±0.05)	3.02 (±0.06)	2.93 (±0.05)	0.063	3.00 (±0.04)	2.90 (±0.05)	2.82 (±0.05)	< 0.05 *
sRML	3.06 (±0.06)	3.06 (±0.07)	2.79 (±0.06)	< 0.01 ¥*	2.96 (±0.06)	2.96 (±0.07)	2.69 (±0.06)	< 0.01 ¥*
sRLL	3.11 (±0.04)	3.01 (±0.05)	2.82 (±0.05)	< 1×10^{-4} ¥*	2.99 (±0.04)	2.89 (±0.04)	2.70 (±0.04)	< 1×10^{-5} ¥*
LMB	6.31 (±0.09)	6.55 (±0.11)	6.49 (±0.10)	0.228	6.17 (±0.09)	6.38 (±0.11)	6.31 (±0.10)	0.322
TriLUL	5.61 (±0.17)	5.48 (±0.13)	5.44 (±0.12)	0.688	5.19 (±0.12)	5.21 (±0.10)	5.17 (±0.10)	0.972
LLB6	5.48 (±0.11)	5.61 (±0.14)	5.39 (±0.16)	0.557	5.24 (±0.08)	5.28 (±0.11)	5.09 (±0.13)	0.455
TriLLB	4.62 (±0.08)	4.58 (±0.08)	4.24 (±0.10)	< 0.01 ¥*	4.54 (±0.08)	4.48 (±0.08)	4.13 (±0.10)	< 0.01 ¥*
sLUL	3.01 (±0.06)	3.03 (±0.08)	2.89 (±0.06)	0.261	2.89 (±0.06)	2.89 (±0.07)	2.77 (±0.06)	0.297
sLML	3.07 (±0.09)	2.85 (±0.07)	2.86 (±0.08)	0.088	2.93 (±0.08)	2.74 (±0.07)	2.73 (±0.07)	0.110
sLLL	3.52 (±0.05)	3.45 (±0.05)	3.14 (±0.05)	< 1×10^{-6} ¥*	3.36 (±0.05)	3.31 (±0.05)	3.00 (±0.05)	< 1×10^{-7} ¥*

Note: The values are presented as means (±SEM). § indicates $P<0.05$ for normal subjects vs. non-severe asthmatics; ¥ indicates $P<0.05$ for non-severe asthmatics vs. severe asthmatics; * indicates $P<0.05$ for normal subjects vs. severe asthmatics.

Table 4.8 ANOVA with Tukey's post-hoc tests of hydraulic diameter (D_h*) normalized by $TLC^{1/3}$ (liter$^{1/3}$) among normal subjects, non-severe and severe asthmatics in major six branches (RB1, RB4, RB10, LB1, LB4 and LB10)

D_h* ($\times$ 100) 6 major paths		Normal subjects	Non-severe asthmatics	Severe asthmatics	ANOVA (P value)
sRUL	RB1	2.88 ($\pm$0.06)	2.73 ($\pm$0.07)	2.75 ($\pm$0.09)	0.355
sRML	RB4	2.51 ($\pm$0.05)	2.43 ($\pm$0.07)	2.30 ($\pm$0.08)	0.08
sRLL	RB10	2.99 ($\pm$0.06)	2.84 ($\pm$0.07)	2.76 ($\pm$0.08)	0.097
sLUL	LB1	2.42 ($\pm$0.05)	2.27 ($\pm$0.08)	2.36 ($\pm$0.07)	0.336
sLML	LB4	2.57 ($\pm$0.08)	2.33 ($\pm$0.07)	2.32 ($\pm$0.07)	< 0.05
sLLL	LB10	3.12 ($\pm$0.07)	3.21 ($\pm$0.07)	2.87 ($\pm$0.09)	< 0.01 ¥

Note: The values are presented as means ($\pm$SEM). § indicates $P<0.05$ for normal subjects vs. non-severe asthmatics; ¥ indicates $P<0.05$ for non-severe asthmatics vs. severe asthmatics; * indicates $P<0.05$ for normal subjects vs. severe asthmatics.

Table 4.9 ANOVA with Tukey's post-hoc tests of hydraulic diameter (D_h*) normalized by $TLC^{1/3}$ ($liter^{1/3}$) among normal subjects, non-severe and severe asthmatics in excluded branches from 6 major paths

D_h* ($\times$ 100) Excluded branches from 6 major paths		Normal subjects	Non-severe asthmatics	Severe asthmatics	ANOVA (P value)
sRUL	RB2	2.85 ($\pm$0.06)	2.66 ($\pm$0.06)	2.67 ($\pm$0.07)	0.074
	RB3	3.27 ($\pm$0.08)	3.31 ($\pm$0.09)	3.04 ($\pm$0.07)	< 0.05
sRML	RB5	2.74 ($\pm$0.09)	2.73 ($\pm$0.09)	2.46 ($\pm$0.07)	< 0.05 *
sRLL	RB6	3.33 ($\pm$0.11)	3.22 ($\pm$0.12)	3.13 ($\pm$0.13)	0.490
	RB7	2.54 ($\pm$0.08)	2.43 ($\pm$0.11)	2.20 ($\pm$0.07)	< 0.05 *
	RB8	2.78 ($\pm$0.05)	2.84 ($\pm$0.07)	2.58 ($\pm$0.08)	< 0.05 ¥
	RB9	2.63 ($\pm$0.07)	2.51 ($\pm$0.07)	2.29 ($\pm$0.07)	< 0.01 *
sLUL	LB2	1.97 ($\pm$0.05)	2.00 ($\pm$0.08)	1.92 ($\pm$0.07)	0.700
	LB3	2.97 ($\pm$0.07)	2.98 ($\pm$0.11)	2.80 ($\pm$0.09)	0.292
sLML	LB5	2.32 ($\pm$0.07)	2.33 ($\pm$0.06)	2.25 ($\pm$0.08)	0.709
sLLL	LB6	3.67 ($\pm$0.06)	3.51 ($\pm$0.08)	3.23 ($\pm$0.09)	< 0.001 *¥
	LB8	3.11 ($\pm$0.09)	3.08 ($\pm$0.09)	2.76 ($\pm$0.09)	< 0.05 *¥
	LB9	2.84 ($\pm$0.06)	2.75 ($\pm$0.07)	2.51 ($\pm$0.08)	< 0.01 *

Note: The values are presented as means ($\pm$SEM). § indicates $P<0.05$ for normal subjects vs. non-severe asthmatics; ¥ indicates $P<0.05$ for non-severe asthmatics vs. severe asthmatics; * indicates $P<0.05$ for normal subjects vs. severe asthmatics.
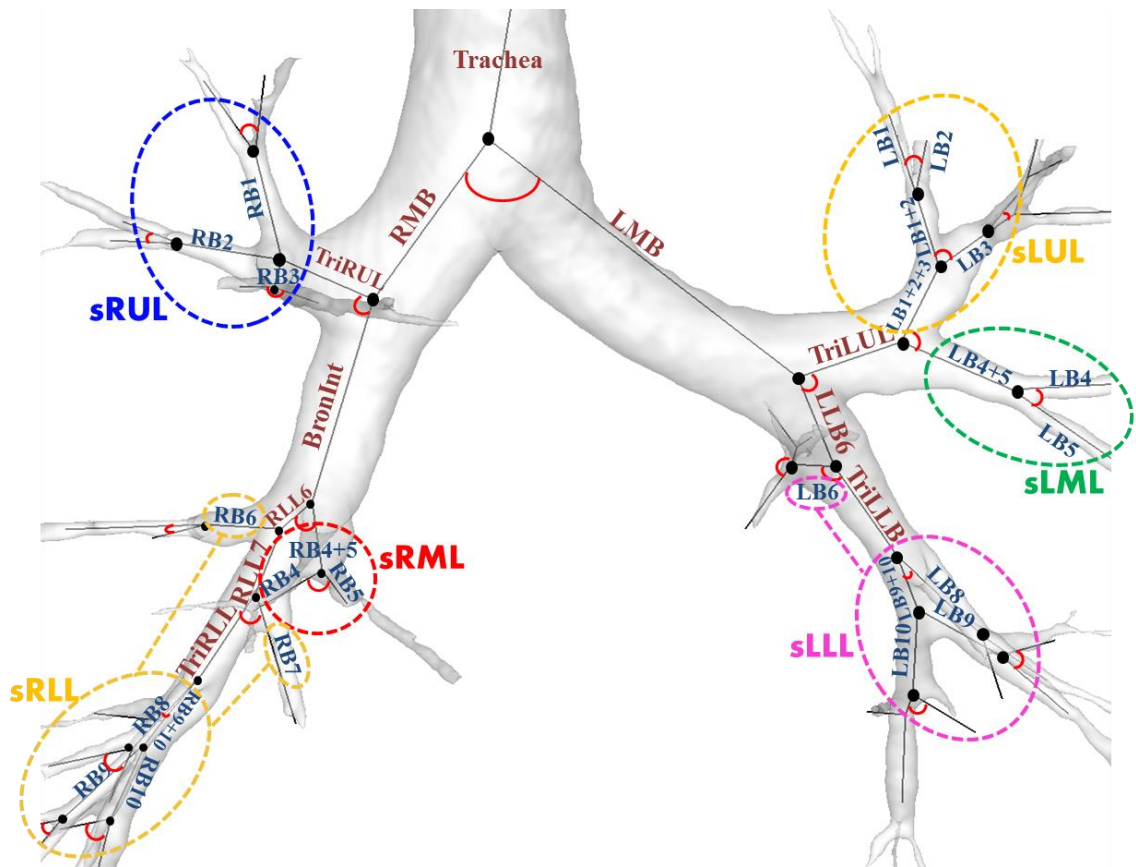
Figure 4.1 Segmental names of airways: Each bifurcation angle of the segment represents the angle between two daughter branches. All of the analysis is performed in the respective segmental region.

A

Total Area (TA)

Luminal Area (LA)

Wall Area (WA)

Wall area = Total area − Luminal area

WA% = WA / TA

B

➢ WA vs. WT

WA

WT

C

Circularity	$\dfrac{\text{major axis}}{\text{minor axis}}$
0.985	1.333
0.977	1.429
0.966	1.538
0.953	1.667
0.937	1.818
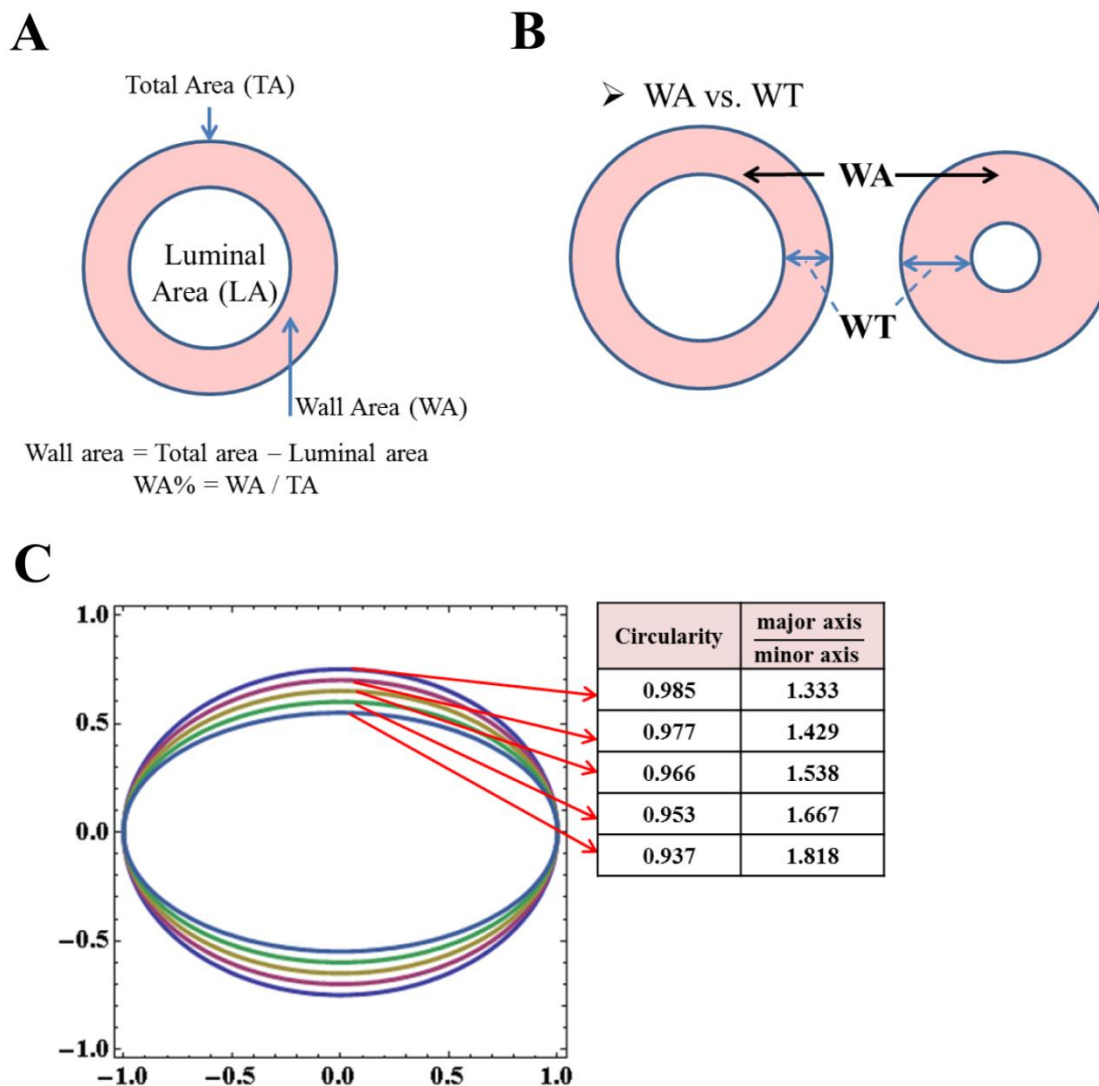
Figure 4.2 A: a schematic of WA%, B: the difference between WA and WT, and C: A schematic of circularity from 0.937 to 1.0 and relationship with the ratio of major axis to minor axis
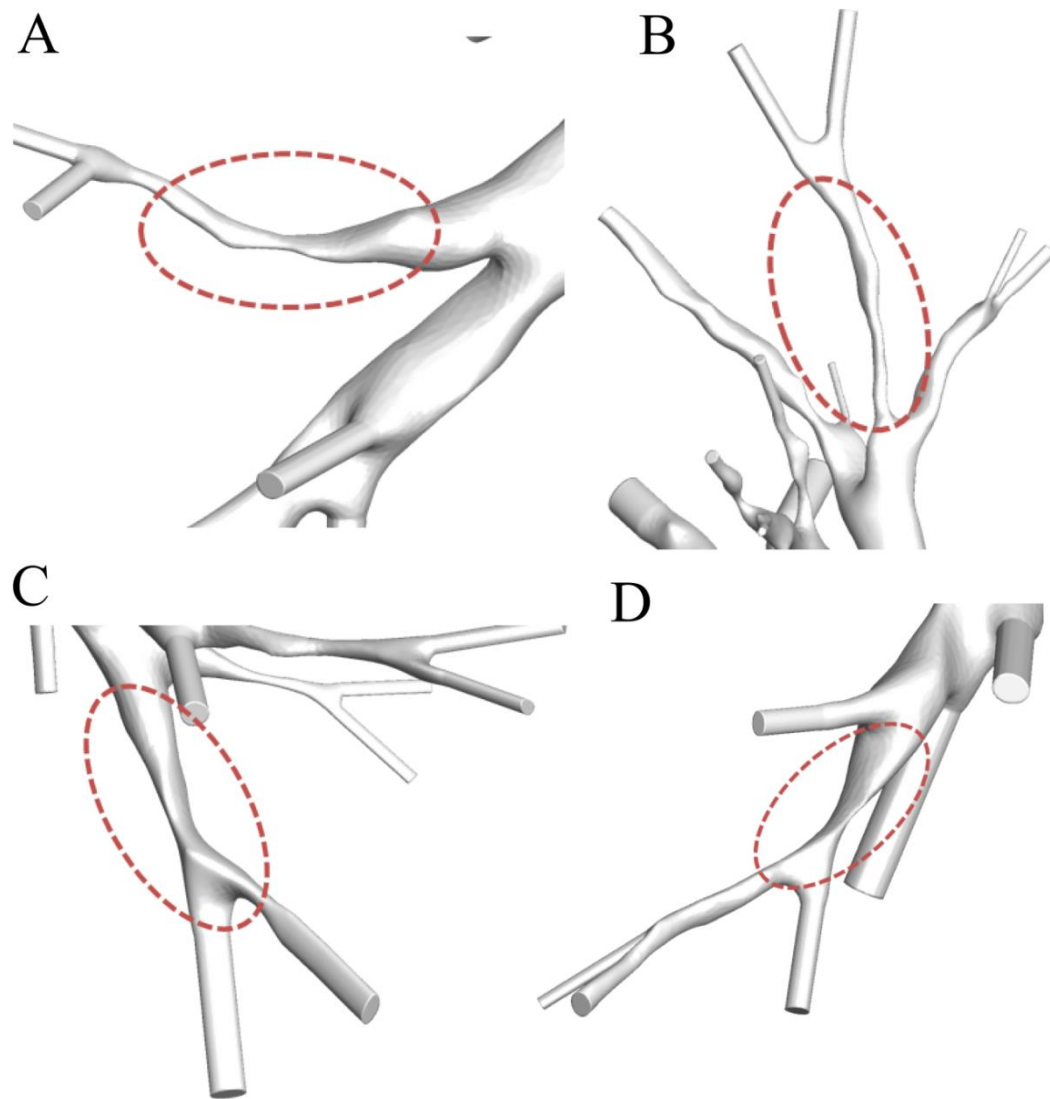
Figure 4.3 A and B show the examples of constricted luminal areas, whereas C and D show the examples of non-circular shapes
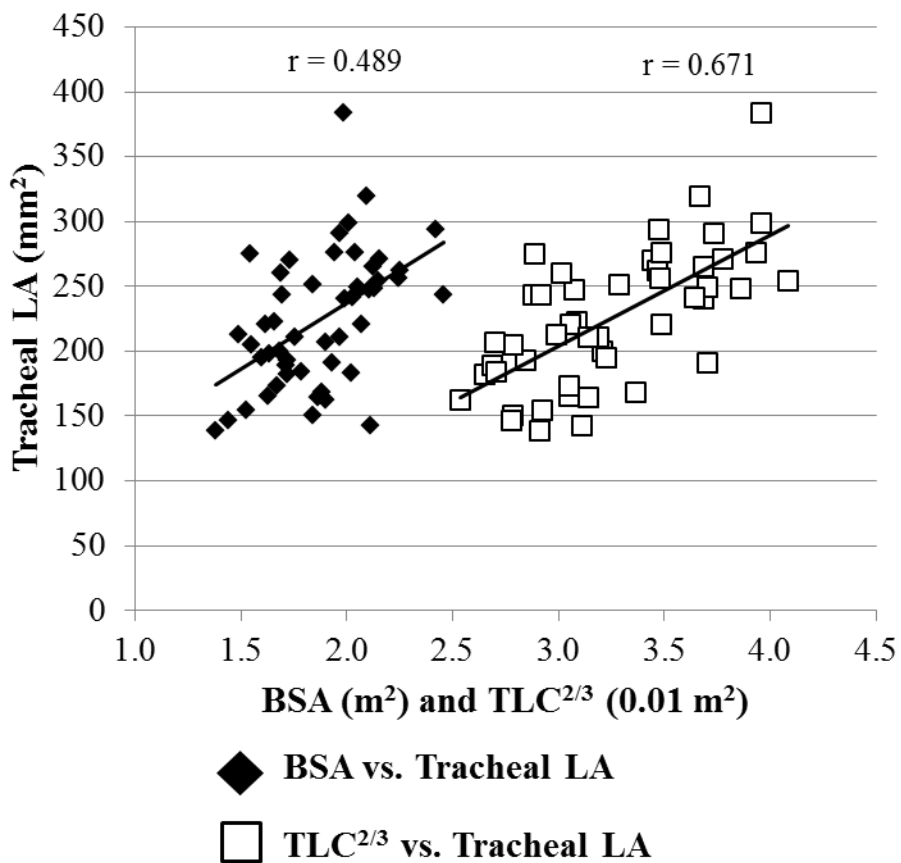
Figure 4.4 Linear regressions of tracheal luminal area (LA) in normal subjects via two different normalizations: body surface area (BSA) and total lung capacity (TLC)
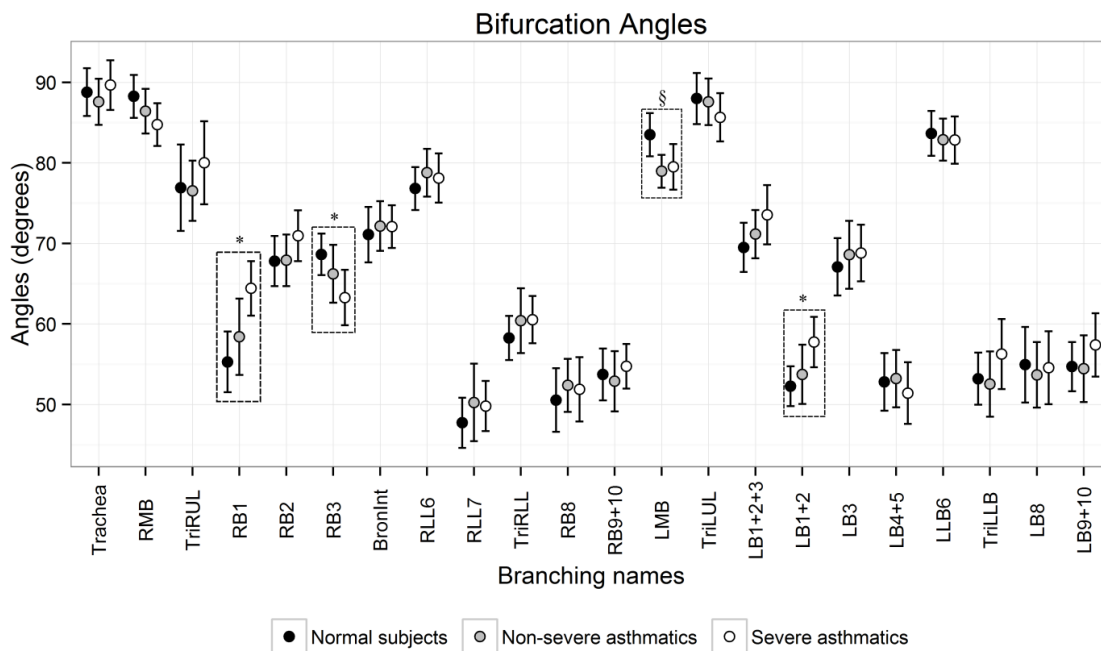
Figure 4.5 Bifurcation angles between daughter branches in 22 segmental regions of normal subjects, non-severe and severe asthmatics. § indicates *P*<0.05 for normal subjects vs. non-severe asthmatics; ¥ indicates *P*<0.05 for non-severe asthmatics vs. severe asthmatics; * indicates *P*<0.05 for normal subjects vs. severe asthmatics.
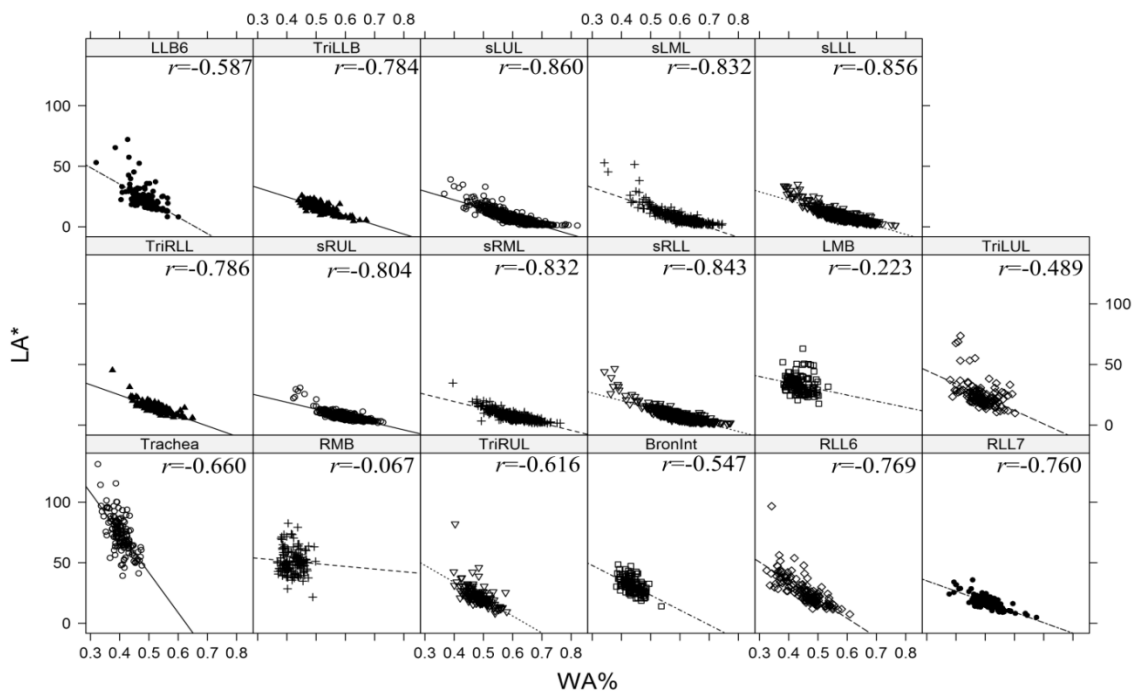
Figure 4.6 Linear regressions and Pearson linear correlations between LA* and WA% in the 17 respective ROIs with all subjects (normal subjects, non-severe and severe asthmatics)
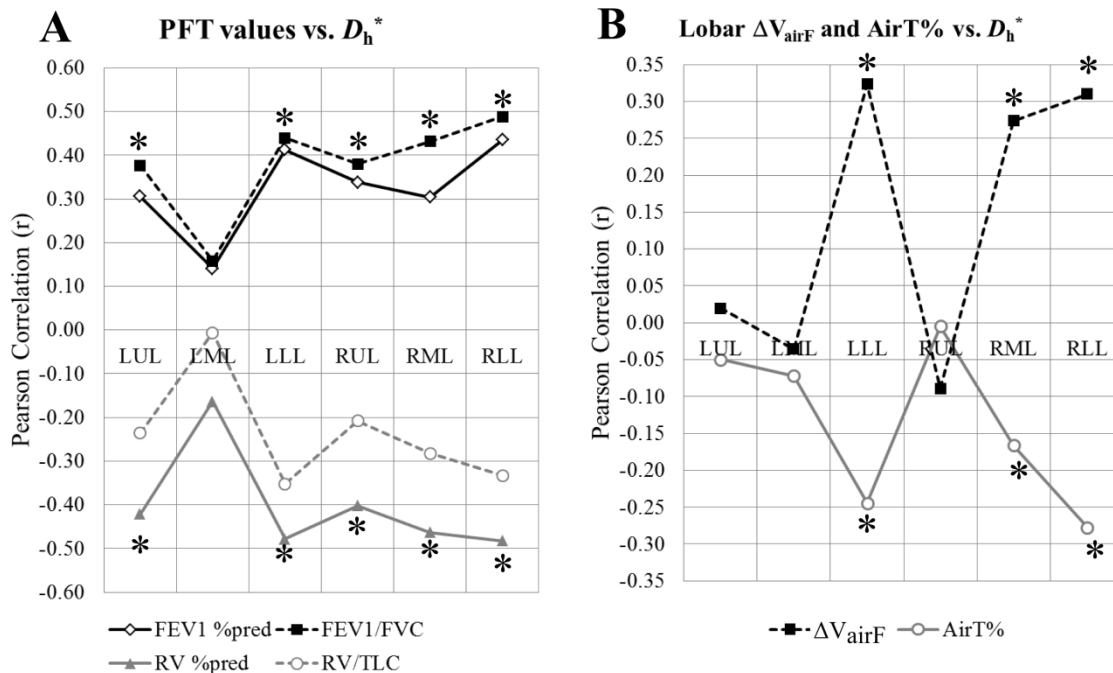
Figure 4.7 Pearson linear correlations of D_h^* (normalized hydraulic diameter) with A: PFT measurements (FEV1 %predicted, FEV1/FVC, RV %predicted, and RV/TLC) and B: AirT% and image-registration measurements (lobar ΔV_{airF}: lobar fraction of air volume change.* denotes that P (T-test) < 0.05.
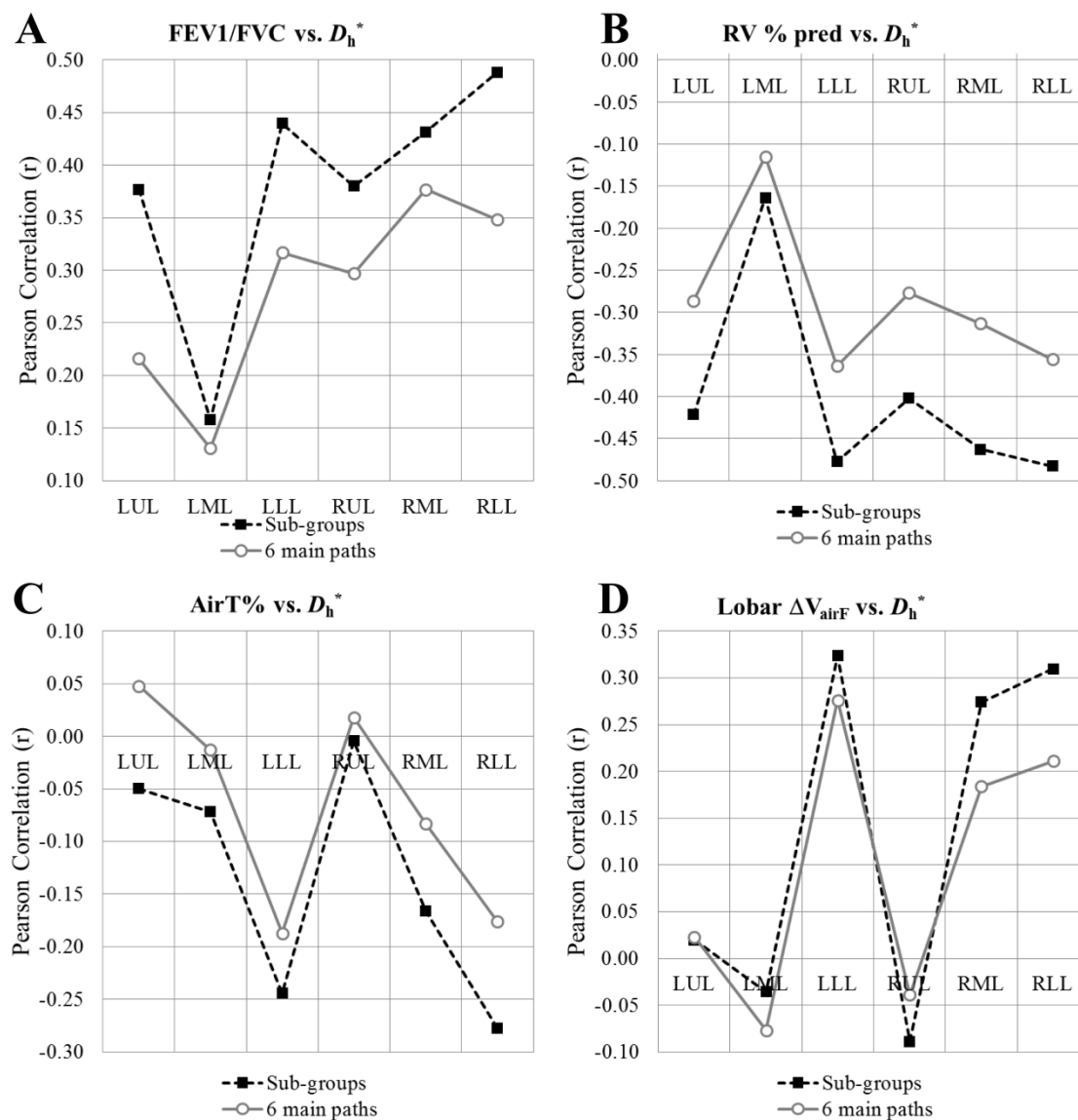
Figure 4.8 Pearson linear correlations of D_h^* (normalized hydraulic diameter) with A: FEV1/FVC, B: RV %predicted, C: AirT% and D: lobar ΔV_{airF}: lobar fraction of air volume change between 6 grouped values (sLUL, sLML, sLLL, sRUL, sRML and sRLL) and 6 major branches (LB1, LB4, LB10, RB1, RB4 and RB10)

CHAPTER 5

REGIONAL CHARACTERISTICS OF PRESSURE DROP AND PARTICLE
DEPOSITION IN SEVERE ASTHMATICS

5.1   Introduction

Phenotypes of asthma could be characterized by airflow obstruction, bronchial
hyper-responsiveness and airway inflammation [16]. However, flow structure and
particle deposition based on structural and functional alterations of asthmatics are yet to
be investigated. In asthmatic studies, ventilation defects and airway structural changes
were investigated by using magnetic resonance image (MRI), positron emission
tomography (PET) and single-photon emission computed tomography (SPECT) [65, 67,
86, 109, 135]. In addition, quantitative computed tomography (QCT) imaging studies
have shown significant alterations such as reduced airway dimension [102], increased
wall thickness [6] and air trapping [15, 110]. Although QCT can provide structural
measurements of the airways up to 6 or 7 generations (~2 mm), quantification of local
functional variables is still limited.

Recently, image registration techniques have been utilized to provide functional
information by matching images at different inflation levels [88, 118, 152]. The
registration derived-variables were validated by comparing ventilation maps from
different imaging modalities [20, 95, 118]. Furthermore, the techniques have shown the
strengths when characterizing functional alterations of disease lungs [11, 51]. For
instance, a study used the technique in differentiating airway vs. parenchymal phenotypes
in a chronic obstructive pulmonary disease (COPD) [51]. Recently, we have shown that
volume changes of severe asthmatics preferentially decreases near basal regions and the
reduced volume changes are compensated with air-volume change in apical regions [25].
In addition, severe asthmatics show the reduced airway dimensions and non-circular
shapes especially in lower lung regions, unlike normal and non-severe asthmatics [23].

Computational fluid dynamics (CFD) technique has become an alternative approach for analyzing flow characteristics and particle depositions in human lungs [52, 87, 93, 112, 158]. In fact, glottal constriction-induced jet-flow of tracheal regions are in laminar-transitional-turbulent flow regimes [91, 92], so that direct numerical simulation (DNS) or large eddy simulation (LES) is required to resolve turbulent eddy viscosity. Most of the researches [157, 158] have been performed with Reynolds averaged Navier-Stokes (RANS), k-ε and k-ω models which temporally average the effect of turbulence, but these approaches do not adequately predict turbulent features. Only a few simulations of CT-resolved-realistic lungs have been performed with LES [27, 28, 32, 101], but most of such studies were limited to normal subjects.

With regard to CFD simulations of asthmatic lungs, a study [77] showed alterations of particle depositions with an asthmatic subject before- and after- asthma attack, and the other study [36] correlated FEV1 with CFD-based resistance before- and after- bronchodilator. However, they imposed parabolic velocity profiles to the trachea regions and uniform pressure boundary conditions to 3D-resolved ending branches, under the k-w turbulence model or laminar assumption. Meanwhile, Backer et al. [37] demonstrates that lobar distributions of air-volume change between SPECT and CT are consistent, and they further emphasized the importance of subject-specific boundary conditions in CFD simulations. On the other hand, Wongviriyawong et al. [146] argued that air-volume change based on static compliances could be different from regional ventilation of the subjects with constricted airways. However, their model used major and minor losses obtained from a single symmetric bifurcation model with a bifurcation angle of 70° [84], and assumed uniform pleural pressure distributions.

The main objectives of this study are to investigate how functional and structural alterations of severe asthmatics observed in existing studies [23-25] affect flow structures and particle depositions, and further to evaluate clinical applications of CFD in localizing hot spots. The results from severe asthmatics are compared with those of normal subjects

in terms of pressure drop and particle deposition. According to our existing population-based analysis [23-25], severe asthmatics are characterized by the shift of lobar air-volume change, increased air-trapping of lower lobes, different bifurcation angle of left main bronchus (LMB) and right apical bronchus (RB1), decreased circularity, reduced hydraulic diameter and increased wall thickness. Therefore, we aim to investigate correlations of the aforementioned functional and structural alterations with CFD-predicted wall shear stress, pressure drop and particle deposition.

5.2   Methods

5.2.1   Human Subjects

The imaging study and protocols for acquiring CT images at both TLC and FRC were approved by the Institutional Review Board of University of Pittsburgh as a part of NIH sponsored multi-center severe asthma research program (SARP) consortium [21, 46, 104, 143]. A total of seven human subjects were obtained from the same institution, among which three subjects were normal subjects and four subjects were severe asthmatics (see Table 5.1). The CT images were taken with GE helical VCT-64 slice scanner with the slice thickness of 0.625 mm (see Table 5.2). Major criteria used to define severe asthma include treatments with oral corticosteroids and high-dose inhaled corticosteroids, besides several minor criteria [143]. The CT scans were acquired in the supine positions, and airway and lobar segmentations were processed using Apollo software (VIDA Diagnostics, Coralville, Iowa).

Symptoms of severe asthmatics could be characterized by the decrease of FEV1 and/or FVC indicating airflow obstruction, and increased RV indicating air-trapping through pulmonary function test (PFT) [125]. In addition to PFT, we found that severe asthmatics are characterized by increased air-trapping near basal regions, and reduced air-volume change in lower lungs together with elevated air-volume change in upper lungs

[24, 25], as compared with the normal group. Based upon our existing analysis [24, 25], we selected three normal subjects and four severe asthmatics with distinctive functional and structural characteristics.

5.2.2 Flow Simulation

A large-eddy simulation (LES) technique with the subgrid-scale (SGS) turbulent eddy viscosity model of Vreman [137] is adopted to resolve laminar-transitional-turbulent flows in the central airways, because turbulent laryngeal jet is induced at the glottal-constricted region above the trachea. The filtered continuity and Navier-Stokes equations read:

$$\nabla \cdot \overline{\mathbf{u}} = 0,$$
(5-1)

$$\frac{\partial \overline{\mathbf{u}}}{\partial t} + \overline{\mathbf{u}} \cdot \nabla \overline{\mathbf{u}} = -\frac{1}{\rho_f} \nabla \overline{p} + \nabla \cdot \left[\left(\nu + \nu_T \right) \nabla \overline{\mathbf{u}} \right],$$
(5-2)

where $\mathbf{u}$, ρ_f, p, ν_f and ν_T are velocity vector, fluid density, pressure, fluid kinematic viscosity and turbulent eddy viscosity, respectively. The properties of ρ_f and ν_f are set to 1.12 kg/m^3 and 1.64×10^{-5} m^2/s, respectively.

A characteristic Galerkin finite element method is employed to discretize the above equations. The current method provides 2nd order temporal and spatial accuracy [27, 90]. A moderate-steady-inspiratory flow-rate of $Q=3.27\times10^{-4}$ m^3/s ($\approx$20 liters/min) is imposed as the inlet condition, being equivalent to the peak flow-rate of a sinusoidal waveform with a tidal volume of 500 mL and a period of 4.8 s. The Reynolds number (Re) in trachea ranges from 1300 to 1700 based on the flow-rate and individual tracheal sizes of three normal and four severe asthmatics. A surface fitting method [100] together with Gmesh [53] is used to construct CT-based airway geometries. The numbers of elements, time step and computational costs are described in Table 5.3. Since SARP study [21, 46, 104, 143] did not gather oropharynx scans, as an alternative we create

synthetic turbulence right above the glottal constricted regions. The turbulent intensity and largest eddy size are set to be 0.29 and 8 mm, respectively, to mimic the turbulent flows found in the CFD simulations with oropharynx [27, 101].

5.2.3   Boundary Condition

Figure 5.1 shows the flow charts from image segmentation and registration to CFD simulations. An improved physiologically-consistent boundary condition is employed as follows to regulate high pressure drop that can be produced sometimes in the existing image registration-derived boundary condition [150]. First, the image registration technique [57] enables to estimate local air-volume change at voxel level between TLC and FRC, and 1D tree structures [49] serve to bridge 3D-resolved ending branches and lung parenchyma by the volume filling method [131]. Airway diameters of peripheral airways beyond the 3D ending branches are generated by Tawhai's model [132]. Pedley's airway resistance model [115] along with the generated 1D segment is used to predict the pressure of terminal bronchioles (P_{alv}).

Locally allowable difference of pleural pressure (ΔP_{pl}) can be calculated by the difference of elastic recoil pressure ($-\Delta P_{E}$). The local ΔP_{E} can be estimated with local air-volumes at TLC (V_{TLC}) and FRC (V_{FRC}) [4, 126]:

$$\Delta P_{E}[Pa] = P_{E,TLC} - \left[B - C\ln\left(\frac{1-\varepsilon}{V_{FRC}/V_{TLC} - \varepsilon} \right) \right], \tag{5-3}$$

where $P_{E,TLC}$, B, C and ε are set to 2000 Pa, 60 Pa, 300 Pa and -0.8, respectively. This relationship is obtained from the experimental data of Smith et al. [124], so that local ΔP_{pl} can be obtained. The local P_{alv} must be larger than ΔP_{pl} during the inspiration, because the inspiration effort to expand the lung from FRC to TLC corresponds to the maximum work of the individual subject [64]. In CFD simulations, flow-rate is slowly

elevated from 0 s to 0.6 s. With increasing flow rate, P_{alv} is continuously monitored and estimated by solving 1D model after running 3D CFD at each time step. Once P_{alv} decreases to lower than local maximum ΔP_{pl}, the flow-rate of the region stops increasing. The reduced flow-rate in a region is compensated with the increased flow-rate of the other regions to satisfy mass conservation. This approach ensures that airway pressure drop falls in known physiologically reasonable range in the presence of constricted airways. In the absence of airway constriction, the above boundary condition is equivalent to the existing registration-derived boundary condition [150].

5.2.4   Pressure Drop

For the quantitative analysis, pressure drop Δp is investigated in 31 segments (Figure 5.2). Δp of internal flow is determined by major loss and minor loss as follows:

$$\Delta p = \underbrace{f \frac{L}{D_h} \frac{\rho_f U^2}{2}}_{Major\ loss} + \underbrace{K \frac{\rho_f U^2}{2}}_{Minor\ loss}, \tag{5-4}$$

where f, L, D_h, U and K denote frictional coefficient, branch length from proximal node to distal node, hydraulic diameter, mean velocity and minor loss coefficient, respectively. The hydraulic diameter is defined as follows:

$$D_h = \frac{4A_c}{P_e}, \tag{5-5}$$

where A_c and P_e denote cross-sectional area and perimeter of the airway. In addition, we used a variable of Circularity (Cr) to assess elliptic shapes of airway's cross-section [138]:

$$Cr = \frac{\text{Perimeter of an area-equivalent circle}}{\text{Perimeter of a luminal area}} = \frac{\pi D_{\text{ave}}}{P_e}, \tag{5-6}$$

where $D_{\text{ave}} = \sqrt{4 \times A_c / \pi}$. With the Equation 5-4, Katz et al. [84] derived minor loss

coefficient K with symmetric bifurcation structures of 70° angles. In addition, Pedley et al.

[115] modeled pressure drop in human airway structure based on the principle of energy

loss:

$$\Delta p = \frac{32 \gamma \rho_f U^{1.5} \sqrt{\nu_f L}}{D_h}. \tag{5-7}$$

The coefficient γ is 0.327 for human bifurcation structures. In this study, we evaluate the

accuracy of two existing airway-resistance models by comparing with the current CFD

results for both normal and severe asthmatic subjects.

5.2.5 Particle Simulation

To compare the characteristics of particle deposition such as air pollutants or

pharmaceutical aerosols between normal subjects and severe asthmatics, particle

transport analysis is conducted using LES-predicted air flow fields. For particle

simulation, Lagrangian particle tracking algorithm [97, 112] is adopted to track particle

trajectories as follows:

$$\frac{d\mathbf{v}_p}{dt} = \frac{U}{\text{Stk} \cdot D_{\text{ave}}} \left(\mathbf{v}_f - \mathbf{v}_p \right) + \frac{\rho_p - \rho_f}{\rho_p} \mathbf{g}, \tag{5-8}$$

where $\mathbf{v}_p$, $\mathbf{v}_f$, ρ_p, ρ_f and $\mathbf{g}$ are particle velocity, fluid velocity corresponding to the particle

location, particle density, fluid density and gravitational acceleration, respectively. The

Stokes number (Stk) is defined as follows:

$$\text{Stk} = \frac{4}{3} \frac{\rho_p}{\rho_f} \frac{d}{D_{ave}} \frac{U}{v_{rel}} \frac{1}{C_D} C_c \alpha^{3.7}$$

$$= \frac{2\rho_p d^2 Q}{9\pi\mu_f D_{ave}^3} C_c \alpha^{3.7} \text{ , if } \text{Re}_p \ll 1$$

$$\tag{5-9}$$

where d, v_{rel}, C_D, C_c and α is the diameter of particles and velocity magnitude of the particles relative to the fluid velocity, the particle drag coefficient [107], the Cunningham slip correction factor [69] and particle-particle interaction factor [47]. The detailed descriptions of particle transport simulation can be found in [89, 101]. The number of particles is set to 10,000, and three different spherical particle sizes of 2.5, 5 and 10 µm are chosen in this study. The particle density and mean free path are 1000 kg/m^3 and 68 nm, respectively. "Particle distribution", "deposition" and "advection" by lobe are defined as particles entering each lobe, those deposited in 3D segments of each lobe and those exiting 3D ending branches of each lobe without being deposited in 3D segments, respectively.

5.3   Results

5.3.1   Pulmonary Function Test

Table 5.1 shows demographic, PFT- and CT-based measurements. In four severe asthmatics, the increased residual volume (RV) % predicted value indicates the increase of air-trapping. FEV1 % predicted values of severe asthmatic (SA) 1 and 2 subjects are relatively close to normal ranges (> 80%), whereas those of SA 3 and 4 subjects are significantly smaller than other subjects. FVC % predicted value that may indicate small airway ($D_{ave} < 2$ mm) disease [31] is significantly small only in SA 4 subject. As a result, only SA 3 subject has the significant drop of FEV1/FVC unlike SA 4 (normal FEV1/FVC

> 70%), implying that SA 3 subject would have significant constriction in CT-resolved large airways. Overall, SA 3 and SA 4 subjects have chronic airflow obstructions rather than other two severe asthmatics (SA 1 and SA 2).

5.3.2   CT-based Functional and Geometric Analysis

CT-based measurements can provide more detailed information than PFT as discussed in previous studies [23, 24]. Table 5.4 shows mean (±SEM) of the sensitive functional and structural variables for normal subjects (NS) and severe asthmatics (SA), which are statistically different between the two groups. The severe asthmatics show the decrease of lower-lobar air-volume changes and the increase of upper-lobar air-volume changes, along with the increased air-trapping (AirT%) in lower lobes, as compared with normal subjects. All of the severe asthmatics show the altered bifurcation angles in LMB and RB1. Circularity of severe asthmatics in RMB is smaller than normal ranges, and normalized wall thickness (WT*) increases in LMB and RB1 except RB1 of SA 3, and D_h* of LLL and RLL in only SA 3 is significantly decreased. Overall, the selected three normal subjects and four severe asthmatics exhibit eight or more characteristics of each group among twelve sensitive variables found before [24, 25].

In addition, Figure 5.3A shows that the Cr values of four severe asthmatics are smaller than those of three normal subjects, thus D_h has to be considered instead of D_{ave} when evaluating major losses for pressure drop. For example, the Cr values of RMB and TriRUL in four severe asthmatics are definitely deviated from those of normal subjects. Especially, SA 3 and 4 having chronic airflow obstructions show relatively smaller Cr than normal subjects in Trachea, RB6, RB9+10 and LMB besides RMB and TriRUL. Both SA 3 and SA 4 have the prominent drop of Cr, but only SA 3 shows small D_h unlike SA 4 in CT resolved airways (Figure 5.3B). We also plotted flow-rate ratio distributions after 1st generation, showing that it regionally depends on the presence of severe asthma (Figure 5.3C). For instance, the flow-rate ratio of TriRUL determining flow distribution

of right-upper-lobe (RUL) is larger in severe asthmatics than normal subjects, whereas the flow-rate ratio of LLB6 determining flow-distribution of left-lower-lobe (LLL) is relatively smaller in severe asthmatics than normal subjects. The alterations of Cr, D_h and flow-rate ratio in severe asthmatics are consistent with existing studies [23-25].

Based on the characteristics of individual subjects, lobar distribution $(U/(M+L)|_{dist})$ and advection $(U/(M+L)|_{adv})$ of particles in response to the shift of air volume change $(U/(M+L)|v)$ are assessed between three normal subjects and four severe asthmatics. The effect of reduced circularity of RMB on the particle deposition in TriRUL (Table 5.5) is assessed between "NS 2, NS 3" and "SA 3, SA 4". The effect of constricted airways of LLL and RLL to particle deposition is assessed with SA 3. The association of bifurcation angle in LMB with the increased WT in LB1+2+3 and LB4+5 (Table 5.6) and particle deposition are evaluated between NS 1 and SA 3 having extreme bifurcation angles to augment the effect for illustration.

5.3.3 Wall Shear Stress and Pressure Drop

Figure 5.4 and Figure 5.5 show the distributions of wall shear stress and pressure, respectively. Overall, the ranges of wall shear stress among the subjects were similar except for NS 1 and SA 3. NS 1 shows a little bit larger wall shear stress than other normal subjects from 1st generation. The NS 1 has smaller D_h as shown in Figure 5.3B, but it has also relatively smaller lung capacity of TLC and FVC and FEV1 than other normal subjects (Table 5.1). Therefore, the increased wall shear stress may not be attributable to airway constriction, but inter-subject variability of D_h. On the other hand, we found significant wall shear stress in SA 3 having the smallest FEV1/FVC (Table 5.1), as expected from reduced D_h (see Figure 5.3B). The D_h of SA 3 gets smaller from the 2nd generation, so that wall shear stress (Figure 5.4) is significantly increased, resulting in significant pressure drop (Figure 5.5) from the beginning of the 2nd generations.

With regard to quantitative analysis, we compared the current CFD results with two existing airway-resistance models for pressure drop based on the assumption of symmetric cylindrical bifurcation [84, 114] (Figure 5.6). Both models [84, 114] are fairly consistent with the current simulation in the selected 31 branches of a normal subject absent of constricted airways. However, these models cannot predict adverse pressure gradient ($\Delta p < 0$, Figure 5.6A), and the estimated pressure drops in a severe asthmatic subject are significantly deviated from the CFD results (Figure 5.6B). Overall, the results obtained by a constant average diameter in a cylindrical branch underestimate pressure drop. In large pressure drop regions, the difference of pressure drops between symmetric models and our simulation is almost four or five folds (Figure 5.6B). We further compared the major losses calculated with D_h and those calculated with D_{ave} (Table 5.7). In normal subjects the difference between the major losses calculated with D_h and D_{ave} is 5-10%, but in asthmatics with severely reduced circularity the difference increases substantially up to 30%. It is noted that two factors limit the applications of existing symmetric models: use of D_h vs. D_{ave} and constant diameter in cylindrical airways. The error in pressure drop due to constant vs varying diameters could be much larger than the error caused by use of D_h vs. D_{ave}.

5.3.4   Particle Deposition and Distribution

Figure 5.7 shows depositions of 10-μm particles in three normal subjects and four severe asthmatics. As expected in smaller D_h, NS 1 and SA 3 subjects show the increase of particle depositions in CT-resolved regions. Figure 5.8 shows global deposition efficiency of three normal and four severe asthmatics according to the Stk in Trachea. Since the Stk of NS 1 is relatively large, particle deposition tends to increase in this subject because Stk is a function of branch's D_{ave} (Equation 5-9). SA 3 subject shows the prominent increase of particle deposition due to both constriction and non-circular shape. In spite of large diameters, SA 4 subject has relatively elevated particle depositions in

similar Stk ranges, suggesting that the decreased circularity (non-circular shape) of SA 4 plays a key role in enhancing particle deposition.

We tested three different particle sizes to evaluate lobar particle distribution and particle advection (see Figure 5.9). With 2.5-µm particles, the U/(M+L)|$_{dist}$ (the particle distribution ratio of upper lobes to middle and lower lobes) is quite close to the ratio of air-volume changes (U/(M+L)|v) as expected, because small particles follow flow streamlines. Although there is slight subject variability, U/(M+L)|$_{dist}$ decreases as particle size increases due in part to the inertial effect that particles can easily move along with the flow to the lower lobes . On the other hand, U/(M+L)|$_{adv}$ (the particle advection ratio of upper lobes to middle and lower lobes) remains almost the same regardless of particle sizes, except for SA 3 subject. The U/(M+L)|$_{adv}$ of SA 3 subject increase with increasing particle size, meaning that large particles are deposited more in the airways of lower lobes. This trend may be attributable to the two major constricted branches of LB10 and RB9+10 in SA 3 (Figure 5.10).

In the TriRUL region, we compared particle depositions between two normal subjects and two severe asthmatics with elliptic shapes, because SA 3 and 4 exhibit significantly decreased circularities in RMB and TriRUL (Table 5.4 and Table 5.5). In Table 5.5, D_{ave} of SA 4 is the largest among four subjects, but D_h is slightly smaller than both NS 2 and NS 3 due to the reduced Cr. Both severe asthmatics have large mean velocity (U) and SA 4 shows the increased wall thickness (WT) than other subjects in TriRUL. Figure 5.11A shows the increased particle deposition efficiency of SA 3 and SA 4 in TriRUL, as compared with NS 2 and NS 3 in the same Stk range of the parent branch. Figure 5.12 displays the distributions of particle deposition in TriRUL. Since the particle deposition of TriRUL is mainly due to non-circular shape, variations of Stk for this case are not sensitive to the variations of particle size (Figure 5.11A and Figure 5.12). Figure 5.11B and C show particle deposition efficiency of the branch exhibiting both constriction and elliptic shapes (Figure 5.10). Since Stk is proportional to $1/D_{ave}^{3}$ with a

given flow-rate (Equation 5-9), in constricted airways particle deposition is very sensitive to particle size.

Furthermore, we found that asthmatics have smaller bifurcation angle between daughter branches of LMB than normal subjects [23]. Therefore, we compared a normal subject (NS 1) and a severe asthmatic subject (SA 3) with two extreme bifurcation angles (Figure 5.13). As shown in Table 5.6, SA 3 subject has the same D_h (6.7 mm), but larger mean velocity U and WT in TriLUL, relative to NS 1 subject. Figure 5.13 shows that the particle deposition in SA 3 increases, although SA 3 has a smaller angle between daughter branches (LB1+2+3 and LB4+5) of TriLUL. A large angle of LMB yields non-uniform flow-distribution in TriLUL due to the airway curvature effect, whereas a small angle of LMB creates almost uniform flow distribution toward the downstream of the bifurcation. Accordingly, the combined effect of the high velocity core and the bifurcation of TriLUL increases particle deposition (Figure 5.14). It is noted that the asthmatic segments of LB1+2+3 and LB4+5 are associated with greater wall thickness as well as more particle deposition than the normal subject (Table 5.6).

5.3.5   Correlation among Wall Shear Stress, Pressure

Drop and Particle Deposition

As shown in Figure 5.15, constriction-induced large velocity (A) creates high wall shear stress (B) in association with high velocity gradient on the wall. The significant pressure drop (D) is required to overcome elevated wall shear stress. Both parent and daughter branches of the constricted segment show the increase of particle deposition (Figure 5.15B). Both higher velocity and smaller D_{ave} contribute to be the increase of Stk (Equation 5-9), leading to the increase of particle deposition. As a result, constriction-induced high velocity, wall shear stress and pressure drop are correlated with particle deposition.

5.4   Discussions

In previous studies [24, 25], we have demonstrated that air-volume change in lower (upper) lobes of severe asthmatics decreases (increases), as compared with normal subjects. In addition, severe asthmatics are characterized by reduced Cr, increased WT and reduced D_h, and smaller bifurcation angle of LMB. Accordingly, this study focused on flow structures and particle depositions according to the chronic structural and functional changes in a moderate inspiratory flow condition (~20 liters/min). Three normal and four severe asthmatics were selected based on the characteristics of distinctive functional alterations such as increased air-trapping, reduced lower air-volume change and increased upper air-volume change. The severe asthmatics (SA 3 and SA 4) with small FEV1 % predicted values show the decrease of Cr, whereas only SA 4 subject with small FEV1/FVC and normal FVC % predicted has small D_h in CT-resolved regions.

Overall pressure drop up to 6-7 generations was less than ~ 50 Pa, which is in physiologically reasonable range of normal subjects [27], except for subject SA 3 having severe airway constriction. Four decades ago, Pedley et al. [114] modeled human airway pressure drop using the principle of energy loss in bifurcation structures. More recently, Katz et al. [84] employed the principle of engineering pipe flow to estimate minor loss coefficients as a function of Re. Wongviriyawong et al. [146] employed the data derived by Katz et al. [84] to model airway resistance in CT resolved airways, concluding that regional air-volume changes derived by static compliances cannot predict regional ventilation of constricted airways. However, airway resistance models developed with the idealistic symmetric cylindrical geometry need justification and verification for constricted asymmetric airways of asthmatics.

Therefore, we compared pressure drops in 3D resolved airways with a normal subject and a severe asthmatic subject with two existing airway-resistance models (see Figure 5.6). CFD results of the normal subjects show fairly close solutions with existing pressure models, although they are not strictly matched in small pressure drop regions

(less than 1 Pa). However, the models could not predict adverse pressure gradient of short branch with smaller inlet and large outlet. In addition, existing models fail to predict pressure drops in constricted airways, especially in large pressure drop regions (larger than 40 Pa). If pressure drops in proximal airways are not correctly estimated, pressure drops in peripheral regions could be overestimated in the case that inlet pressure and terminal pressures are confined as in [146]. In fact, pressure drops in airways are determined by the shear stress acting on airway wall, so that pressure drops could be totally different if airways exhibit elliptic and/or irregular shapes in a branching segment. In addition, the minimum FEV_1 volume among our subjects is ~ 1 liter (SA 3), whereas our simulation is performed in 0.327 liter/s. In this range, it is hard to conclude that air-volume changes derived from static compliances are different from dynamic breathing, as long as pressure distribution is much smaller than the variance of pleural pressure (~ 3 kPa) [144].

Investigating characteristics of particle deposition in severe asthmatics is important for inhaled pharmaceutical drugs, airborne bacteria or air pollutants. Lobar distributions of small particles are fairly consistent with air-volume distribution (Figure 5.9). With increasing particle size, the delivery of particles to lower lobes may increase because of the increased inertial effect of large particles. On the other hand, regardless of particle size, the advection ratio of particle distribution remains the same except for subjects with constricted airways in lower lobes, e.g. SA 3. This is because 3D-resolved airways of lower lobes (~6 generations) have more branches than those of upper lobes (~4 generations), so that it is possible that particles distributed toward lower lobes due to the inertial effects would be more deposited in the regions. The prominent increase of $U/(M+L)|_{adv}$ in SA 3 would be due to significantly constricted airways (RB9+10 and LB10) in lower lobes (Figure 5.10).

In severe asthmatics, the structural variables of circularity, bifurcation angle, and constriction are found to significantly affect particle deposition. In SA 3 and SA 4 with

chronic airflow obstructions, non-circular shapes of airways are detected in RMB and TriRUL, along with increased flow in TriRUL (Table 5.5). Particle depositions in TriRUL having non-circular shapes are relatively larger than other normal subjects having airways of circular shapes (see Figure 5.11A and Figure 5.12). In addition, both the reduced bifurcation angle of LMB and the increased flow of TriLUL in the severe asthmatic subject generate the uniform flow distribution (Figure 5.13), which subsequently leads to increased particle deposition on downstream. Presumably, the wall shear stress due to increased flow and particle distribution toward upper lobes in severe asthmatics may increase the chance of inflammation in the upper lobar regions, which may reflect on the increased wall thickness as in LB1+2+3 and LB4+5 (Table 5.6). Lastly, abrupt constriction of airways as shown in Table 5.6 corresponds to the reduced D_h of airways, which then subsequently create strong jet flows downstream. This is accompanied with the significant increase of Stk because Stk is proportional to D_{ave}^{-3}. In fact, the increase in deposition of large particle may be largely caused by airway constriction.

In conclusion, we applied a high-fidelity CFD model together with CT image-based airway models to study pressure drop and particle deposition in both normal and asthmatic lungs. With the aid of image registration technique, the subject-specific physiologically-realistic-flow boundary condition is derived based on air-volume difference between two CT lung images of the same human subject. We compared CFD-predicted pressure drop with those of existing models derived from idealistic symmetric cylindrical bifurcation structures. For a normal subject, both models predicted reasonable pressure drops, but they failed to estimate pressure drop with heterogeneous airway structures as in asthmatic subjects. As expected from flow-rate distribution, particle distribution and particle advection to upper lobes are larger in severe asthmatics, relative to normal subjects. In both normal and severe asthmatics, with increasing particle size, particles are distributed more toward lower lobar regions due to the inertial effects.

Alterations of bifurcation angle, circularity, diameter, flow-rate ratio of the airways in severe asthmatics result in an increase of particle deposition. Especially, the constricted airways contribute to high wall shear stress, elevated pressure drop, and significantly increased particle deposition.

Table 5.1 Demographic, pulmonary function test (PFT)-based and CT-based information of three normal subjects and four severe asthmatics

		Normal subjects (NS)			Severe asthmatics (SA)			
		NS 1	NS 2	NS 3	SA 1	SA 2	SA 3	SA4
Demo-graphy	Sex	F	F	F	F	M	F	F
	Age (yrs.)	57	59	29	59	60	48	61
	BMI	19.7	23.7	22.2	30.5	22.9	23.9	32.4
	Asthma Duration	-	-	-	3.4	38.8	19.7	10.6
PFT	TLC (liters) (% predicted)	4.65 (93%)	5.96 (107%)	5.24 (101%)	4.71 (101%)	5.55 (113%)	5.55 (128%)	6.95 (98%)
	FRC (liters) (% predicted)	2.51 (92%)	3.40 (116%)	2.52 (91%)	2.34 (90%)	3.17 (117%)	2.87 (115%)	4.13 (113%)
	RV (liters) (% predicted)	1.66 (88%)	2.24 (108%)	1.42 (96%)	2.28 (126%)	2.65 (140%)	2.34 (151%)	3.95 (163%)
	RV/TLC	36%	38%	27%	48%	48%	42%	57%
	FVC (liters) (% predicted)	3.16 (92%)	3.82 (100%)	4.00 (101%)	2.43 (78%)	2.78 (84%)	2.52 (80%)	1.83 (39%)
	FEV1 (liters) (% predicted)	2.53 (95%)	2.97 (100%)	3.15 (94%)	1.98 (82%)	1.95 (76%)	1.02 (40%)	1.19 (34%)
	FEV1/FVC	80%	78%	79%	82%	70%	41%	65%
CT	TLC (liters)	3.65	5.37	4.31	3.90	4.93	4.33	5.64
	FRC (liters)	1.41	2.04	1.79	1.95	2.77	1.77	2.85

Note: All of normal subjects and severe asthmatics are Caucasians and non-smokers. PFT and CT measurements are obtained in upright and supine positions, respectively.

Table 5.2 The scanner and the scanning protocol used for both normal subjects and severe asthmatics

	Scanner and protocol
Scanner model	GE VCT 64 slice
Scan type	Helical
Rotation time (s)	0.5
Detector configuration (channel # x mm)	64×0.625 mm
Pitch	0.984
Peak kilovoltage (kVp)	120
miliampere (mA)	S-145 M-180 L-270
Dose modulation	Auto mA OFF
Reconstruction Algorithm	Standard or Detail
Lung Algorithm	None
Additional Image filters	No Selection
Thickness (mm)	0.625
Interval (mm)	0.5
Iterative reconstruction (noise reduction algorithm)	No Selection
Scan Time (s) 30cm length	< 10

Note: mA was varied for protocol based on BMI size (S: BMI < 20, M: 20 ≤ BMI ≤ 30, L: BMI > 30).

Table 5.3 The number of elements, simulation time step, and computation costs

	Normal subjects (NS)			Severe asthmatics (SA)			
	NS 1	NS 2	NS 3	SA 1	SA 2	SA 3	SA 4
Elements (Tetrahedral)	4,765,726	3,980,840	4,966,096	4,200,905	4,298,995	4,132803	4,765,726
Time step (s)	5×10^{-6}	5×10^{-6}	5×10^{-6}	5×10^{-6}	5×10^{-6}	3×10^{-6}	5×10^{-6}
CPU cores	192	128	192	192	128	160	160
Simulation times (hours)	~240	~353	~230	~333	~264	~408	~240
Total cost (hours)	~107,712	~64,320	~32,256	~63,936	~33,792	~65,280	~38,400

Table 5.4 The ratio of air-volume change in upper lobes to air-volume change in middle and lower lobes (U/(M+L)|v), AirT%, Bifurcation angle, Cr, WT normalized by PFT-based $TLC^{1/3}$ (WT*) and D_h normalized by PFT-based $TLC^{2/3}$ (D_h*).

	U/(M+L)|v	AirT%		Bif. Angle		Cr		WT*		D_h*	
		RLL	LLL	LMB	RB1	RMB	LMB	LMB	RB1	LLL	RLL
NS	0.57 (±0.01)	2.3 (±0.5)	3.2 (±0.6)	83.5 (±1.3)	55.3 (±1.9)	0.971 (±0.002)	0.977 (±0.001)	2.04 (±0.04)	1.67 (±0.02)	3.36 (±0.05)	2.99 (±0.04)
SA	0.80 (±0.03)	9.5 (±1.6)	10.8 (±1.8)	79.5 (±1.4)	64.4 (±1.7)	0.958 (±0.003)	0.973 (±0.001)	2.20 (±0.04)	1.74 (±0.03)	3.00 (±0.05)	2.70 (±0.04)
NS 1	0.548	0.2	0.4	87.6	48.6	0.959	0.978	2.00	1.65	3.60	3.11
NS 2	0.640	0.3	0.2	73.9	80.0	0.974	0.975	1.92	1.79	3.26	2.99
NS 3	0.655	1.0	0.5	74.0	-	0.962	0.977	2.01	1.37	2.74	3.35
SA 1	0.880	7.2	7.7	72.0	82.4	0.934	0.983	2.26	2.07	3.13	3.24
SA 2	0.703	36.9	50.9	75.3	78.7	0.938	0.980	2.55	1.93	3.48	3.26
SA 3	0.816	24.6	11.1	63.0	74.8	0.927	0.961	2.34	1.58	2.51	1.91
SA 4	0.835	43.3	52.5	71.7	63.1	0.926	0.954	2.42	1.75	3.50	2.86

RLL and LLL indicate right-lower-lobe and left-lower-lobe respectively.

Table 5.5 D_{ave}, circularity, D_h and mean velocity of two normal subjects (NS 2 and NS 3) and two severe asthmatics (SA 3 and SA 4) in TriRUL region

		Normal subjects		Severe asthmatics	
		NS 2	NS 3	SA 3	SA 4
TriRUL	D_{ave} (mm)	8.3	8.2	6.1	8.5
	Cr (Circularity)	0.95	0.96	0.82	0.88
	D_h (mm)	7.9	7.8	5.0	7.6
	U (mean velocity, m/s)	1.03	1.02	2.29	1.28
	WT*	2.03	1.77	2.05	2.26
	WT (wall thickness, mm)	3.68	3.07	3.62	4.31

Note: Mean (±SEM) of WT* of 50 normal subjects from the previous study (Chapter 4) in TriRUL is 2.01 (±0.04).

Table 5.6 D_{ave}, circularity, D_h and mean velocity of two normal subjects (NS 2 and NS 3) and two severe asthmatics (SA 3 and SA 4) in TriLUL region

		Normal (NS 1)	Severe asthmatic (SA 3)
TriLUL	D_{ave} (mm)	7.0	6.9
	Cr (Circularity)	0.96	0.97
	D_h (mm)	6.7	6.7
	U (mean velocity, m/s)	1.58	2.16
	WT*	1.82	2.16
	WT (wall thickness, mm)	3.04	3.82
LB1+2+3	WT*	1.71	2.07
	WT (wall thickness, mm)	2.86	3.67
LB4+5	WT*	1.64	1.98
	WT (wall thickness, mm)	2.74	3.50

Note: Mean (±SEM) of WT* of 50 normal subjects in the previous study (Chapter 4) in TriLUL, LB1+2+3 and LB4+5 are 2.15 (±0.07), 1.87 (±0.03) and 1.85 (±0.04), respectively.

Table 5.7 The ratio of major loss calculated by D_{ave} to that calculated by D_h in RMB, TriRUL, RB6 and RB9+10 regions

	Normal subjects			Severe asthmatics			
	NS 1	NS 2	NS 3	SA 1	SA 2	SA 3	SA 4
RMB	0.925	0.952	0.925	0.871	0.880	0.860	0.858
TriRUL	0.912	0.911	0.920	0.879	0.844	0.679	0.783
RB6	0.914	0.895	0.902	0.951	0.951	0.773	0.663
RB9+10	0.921	0.943	0.949	0.929	-	0.830	0.858
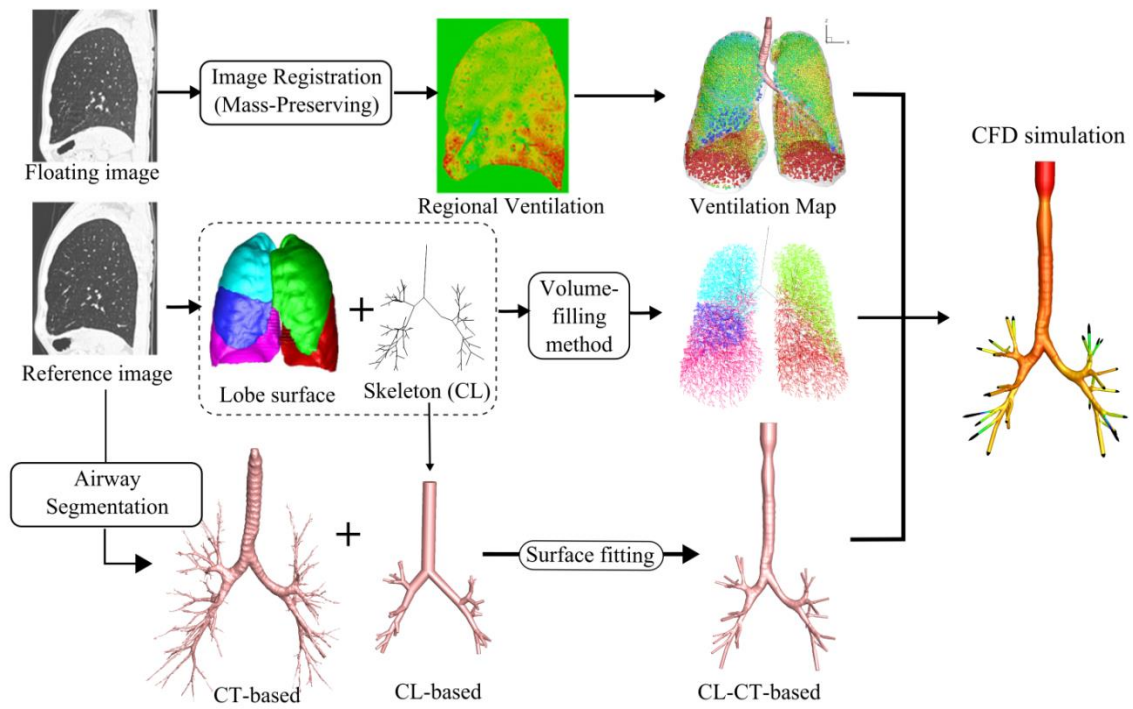
Figure 5.1 Flow charts of connecting CT image-based structure and functional information for physiologically consistent CFD simulations
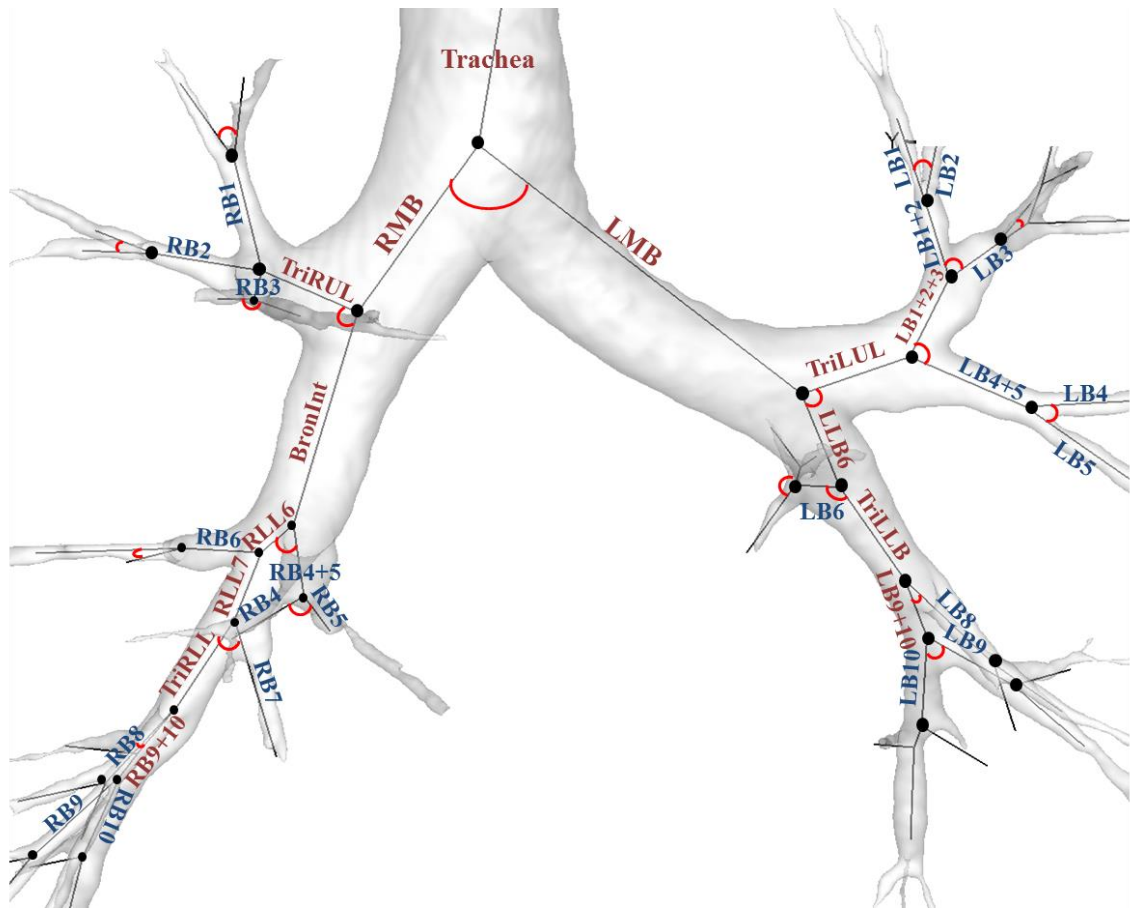
Figure 5.2 Segmental names of airways: Each angle of the segment represents the bifurcation angle between two daughter branches.
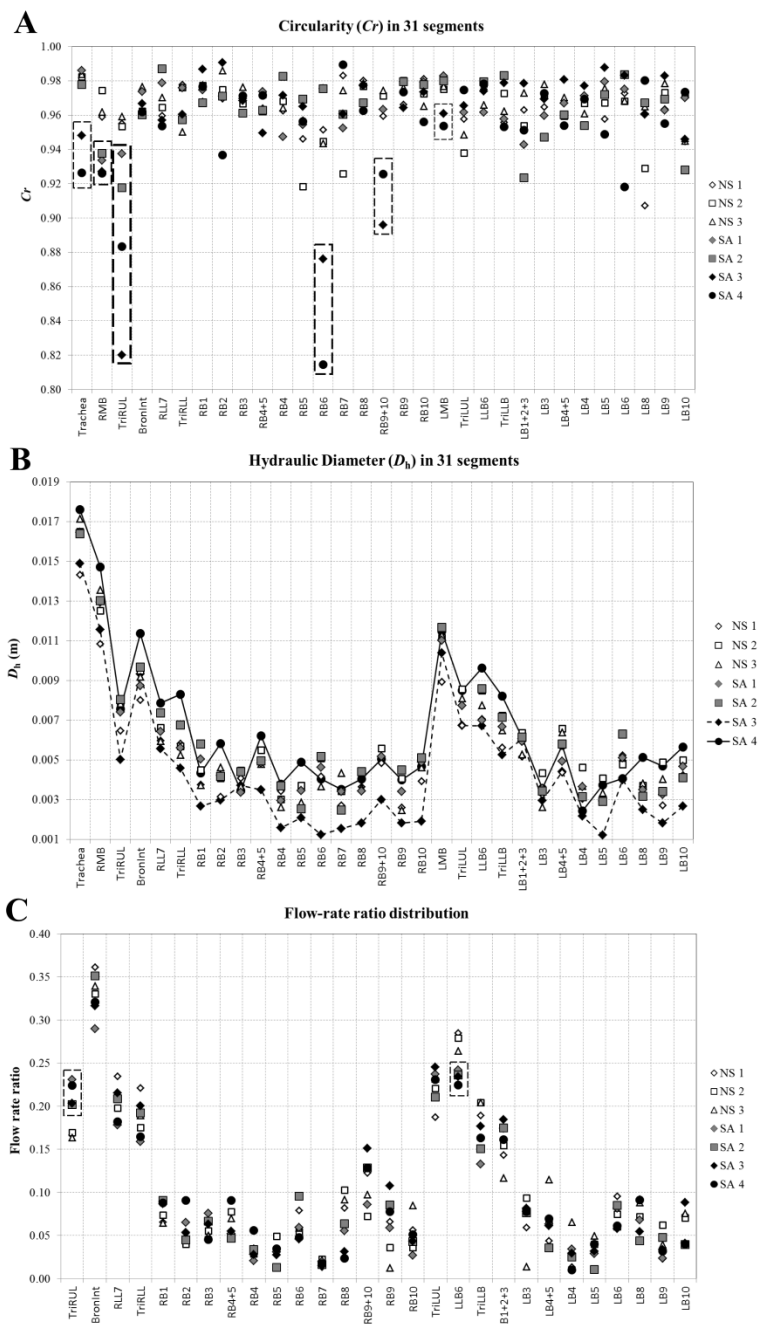
Figure 5.3 Structural variability of Cr (A) and D_h (B) for 31 segments and functional variability of flow-rate ratio distribution (C) after 1st generation in three normal and four severe asthmatics
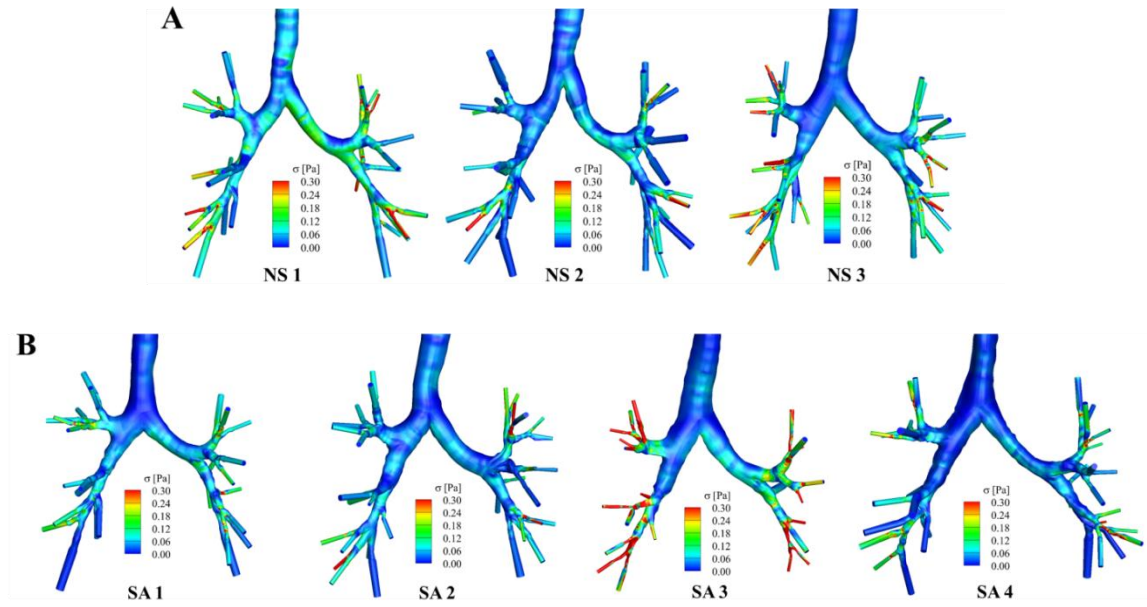
Figure 5.4 Regional distribution of wall shear stress in A: normal subjects and B: four severe asthmatics in steady inspiratory flow-rate of ~20 liters/min
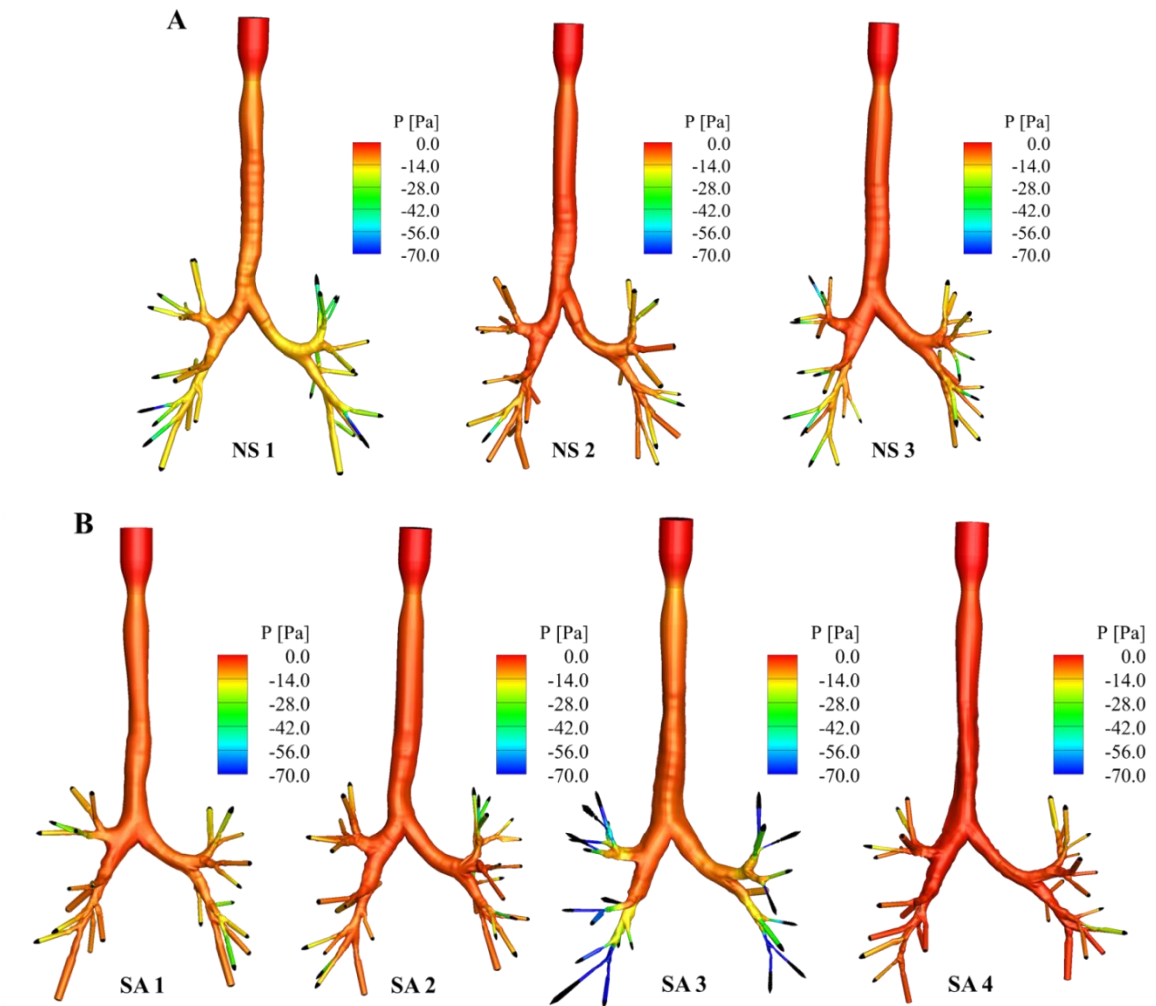
Figure 5.5 Regional distribution of pressure in A: normal subjects and B: severe asthmatics in steady inspiratory flow-rate of ~20 liters/min
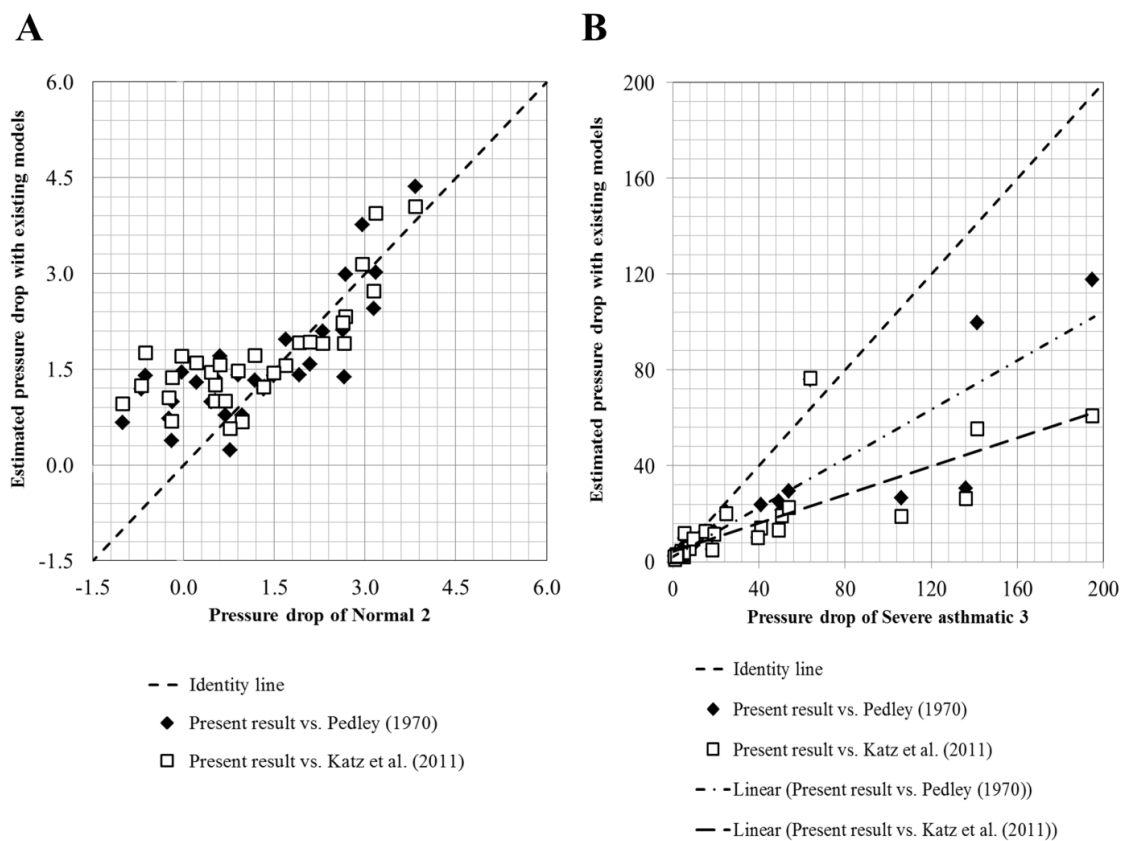
Figure 5.6 Pressure drops of 31 branching segments in A: a normal and B: a severe asthmatic subject with current CFD simulations and those calculated by existing models by Pedley et al. (1970) and Katz et al. (2011)
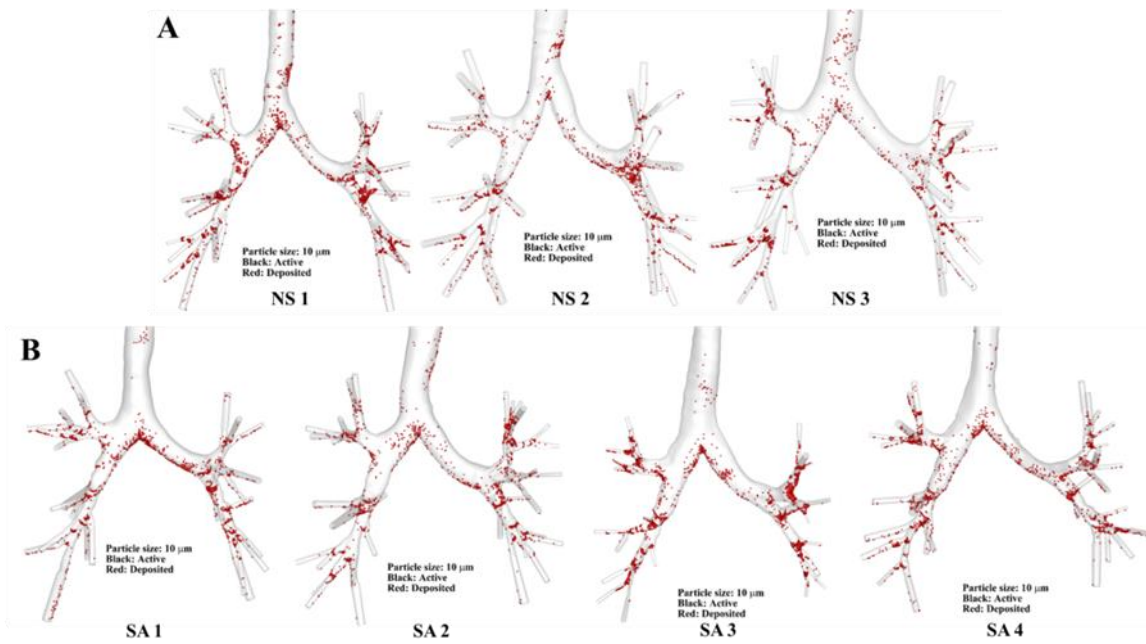
Figure 5.7 Regional depositions with particles with size of 10 µm in A: normal subjects B: and severe asthmatics
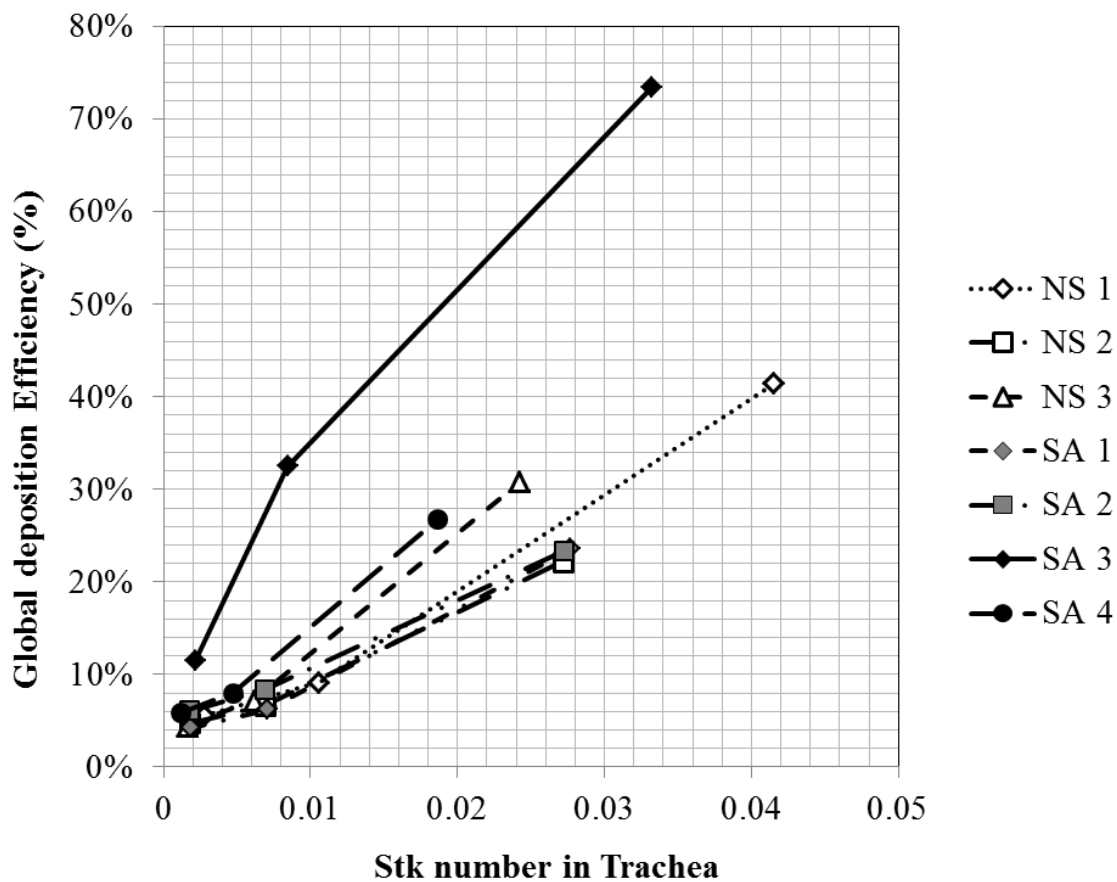
Figure 5.8 Global deposition efficiency according to Stk in trachea based on three different particle sizes (2.5, 5 and 10 μm) in three normal subjects and four severe asthmatics
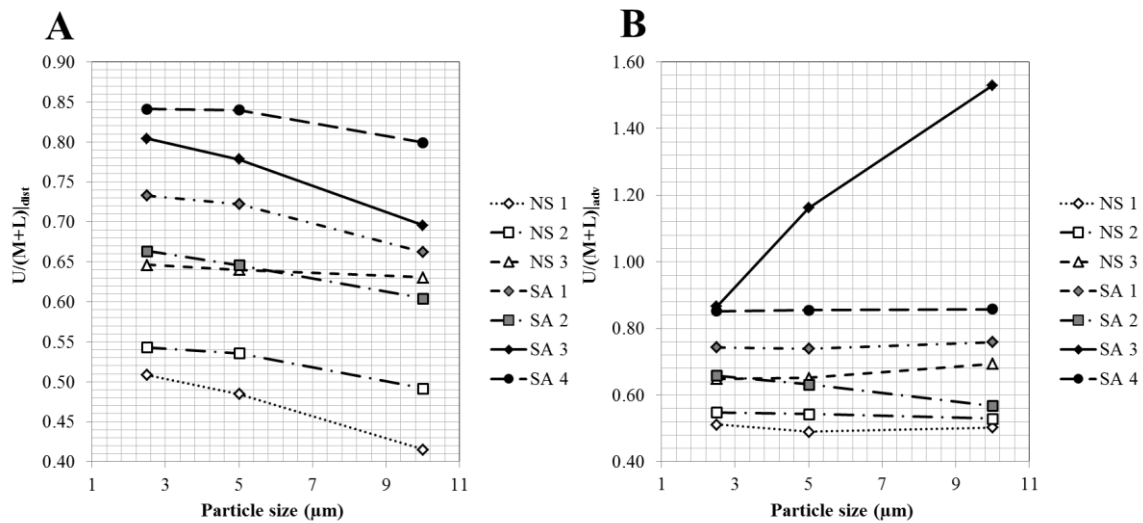
Figure 5.9 A: U/(M+L)|dist (The particle distribution ratio of upper lobes to middle and lower lobes) and B: U/(M+L)|adv (The particle advection ratio of upper lobes to middle and lower lobes)
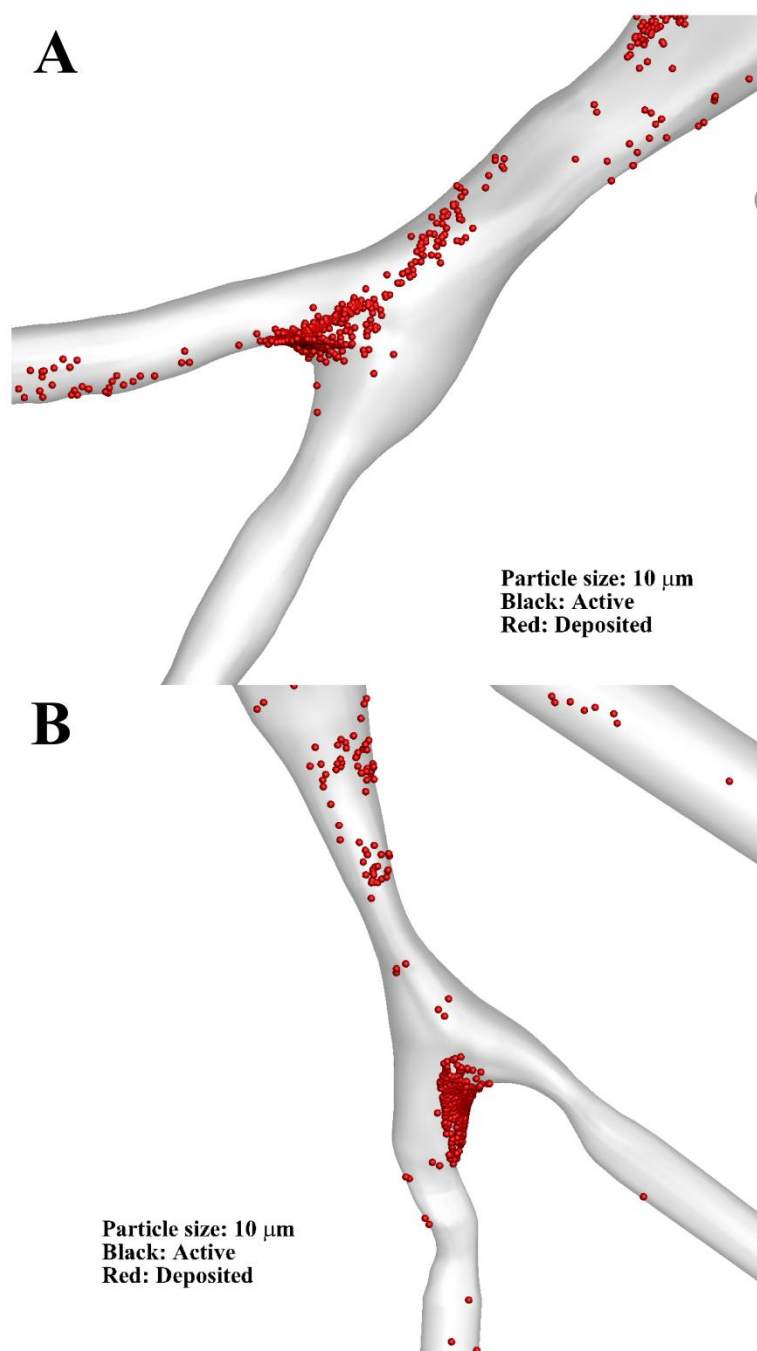
Figure 5.10. Two representative constricted regions of A: RB9+10 and B: LB10 in lower lobes in SA 3 subject
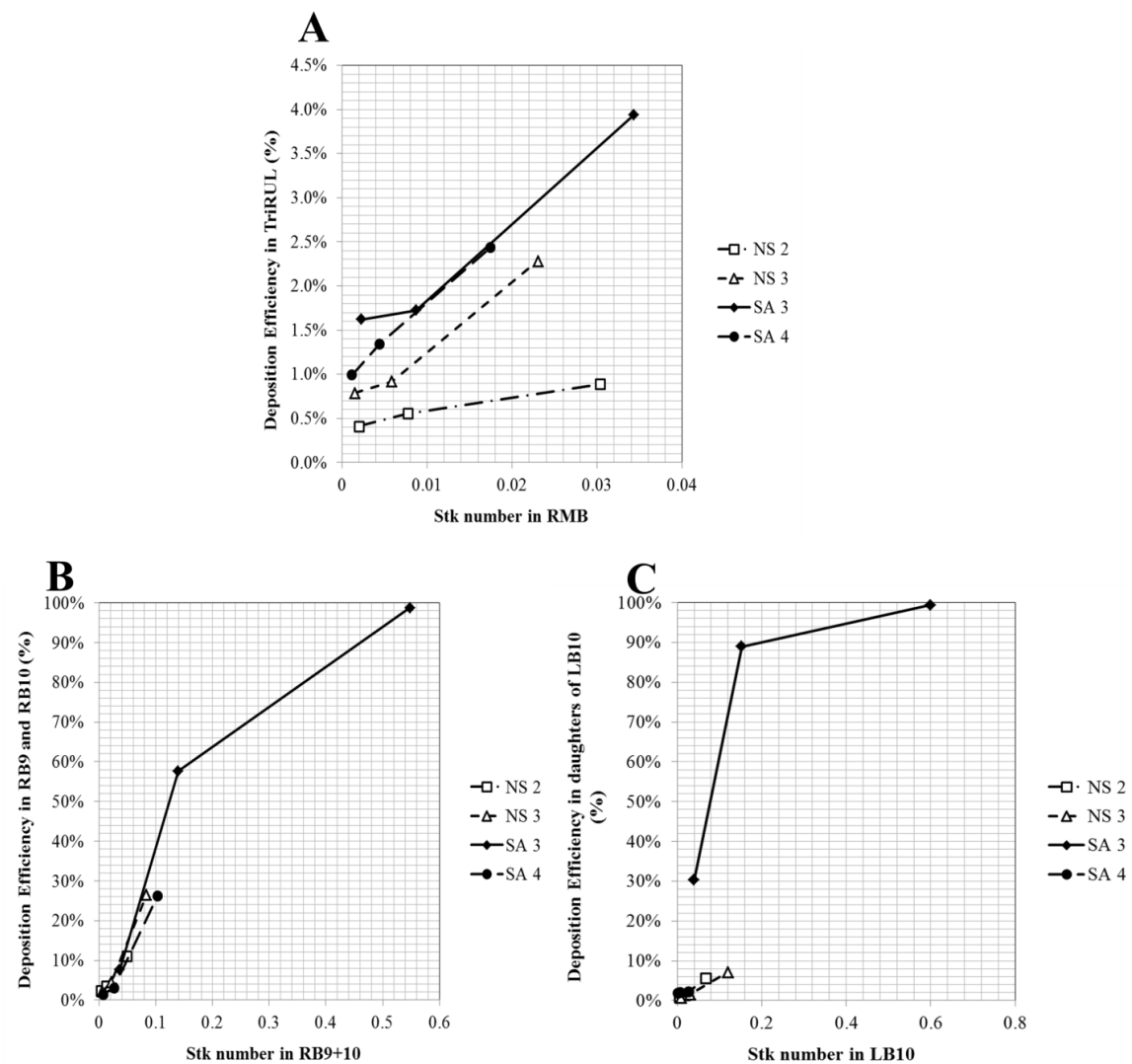
Figure 5.11 Particle deposition efficiency in A: TriRUL, B: RB9 and RB10 and C: LB10 daughters according to Stk of parent branch
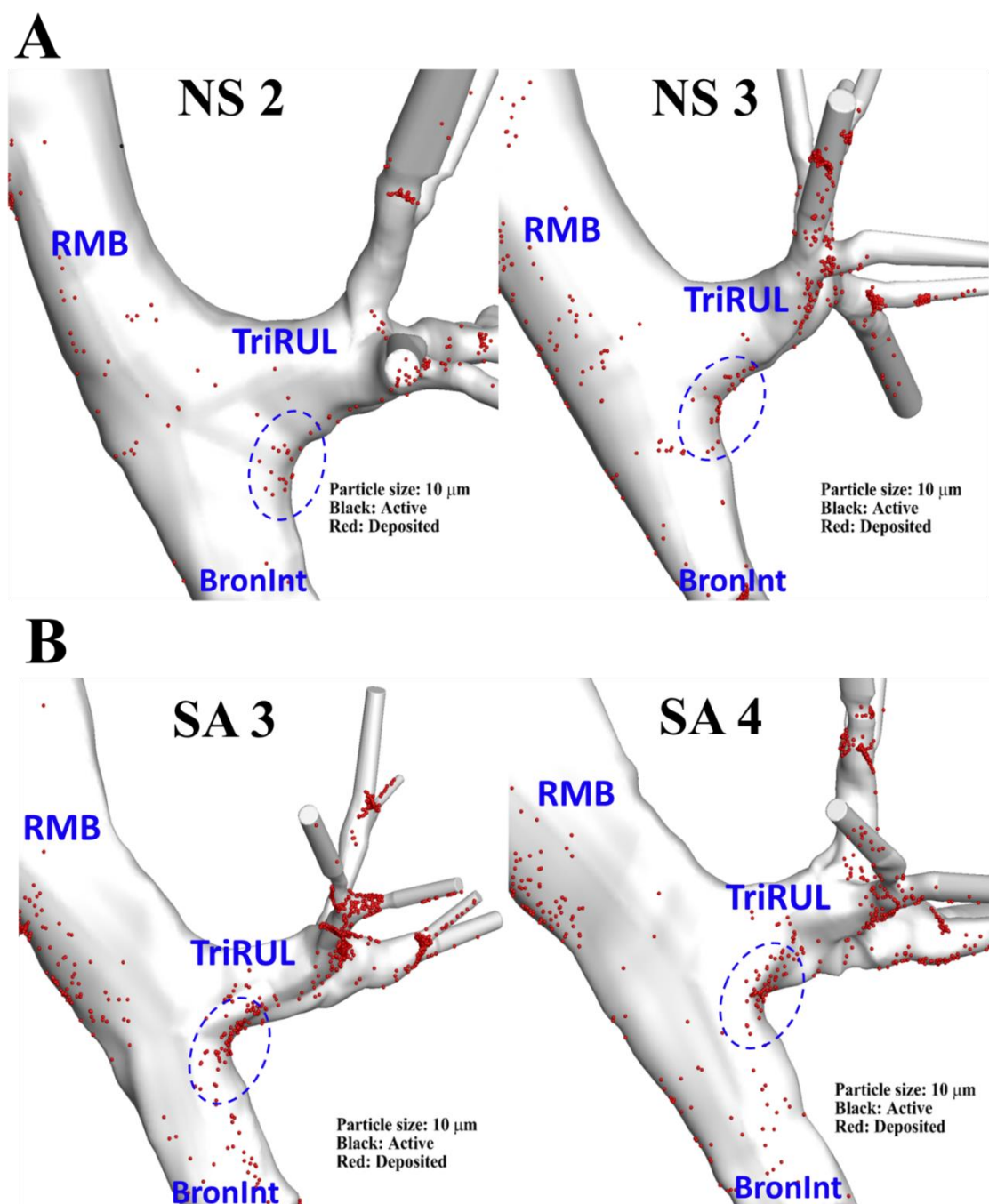
Figure 5.12 Correlations among non-circularity, bifurcation angles, and particle deposition in TriRUL regions between A: normal subjects and B: severe asthmatics. All of the images are plotted as back-view.
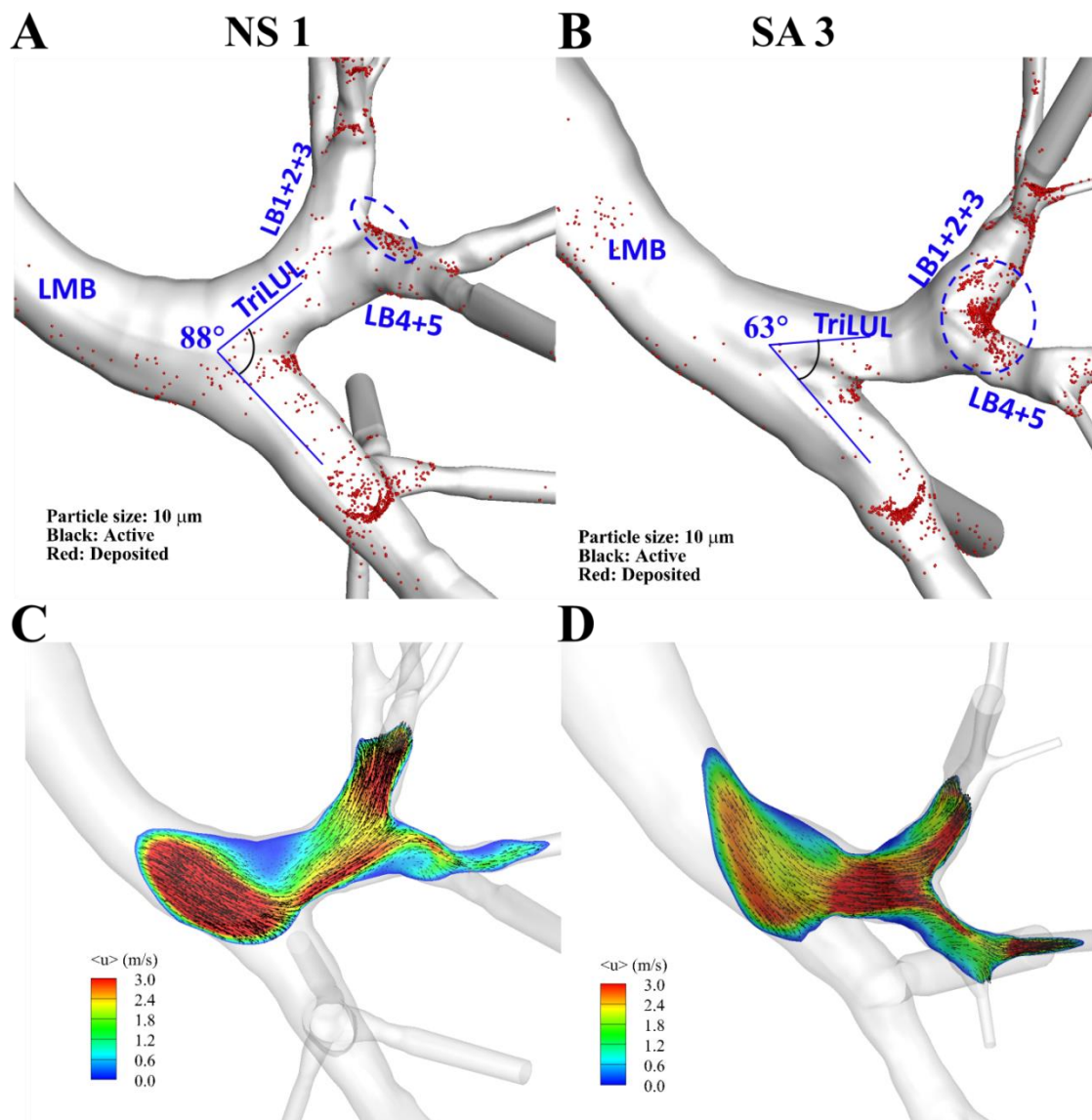
Figure 5.13 Correlations among particle deposition, bifurcation angle, and mean velocity in TriLUL between normal subject 1 and severe asthmatic 3
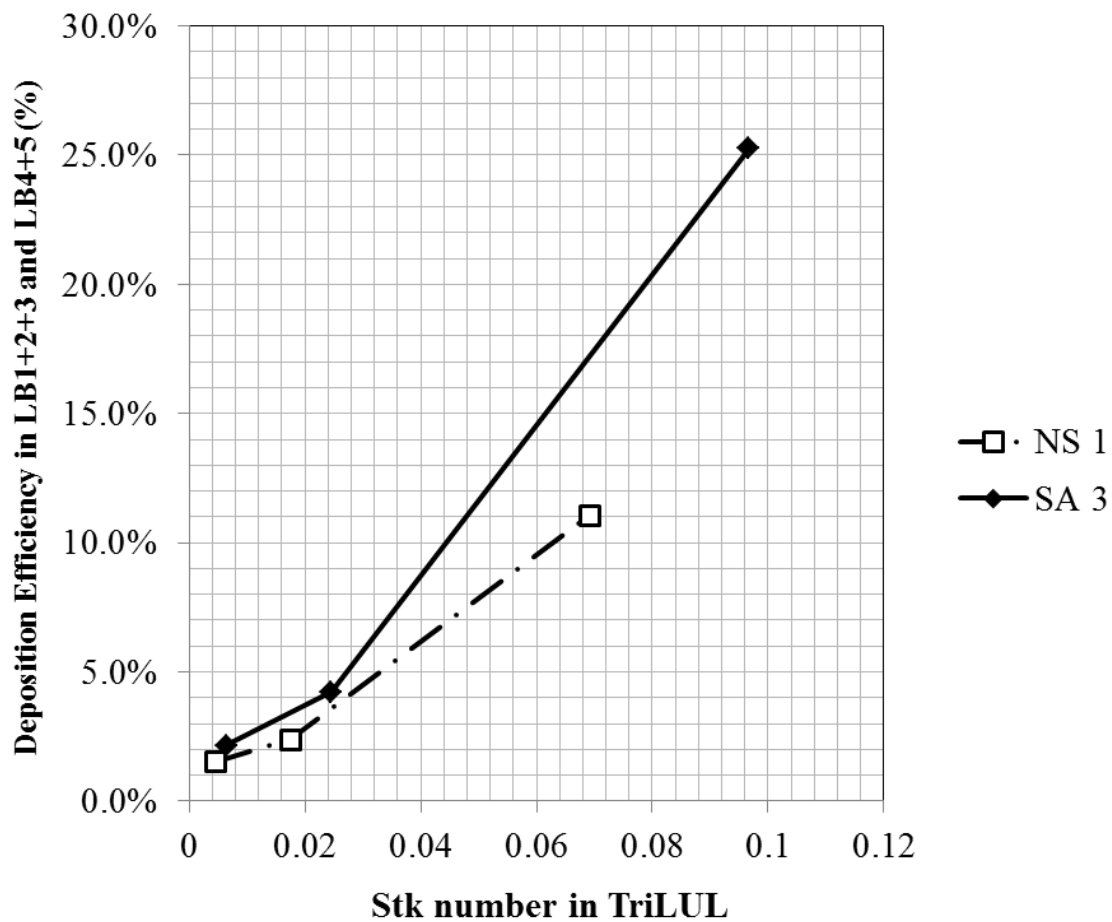
Figure 5.14 Particle deposition efficiency in LB1+2+3 and LB4+5 according to Stk of parent branch (TriLUL)
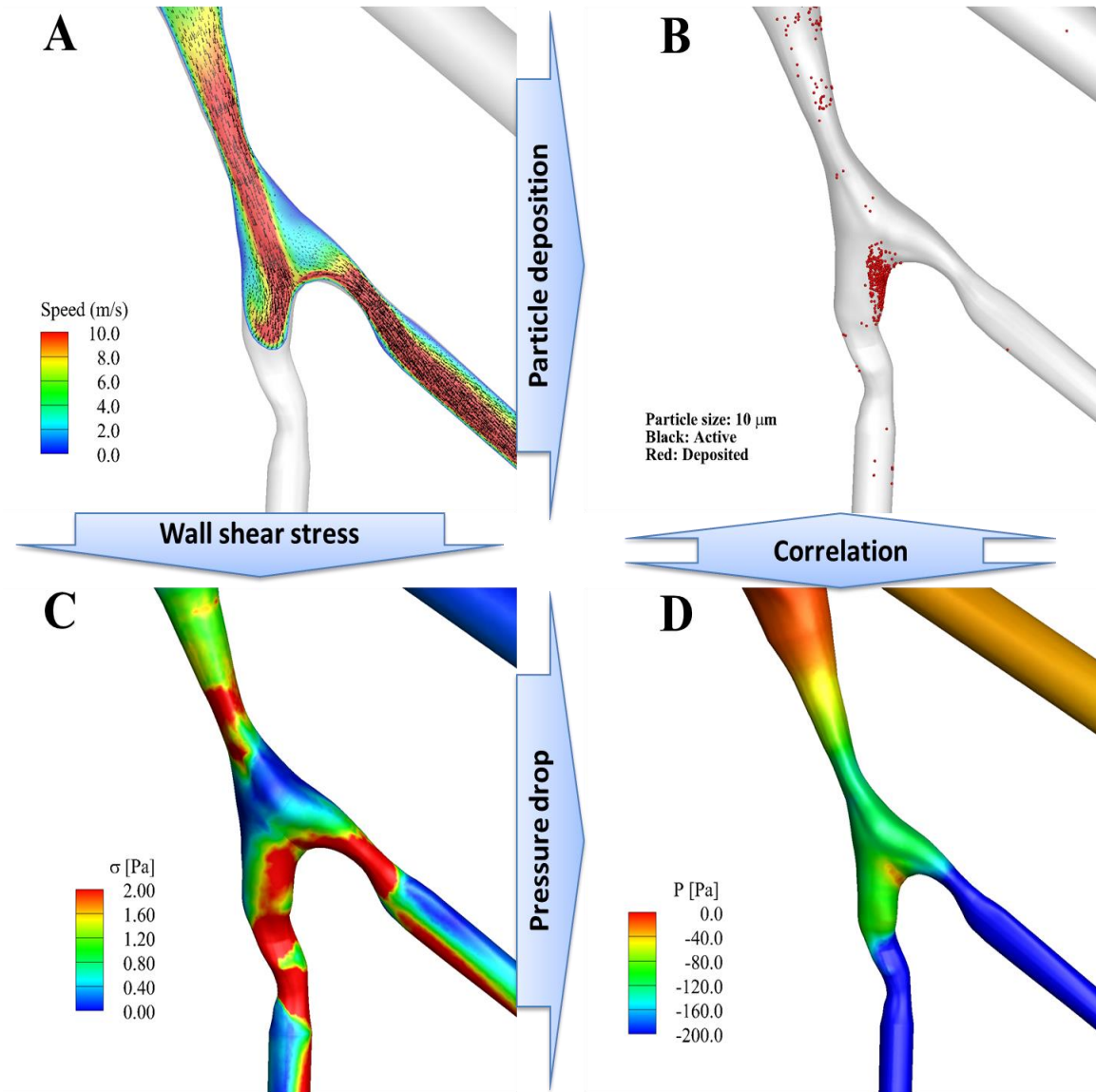
Figure 5.15 Correlations among A: high velocity due to constriction, B: particle deposition, C: wall shear stress and D: pressure drop.

CHAPTER 6

SUMMARY

6.1   Registration-Based Assessment of the Regional Lung

         Function in Normal Subjects vs. Severe Asthmatics

         As an evaluation of the utility of such an imaging approach, we explored two
groups at the extremes of population ranging from normal subjects to severe asthmatics.
A mass preserving image registration technique was employed to match CT images at
total lung capacity (TLC) and functional residual capacity (FRC) for assessments of
regional air volume change and lung deformation between the two states. Fourteen
normal subjects and thirty severe asthmatics were analyzed via image registration-derived
metrics together with their pulmonary function test (PFT) and CT-based air-trapping.
Relative to the normal subjects, the severe asthmatics demonstrated reduced air volume
change (consistent with air trapping) and more isotropic deformation in the basal lung
regions, while demonstrating increased air volume change associated with increased
anisotropic deformation in the apical lung regions. These differences were found despite
the fact that both PFT-derived TLC and FRC in the two groups are near 100% of
predicted values. Data suggested that reduced basal-lung air volume change in severe
asthmatics is compensated by increased apical-lung air volume change and that relative
increase in apical-lung air volume change in severe asthmatics is accompanied by
enhanced anisotropic deformation. In conclusion, CT-based deformation, assessed via
inspiration vs. expiration scans, could provide a tool for distinguishing differences in lung
mechanics when applied to the extreme ends of a population range.

6.2   Effects of Protocol Difference on Air-trapping and

Registration-based Lung Assessments

Lung air-trapping and air volume change can be estimated via quantitative computed tomography (CT) using one-image CT-density threshold-based measures on expiration or two-image registration-based measures. However, the effects of scanner differences and imaging protocol adherence on quantitative assessment are known to be problematic. Therefore, we studied the effects of using different CT scanners and protocols in a multi-center study of asthma and propose new methods that can adjust inter-site and inter-subject variations. CT images of 50 normal, 42 non-severe asthmatic and 52 severe asthmatic subjects at total lung capacity (TLC) and functional residual capacity (FRC) were acquired using three different scanners and two different coaching methods. Tracheal density was extracted to correct Hounsfield Unit of air (HU_{air}), and a fraction-based approach with the corrected HU_{air} was applied to quantify air-trapping at FRC. The fraction-based measure was enhanced by adding a lung shape metric at TLC and a registration-based measure of air volume change between TLC and FRC. The fraction-based measure of air-trapping was able to collapse data into two regression lines with distinct slopes that differentiate severe asthmatics from normal subjects and non-severe asthmatics. Furthermore, both lung shape and air volume change were found to be discriminant variables for differentiating three populations of normal subjects, non-severe asthmatics and severe asthmatics. In conjunction with the variables of lung shape and air volume change, the fraction-based measure has enabled differentiation of three populations, allowing for the differentiation of severe from non-severe and non-severe from normal populations.

6.3   Structural Assessment of Airways in Asthmatic
Populations

Existing studies on alterations of wall thickness (WT) and luminal area (LA) in asthmatics were inconclusive and their correlations with airway bifurcation angle, circularity and hydraulic diameter (D_h) remain unclear. Therefore, we examined the correlations of these structural variables with pulmonary function test (PFT) and image-based functional variables among three populations: normal subjects, non-severe and severe asthmatics. 50 normal subjects, 42 non-severe and 52 severe asthmatics were studied. The structural variables of WT, LA, bifurcation angle, circularity and D_h that reflects the combined effect of airway constriction and circularity were measured from CT images. The image-based functional variables included air-trapping at functional residual capacity (FRC) and lobar air volume change between total lung capacity (TLC) and FRC. TLC measured in PFT was used for normalization of dimensional variables. The bulk normalized WT increased in both non-severe and severe asthmatics. In severe asthmatics, the normalized LA was mainly reduced in the lower-lobar segments, and bifurcation angles of apical bronchi (LB1+2 and RB1) were larger than those of normal subjects, being correlated with the increase of upper-lobar air volume change. Furthermore, the circularity and D_h significantly decreased in severe asthmatics, and the D_h is correlated with PFT-based forced expiratory volume in 1 s (FEV1), residual volume (RV) % predicted values, air-trapping and air-volume change. The bulk normalized WT can be used to distinguish asthmatics from normal subjects. The bifurcation angle, circularity, normalized LA and D_h can be used to differentiate severe asthmatics from non-severe asthmatics. D_h serves as the most significant variable that bridges airway segmental features and global lung functions.

6.4   Regional Characteristics of Pressure Drop and

Particle Deposition in Severe Asthmatics

Severe asthmatics were characterized by structural alterations of bifurcation angle, non-circular shape, reduced diameter of airways and airway wall thickness, as well as functional alterations of air-trapping and air-volume change shifting from basal region to apical region. A high-fidelity large-eddy-simulation (LES) CFD model for transitional and turbulent flows was applied to study air-flow characteristics and particle deposition in both normal and severe asthmatic lungs. Airway models of three normal subjects and four severe asthmatics were constructed from computed tomography (CT) volumetric images. With image registration, subject-specific physiological flow boundary conditions were derived based on air-volume difference between CT images at total lung capacity (TLC) and functional residual capacity (FRC). Particle transport simulations were performed on CFD-predicted flow fields with 2.5, 5 and 10-µm particles. The CFD results were compared with existing airway-resistance models developed upon the assumption of symmetric cylindrical bifurcation. Existing resistance models could not estimate the pressure drop of the severe asthmatic subject with constricted airways. In severe asthmatics, the increased air-volume change of upper lobes in severe asthmatics affected the increase of particle distribution toward upper lobes, especially for small 2.5-µm particles. The structural alterations of airway bifurcation angle, circularity and diameter in severe asthmatics were associated with the increase of particle deposition. Especially, the constricted airways were correlated with high wall shear stress, leading to increased pressure drop and particle deposition. These characteristics were also spatially correlated with increased airway wall thickness. Chronic functional and structural alterations of severe asthmatics are significantly associated with particle distribution and deposition in local regions at segmental scale.

6.5   Limitations

In CHAPTER 3, we performed population-based statistical analysis, but most of the analysis was evaluated with the given explanatory variables. However, some other variables may also be important and shall be considered in future studies. For example, the inter-center variations of tracheal CT density and air-volumes at TLC and FRC might be associated with socioeconomic and environmental effects besides protocol differences. In addition, In CHAPTER 4, we performed linear correlation tests to investigate the relationships between structural and functional variables. However, for more reliable correlation analysis, logarithmic transformation of data is desirable to improve the data distribution. Thus, the multivariate regression models of transformed data including socioeconomic and environmental effects may provide improved associations for all of the structural and functional variables.

In CHAPTER 5, we performed CFD simulations on limited samples having only three normal subjects and four severe asthmatics. This is because LES-based turbulent simulations require significant computational costs as shown in Table 5.3. To obtain more statistically reliable results, it is a necessity to increase the number of representative subjects from each group. In addition, our CFD simulations were performed under the assumptions of rigid airway wall, static surface-boundary of TLC image and steady-inspiratory flow. Thus, the effects of tissue compliances, displacements of surface boundary and dynamic breathing were not considered because of limited knowledge about tissue properties and significant computational costs for breathing lung simulations. In fact, change of bifurcation angle between TLC and FRC and compliant airways would affect particle deposition and pressure drop, respectively. Therefore, some of the results and discussions in this dissertation require further validation with simulations using more realistic conditions as listed above.

6.6   Future Studies

6.6.1   Multi-Center Study

We performed a population study of air-trapping (CHAPTER 3) with a fraction threshold-based air-trapping method that can control inter-site variability of scanners and breath-hold coaching methods. The proposed method facilitates increasing the number of samples via multi-center studies, because the proposed method is not sensitive to the variations of scanners and breath-hold coaching. The increased number of samples can reduce statistical error and provide more reliable results. In addition, the performance of proposed slope-based classification can be validated via blind tests with CT images of asthmatics from different centers.

6.6.2   Cluster Analysis

We found unique characteristics of structural variables such as wall thickness, hydraulic diameter, circularities and bifurcation angle of asthmatic populations (CHAPTER 4). In fact, the classification between non-severe asthmatics and severe asthmatics only depends on the treatments of oral corticosteroid and high-dose inhaled corticosteroids besides severe minor criteria [104, 143]. Thus, the classification may not reflect the functional and structural alterations such as air-trapping, wall thickening and chronic constriction. Accordingly, the aforementioned altered characteristics could be utilized to classify asthmatic subjects into sub-populations via cluster analysis. The imaging cluster analysis would be associated with clinical phenotypes such as allergy, onset of asthma and FEV1 [79], which can be utilized to develop therapeutic interventions for each cluster.

6.6.3   Application to COPD

COPD is characterized by the increased emphysema and elevated air-trapping with CT scans at TLC and FRC levels. The assessment is performed with CT density threshold-based method, but the method turns out problematic in the multi-center study. Therefore, the proposed fraction-based method can be applied to evaluate emphysema at TLC and air-trapping at FRC in COPD populations. In addition, in the COPD study, image registration can be utilized to assess local air-volume change and deformation, and CFD technique can be employed to investigate flow structure and particle deposition with registration-derived air-volume change. The comprehensive analysis of COPD via image registration and CFD may shed light on structural and functional differences of COPD vs. Normal and COPD vs. asthma.

BIBLIOGRAPHY

[1] Altes TA, Powers PL, Knight-Scott J, Rakes G, Platts-Mills TA, de Lange EE, Alford BA, Mugler JP and Brookeman JR., 2001. Hyperpolarized 3He MR lung ventilation imaging in asthmatics: preliminary findings. *J Magn Reson Imaging* 13 (3), 378-384.

[2] Amelon R, Cao K, Ding K, Christensen GE, Reinhardt JM and Raghavan ML., 2011. Three-dimensional characterization of regional lung deformation. *J Biomech* 44 (13), 2489-2495.

[3] Amis TC, Jones HA and Hughes JM., 1984. Effect of posture on inter-regional distribution of pulmonary ventilation in man. *Respir Physiol* 56 (2), 145-167.

[4] Andreassen S, Steimle KL, Mogensen ML, de la Serna, Jorge Bernardino, Rees S and Karbing DS., 2010. The effect of tissue elastic properties and surfactant on alveolar stability. *J Appl Physiol* 109 (5), 1369-1377.

[5] Arppe A., 2012. polytomous: Polytomous logistic regression for fixed and mixed effects. R package version 0.1.4 .

[6] Aysola RS, Hoffman EA, Gierada D, Wenzel S, Cook-Granroth J, Tarsi J, Zheng J, Schechtman KB, Ramkumar TP, Cochran R, Xueping E, Christie C, Newell J, Fain S, Altes TA and Castro M., 2008. Airway remodeling measured by multidetector CT is increased in severe asthma and correlates with pathology. *Chest* 134 (6), 1183-1191.

[7] Aysola R, de Lange EE, Castro M and Altes TA., 2010. Demonstration of the heterogeneous distribution of asthma in the lungs using CT and hyperpolarized helium-3 MRI. *J Magn Reson Imaging* 32 (6), 1379-1387.

[8] Bake B, Bjure J, Grimby G, Milic-Emili J and Nilsson NJ., 1967. Regional distribution of inspired gas in supine man. *Scand J Respir Dis* 48 (3), 189-196.

[9] Bakker ME, Stolk J, Putter H, Shaker SB, Parr DG, Piitulainen E, Russi EW, Dirksen A, Stockley RA and Reiber JH., 2005. Variability in densitometric assessment of pulmonary emphysema with computed tomography. *Invest Radiol* 40 (12), 777-783.

[10] Beigelman-Aubry C, Capderou A, Grenier PA, Straus C, Becquemin M, Similowski T and Zelter M., 2002. Mild Intermittent Asthma: CT Assessment of Bronchial Cross-sectional Area and Lung Attenuation at Controlled Lung Volume1. *Radiology* 223 (1), 181-187.

[11] Bodduluri S, Newell Jr. JD, Hoffman EA and Reinhardt JM., 2013. Registration-Based Lung Mechanical Analysis of Chronic Obstructive Pulmonary Disease (COPD) Using a Supervised Machine Learning Framework. *Acad Radiol* 20 (5), 527-536.

[12] Breatnach E, Abbott GC and Fraser RG., 1984. Dimensions of the normal human trachea. *Am J Roentgenol* 142 (5), 903-906.

[13] Brown MS, Kim HJ, Abtin F, Da Costa I, Pais R, Ahmad S, Angel E, Ni C, Kleerup EC and Gjertson DW., 2010. Reproducibility of lung and lobar volume measurements using computed tomography. *Acad Radiol* 17 (3), 316-322.

[14] Brown MS, McNitt-Gray MF, Goldin JG, Greaser LE, Hayward UM, Sayre JW, Arid MK and Aberle DR., 1999. Automated measurement of single and total lung volume from CT. *J Comput Assist Tomogr* 23 (4), 632-640.

[15] Busacker A, Newell Jr JD, Keefe T, Hoffman EA, Granroth JC, Castro M, Fain S and Wenzel S., 2009. A multivariate analysis of risk factors for the air-trapping asthmatic phenotype as measured by quantitative CT analysis. *Chest* 135 (1), 48-56.

[16] Busse WW and Lemanske Jr RF., 2001. Asthma. *N Engl J Med* 344 (5), 350-362.

[17] Campana L, Kenyon J, Zhalehdoust-Sani S, Tzeng YS, Sun Y, Albert M and Lutchen KR., 2009. Probing airway conditions governing ventilation defects in asthma via hyperpolarized MRI image functional modeling. *J Appl Physiol* 106 (4), 1293-1300.

[18] Carroll N, Cooke C and James A., 1997. The distribution of eosinophils and lymphocytes in the large and small airways of asthmatics. *Eur Respir J* 10 (2), 292-300.

[19] Castillo R, Castillo E, Guerra R, Johnson VE, McPhail T, Garg AK and Guerrero T., 2009. A framework for evaluation of deformable image registration spatial accuracy using large landmark point sets. *Phys Med Biol* 54 (7), 1849.

[20] Castillo R, Castillo E, Martinez J and Guerrero T., 2010. Ventilation from four-dimensional computed tomography: density versus Jacobian methods. *Phys Med Biol* 55 (16), 4661.

[21] Castro M, Fain SB, Hoffman EA, Gierada DS, Erzurum SC, Wenzel S and National Heart, Lung and Blood Institute's Severe Asthma Research Program., 2011. Lung imaging in asthmatic patients: the picture is clearer. *J Allergy Clin Immunol* 128 (3), 467.

[22] Centers for Disease Control and Prevention., 2011. *Vital Signs*.

[23] Choi S, Hoffman EA, Wenzel SE, Castro M and Lin C., 2014. Structural Assessment of Heterogeneous Airways in Severe Asthmatics via Quantitative Computed Tomography. *to be submitted* .

[24] Choi S, Hoffman EA, Wenzel SE, Castro M and Lin C., 2013. Improved CT-Based Estimate of Pulmonary Gas Trapping Accounting for Scanner and Lung Volume Variations in a Multi-center Study. *under peer-review* .

[25] Choi S, Hoffman EA, Wenzel SE, Tawhai MH, Yin Y, Castro M and Lin C., 2013. Registration-based Assessment of Regional Lung Function via Volumetric CT Images of Normal Subjects vs. Severe Asthmatics. *J Appl Physiol* 115 (5), 730-742.

[26] Choi Y and Lee S., 2000. Injectivity conditions of 2D and 3D uniform cubic B-spline functions. *Graphical Models* 62 (6), 411-427.

[27] Choi J, Tawhai MH, Hoffman EA and Lin C., 2009. On intra- and intersubject variabilities of airflow in the human lungs. *Phys Fluids* 21 (10), 101901.

[28] Choi J, Xia G, Tawhai M and Hoffman EaL,Ching-Long., 2010. Numerical Study of High-Frequency Oscillatory Air Flow and Convective Mixing in a CT-Based Human Airway Model. *Ann Biomed Eng* 38 (12), 3550-3571.

[29] Clausen J., 1997. Measurement of absolute lung volumes by imaging techniques. *Eur Respir J* 10 2427-2431.

[30] Coates A, Peslin R, Rodenstein D and Stocks J., 1997. Measurement of lung volumes by plethysmography. *Eur Respir J* 10 (6), 1415-1427.

[31] Cohen J, Postma DS, Vink-Klooster K, van der Bij W, Verschuuren E, ten Hacken NH, Koëter GH and Douma WR., 2007. FVC to Slow Inspiratory Vital Capacity RatioA Potential Marker for Small Airways Obstruction. *Chest* 132 (4), 1198-1203.

[32] Comerford A, Gravemeier V and Wall W., 2013. An algebraic variational multiscale-multigrid method for large-eddy simulation of turbulent pulsatile flows in complex geometries with detailed insight into pulmonary airway flow. *Int J Numer Methods Fluids* 71 (10), 1207-1225.

[33] Couper D, Lavange LM, Han M, Barr RG, Bleecker E, Hoffman EA, Kanner R, Kleerup E, Martinez FJ, Woodruff PG, Rennard S and for the SPIROMICS Research Group., 2013. Design of the Subpopulations and Intermediate Outcomes in COPD Study (SPIROMICS). *Thorax* .

[34] Coxson H, Mayo J, Behzad H, Moore B, Verburgt L, Staples C, Pare P and Hogg J., 1995. Measurement of lung expansion with computed tomography and comparison with quantitative histology. *J Appl Physiol* 79 (5), 1525-1530.

[35] Crum WR, Hartkens T and Hill DL., 2004. Non-rigid image registration: theory and practice. *Br J Radiol* 77 (Spec No 2), S140-S153.

[36] De Backer J, Vos W, Devolder A, Verhulst S, Germonpré P, Wuyts F, Parizel P and De Backer W., 2008. Computational fluid dynamics can detect changes in airway resistance in asthmatics after acute bronchodilation. *J Biomech* 41 (1), 106-113.

[37] De Backer JW, Vos WG, Vinchurkar SC, Claes R, Drollmann A, Wulfrank D, Parizel PM, Germonpre P and De Backer W., 2010. Validation of computational fluid dynamics in CT-based airway models with SPECT/CT. *Radiology* 257 (3), 854-862.

[38] De Jong P, Long F, Wong J, Merkus P, Tiddens H, Hogg J and Coxson H., 2006. Computed tomographic estimation of lung dimensions throughout the growth period. *Eur Respir J* 27 (2), 261-267.

[39] De Jong P, Müller N, Pare P and Coxson H., 2005. Computed tomographic imaging of the airways: relationship to structure and function. *Eur Respir J* 26 (1), 140-152.

[40] de Lange EE, Altes TA, Patrie JT, Battiston JJ, Juersivich AP, Mugler JP and Platts-Mills TA., 2009. Changes in Regional Airflow Obstruction over Time in the Lungs of Patients with Asthma: Evaluation with 3He MR Imaging. *Radiology* 250 (2), 567-575.

[41] de Lange EE, Altes TA, Patrie JT, Parmar J, Brookeman JR, Mugler JP and Platts-Mills TA., 2007. The variability of regional airflow obstruction within the lungs of patients with asthma: assessment with hyperpolarized helium-3 magnetic resonance imaging. *J Allergy Clin Immunol* 119 (5), 1072-1078.

[42] Ding K, Yin Y, Cao K, Christensen GE, Lin CL, Hoffman EA and Reinhardt JM., 2009. Evaluation of lobar biomechanics during respiration using image registration. *MICCAI* 5761 739-746.

[43] Doeing DC and Solway J., 2013. Airway smooth muscle in the pathophysiology and treatment of asthma. *J Appl Physiol* 114 (7), 834-843.

[44] Engel LA and Prefaut C., 1981. Cranio-caudal distribution of inspired gas and perfusion in supine man. *Respir Physiol* 45 (1), 43-53.

[45] Fain SB, Gonzalez-Fernandez G, Peterson ET, Evans MD, Sorkness RL, Jarjour NN, Busse WW and Kuhlman JE., 2008. Evaluation of structure-function relationships in asthma using multidetector CT and hyperpolarized He-3 MRI. *Acad Radiol* 15 (6), 753-762.

[46] Fain SB, Peterson ET, Sorkness RL, Wenzel S, Castro M and Busse WW., 2009. Severe Asthma Research Program–Phenotyping and Quantification of Severe Asthma. *Imaging Decisions MRI* 13 (1), 24-27.

[47] Finlay WH., 2001. *The mechanics of inhaled pharmaceutical aerosols: an introduction.* Academic Press, Waltham.

[48] Froese AB and Bryan AC., 1974. Effects of Anesthesia and Paralysis on Diaphragmatic Mechanics in Man. *Anesthesiology* 41 (3), 242-255.

[49] Fuld MK, Easley RB, Saba OI, Chon D, Reinhardt JM, Hoffman EA and Simon BA., 2008. CT-measured regional specific volume change reflects regional ventilation in supine sheep. *J Appl Physiol* 104 (4), 1177-1184.

[50] Fuld MK, Grout RW, Guo J, Morgan JH and Hoffman EA., 2012. Systems for Lung Volume Standardization during Static and Dynamic MDCT-based Quantitative Assessment of Pulmonary Structure and Function. *Acad Radiol* 19 (8), 930-940.

[51] Galban CJ, Han MK, Boes JL, Chughtai KA, Meyer CR, Johnson TD, Galban S, Rehemtulla A, Kazerooni EA, Martinez FJ and Ross BD., 2012. Computed tomography-based biomarker provides unique signature for diagnosis of COPD phenotypes and disease progression. *Nat Med* 18 (11), 1711-1715.

[52] Gemci T, Ponyavin V, Chen Y, Chen H and Collins R., 2008. Computational model of airflow in upper 17 generations of human respiratory tract. *J Biomech* 41 (9), 2047.

[53] Geuzaine C and Remacle J., 2009. Gmsh: A 3-D finite element mesh generator with built-in pre-and post-processing facilities. *Int J Numer Methods Eng* 79 (11), 1309-1331.

[54] Gevenois PA, De Vuyst P, De Maertelaer V, Zanen J, Jacobovitz D, Cosio MG and Yernault J., 1996. Comparison of computed density and microscopic morphometry in pulmonary emphysema. *Am J Respir Crit Care Med* 154 (1), 187-192.

[55] Gevenois PA, de Maertelaer V, De Vuyst P, Zanen J and Yernault JC., 1995. Comparison of computed density and macroscopic morphometry in pulmonary emphysema. *Am J Respir Crit Care Med* 152 (2), 653-657.

[56] Gono H, Fujimoto K, Kawakami S and Kubo K., 2003. Evaluation of airway wall thickness and air trapping by HRCT in asymptomatic asthma. *Eur Respir J* 22 (6), 965-971.

[57] Grenier PA, Beigelman-Aubry C, Fetita C and Preteux F., 2004. Large airways at CT: Bronchiectasis, Asthma and COPD. 39-55, *Functional Imaging of the Chest* 1st, Springer, Heidelberg.

[58] Griscom NT and Wohl ME., 1986. Dimensions of the growing trachea related to age and gender. *Am J Roentgenol* 146 (2), 233-237.

[59] Gupta S, Siddiqui S, Haldar P, Entwisle JJ, Mawby D, Wardlaw AJ, Bradding P, Pavord ID, Green RH and Brightling CE., 2010. Quantitative analysis of high-resolution computed tomography scans in severe asthma subphenotypes. *Thorax* 65 (9), 775-781.

[60] Gupta S, Siddiqui S, Haldar P, Raj JV, Entwisle JJ, Wardlaw AJ, Bradding P, Pavord ID, Green RH and Brightling CE., 2009. Qualitative analysis of high-resolution CT scans in severe asthma. *Chest* 136 (6), 1521-1528.

[61] Gupta S, Hartley R, Khan UT, Singapuri A, Hargadon B, Monteiro W, Pavord ID, Sousa AR, Marshall RP and Subramanian D., 2013. Quantitative computed tomography-derived clusters: Redefining airway remodeling in asthmatic patients. *J Allergy Clin Immunol* 133 (3), 729-738.

[62] Halaweish AF, Hoffman EA, Thedens DR, Fuld MK, Sieren JP and van Beek EJ., 2013. Effect of Lung Inflation Level on Hyperpolarized 3He Apparent Diffusion Coefficient Measurements in Never-Smokers. *Radiology* 268 (2), 572-580.

[63] Hankinson JL, Odencrantz JR and Fedan KB., 1999. Spirometric reference values from a sample of the general US population. *Am J Respir Crit Care Med* 159 (1), 179-187.

[64] Harris RS., 2005. Pressure-volume curves of the respiratory system. *Respir Care* 50 (1), 78-99.

[65] Harris RS, Fujii-Rios H, Winkler T, Musch G, Vidal Melo MF and Venegas JG., 2012. Ventilation Defect Formation in Healthy and Asthma Subjects Is Determined by Lung Inflation. *PLoS One* 7 (12), e53216.

[66] Harris RS, Winkler T, Musch G, Vidal Melo MF, Schroeder T, Tgavalekos N and Venegas JG., 2009. The prone position results in smaller ventilation defects during bronchoconstriction in asthma. *J Appl Physiol* 107 (1), 266-274.

[67] Harris RS, Winkler T, Tgavalekos N, Musch G, Melo MF, Schroeder T, Chang Y and Venegas JG., 2006. Regional pulmonary perfusion, inflation, and ventilation defects in bronchoconstricted patients with asthma. *Am J Respir Crit Care Med* 174 (3), 245-253.

[68] Heckscher T, Bass H, Oriol A, Rose B, Anthonisen N and Bates D., 1968. Regional lung function in patients with bronchial asthma. *J Clin Invest* 47 (5), 1063.

[69] Hinds WC., 1982. *Aerosol technology: properties, behavior, and measurement of airborne particles.* Wiley-Interscience, New York.

[70] Hoffman EA., 1985. Effect of body orientation on regional lung expansion: a computed tomographic approach. *J Appl Physiol* 59 (2), 468-480.

[71] Hoffman EA and Ritman EL., 1985. Effect of body orientation on regional lung expansion in dog and sloth. *J Appl Physiol* 59 (2), 481-491.

[72] Hoffman EA, Simon BA and McLennan G., 2006. State of the Art. A Structural and Functional Assessment of the Lung via Multidetector-Row Computed Tomography Phenotyping Chronic Obstructive Pulmonary Disease. *Proc Am Thorac Soc* 3 (6), 519-532.

[73] Holden M., 2008. A review of geometric transformations for nonrigid body registration. *IEEE Trans Med Imag* 27 (1), 111-128.

[74] Hothorn T, Bretz F and Westfall P., 2008. Simultaneous Inference in General Parametric Models. *Biometrical Journal* 50 (3), 346-363.

[75] Hu S, Hoffman EA and Reinhardt JM., 2001. Automatic lung segmentation for accurate quantitation of volumetric X-ray CT images. *IEEE Trans Med Imag* 20 (6), 490-498.

[76] Ibanez J and Raurich J., 1982. Normal values of functional residual capacity in the sitting and supine positions. *Intensive Care Med* 8 (4), 173-177.

[77] Inthavong K, Tu J, Ye Y, Ding S, Subic A and Thien F., 2010. Effects of airway obstruction induced by asthma attack on particle deposition. *J Aerosol Sci* 41 (6), 587-601.

[78] James AL, Paré PD and Hogg JC., 1989. The mechanics of airway narrowing in asthma. *Am Rev Respir Dis* 139 (1), 242-246.

[79] Jarjour NN, Erzurum SC, Bleecker ER, Calhoun WJ, Castro M, Comhair SA, Chung KF, Curran-Everett D, Dweik RA, Fain SB, Fitzpatrick AM, Gaston BM, Israel E, Hastie A, Hoffman EA, Holguin F, Levy BD, Meyers DA, Moore WC, Peters SP, Sorkness RL, Teague WG, Wenzel SE, Busse WW and NHLBI Severe Asthma Research Program (SARP)., 2012. Severe Asthma Lessons Learned from the National Heart, Lung, and Blood Institute Severe Asthma Research Program. *Am J Respir Crit Care Med* 185 (4), 356-362.

[80] Jeffery PK., 2001. Remodeling in asthma and chronic obstructive lung disease. *Am J Respir Crit Care Med* 164 (supplement_2), S28-S38.

[81] Johnson PRA, Roth M, Tamm M, Hughes M, Ge Q, King G, Burgess JK and Black JL., 2001. Airway smooth muscle cell proliferation is increased in asthma. *Am J Respir Crit Care Med* 164 (3), 474-477.

[82] Kang M, Hwang J and Lee J., 2011. Effect of geometric variations on pressure loss for a model bifurcation of the human lung airway. *J Biomech* 44 (6), 1196-1199.

[83] Kasahara K, Shiba K, Ozawa T, Okuda K and Adachi M., 2002. Correlation between the bronchial subepithelial layer and whole airway wall thickness in patients with asthma. *Thorax* 57 (3), 242-246.

[84] Katz IM, Martin AR, Muller P, Terzibachi K, Feng C, Caillibotte G, Sandeau J and Texereau J., 2011. The ventilation distribution of helium–oxygen mixtures and the role of inertial losses in the presence of heterogeneous airway obstructions. *J Biomech* 44 (6), 1137-1143.

[85] Kim SS, Seo JB, Kim N, Chae EJ, Lee YK, Oh YM and Lee SD., 2012. Improved correlation between CT emphysema quantification and pulmonary function test by density correction of volumetric CT data based on air and aortic density. *Eur J Radiol* http://dx.doi.org/10.1016/j.ejrad.2012.02.021 .

[86] King GG, Harris B and Mahadev S., 2010. V/Q SPECT: utility for investigation of pulmonary physiology. *Semin Nucl Med* 40 (6), 467-473.

[87] Kleinstreuer C, Zhang Z and Li Z., 2008. Modeling airflow and particle transport/deposition in pulmonary airways. 163 (1), 128-138.

[88] Kumar H, Vasilescu DM, Yin Y, Hoffman EA, Tawhai MH and Lin C., 2013. Multiscale imaging and registration-driven model for pulmonary acinar mechanics in the mouse. *J Appl Physiol* 114 (8), 971-978.

[89] Lambert AR, O'shaughnessy PT, Tawhai MH, Hoffman EA and Lin C., 2010. Regional Deposition of Particles in an Image-Based Airway Model: Large-Eddy Simulation and Left-Right Lung Ventilation Asymmetry. *Aerosol Sci Technol* 45 (1), 11-25.

[90] Lin C, Lee H, Lee T and Weber LJ., 2005. A level set characteristic Galerkin finite element method for free surface flows. *Int J Numer Methods Fluids* 49 (5), 521-547.

[91] Lin C, Tawhai MH, Mclennan G and Hoffman EA., 2009. Computational fluid dynamics. *IEEE Eng Med Biol* 28 (3), 25.

[92] Lin C, Tawhai MH, Mclennan G and Hoffman EA., 2007. Characteristics of the turbulent laryngeal jet and its effect on airflow in the human intra-thoracic airways. *Respir Physiol Neurobiol* 157 (2-3), 295-309.

[93] Luo HY and Liu Y., 2009. Particle deposition in a CT-scanned human lung airway. *J Biomech* 42 (12), 1869.

[94] Mase GT, Smelser R and Mase GE., 2009. *Continuum mechanics for engineers (series: computational mechanics and applied analysis).* 3rd, CRC Press, Florida.

[95] Mathew L, Wheatley A, Castillo R, Castillo E, Rodrigues G, Guerrero T and Parraga G., 2012. Hyperpolarized 3He Magnetic Resonance Imaging: Comparison with Four-dimensional X-ray Computed Tomography Imaging in Lung Cancer. *Acad Radiol* 19 (12), 1546-1553.

[96] Matsuoka S, Kurihara Y, Yagihashi K, Hoshino M, Watanabe N and Nakajima Y., 2008. Quantitative assessment of air trapping in chronic obstructive pulmonary disease using inspiratory and expiratory volumetric MDCT. *Am J Roentgenol* 190 (3), 762-769.

[97] Maxey MR and Riley JJ., 1983. Equation of motion for a small rigid sphere in a nonuniform flow. *Phys Fluids* 26 (4), 883-889.

[98] Mets O, de Jong P, van Ginneken B, Gietema H and Lammers J., 2012. Quantitative computed tomography in COPD: possibilities and limitations. *Lung* 190 (2), 133-145.

[99] Michael A. Lawrence., 2012. ez: Easy analysis and visualization of factorial experiments. R package version 4.1-1 http://CRAN.R-project.org/package=ez.

[100] Miyawaki S., 2013. AUTOMATIC CONSTRUCTION AND MESHING OF MULTISCALE IMAGE-BASED HUMAN AIRWAY MODELS FOR SIMULATIONS OF AEROSOL DELIVERY. *University of Iowa* .

[101] Miyawaki S, Tawhai MH, Hoffman EA and Lin C., 2012. Effect of carrier gas properties on aerosol distribution in a CT-based human airway numerical model. *Ann Biomed Eng* 40 (7), 1495-1507.

[102] Montaudon M, Lederlin M, Reich S, Begueret H, Tunon-de-Lara JM, Marthan R, Berger P and Laurent F., 2009. Bronchial Measurements in Patients with Asthma: Comparison of Quantitative Thin-Section CT Findings with Those in Healthy Subjects and Correlation with Pathologic Findings1. *Radiology* 253 (3), 844-853.

[103] Montesantos S, Katz I, Fleming J, Majoral C, Pichelin M, Dubau C, Piednoir B, Conway J, Texereau J and Caillibotte G., 2013. Airway Morphology From High Resolution Computed Tomography in Healthy Subjects and Patients With Moderate Persistent Asthma. *Anat Rec* 296 (6), 852-866.

[104] Moore WC, Bleecker ER, Curran-Everett D, Erzurum SC, Ameredes BT, Bacharier L, Calhoun WJ, Castro M, Chung KF, Clark MP, Dweik RA, Fitzpatrick AM, Gaston B, Hew M, Hussain I, Jarjour NN, Israel E, Levy BD, Murphy JR, Peter SP, Teague WG, Meyers DA, Busse WW, Wenzel SE and National Heart, Lung and Blood Institute's Severe Asthma Research Program., 2007. Characterization of the

severe asthma phenotype by the national heart, lung, and blood institute's severe asthma research program. *J Allergy Clin Immunol* 119 (2), 405-413.

[105] Moore WC, Meyers DA, Wenzel SE, Teague WG, Li H, Li X, D'Agostino Jr R, Castro M, Curran-Everett D, Fitzpatrick AM, Gaston B, Jarjour NN, Sorkness R, Calhoun WJ, Chung KF, Comhair SA, Dweik RA, Israel E, Peters SP, Busse WW, Erzurum SC, Bleecker ER and National Heart, Lung and Blood Institute's Severe Asthma Research Program., 2010. Identification of asthma phenotypes using cluster analysis in the Severe Asthma Research Program. *Am J Respir Crit Care Med* 181 (4), 315-323.

[106] Moreno F and Lyons HA., 1961. Effect of body posture on lung volumes. *J Appl Physiol* 16 (1), 27-29.

[107] Morsi S and Alexander A., 1972. An investigation of particle trajectories in two-phase flow systems. *J Fluid Mech* 55 (02), 193-208.

[108] Muller N, Staples C, Miller R and Abboud R., 1988. "Density mask." An objective method to quantitate emphysema using computed tomography. *Chest* 94 (4), 782-787.

[109] Musch G, Layfield JD, Harris RS, Melo MF, Winkler T, Callahan RJ, Fischman AJ and Venegas JG., 2002. Topographical distribution of pulmonary perfusion and ventilation, assessed by PET in supine and prone humans. *J Appl Physiol* 93 (5), 1841-1851.

[110] Newman KB, Lynch DA, Newman LS, Ellegood D and Newell Jr JD., 1994. Quantitative computed tomography detects air trapping due to asthma. *Chest* 106 (1), 105-109.

[111] Niimi A, Matsumoto H, Amitani R, Nakano Y, Mishima M, Minakuchi M, Nishimura K, Itoh H and Izumi T., 2000. Airway wall thickness in asthma assessed by computed tomography: relation to clinical indices. *Am J Respir Crit Care Med* 162 (4), 1518-1523.

[112] Nowak N, Kakade PP and Annapragada AV., 2003. Computational Fluid Dynamics Simulation of Airflow and Aerosol Deposition in Human Lungs. *Ann Biomed Eng* 31 (4), 374-390.

[113] Park SJ, Lee CH, Goo JM, Kim JH, Park E, Jung J, Park H and Cho S., 2012. Quantitative analysis of dynamic airway changes after methacholine and salbutamol inhalation on xenon-enhanced chest CT. *Eur Radiol* 22 (11), 2441-2450.

[114] Pedley T, Schroter R and Sudlow M., 1970. Energy losses and pressure drop in models of human airways. *Respir Physiol* 9 (3), 371-386.

[115] Pedley T, Schroter R and Sudlow M., 1970. The prediction of pressure drop and variation of resistance within the human bronchial airways. *Respir Physiol* 9 (3), 387-405.

[116] Plathow C, Ley S, Fink C, Puderbach M, Heilmann M, Zuna I and Kauczor HU., 2004. Evaluation of chest motion and volumetry during the breathing cycle by dynamic MRI in healthy subjects: comparison with pulmonary function tests. *Invest Radiol* 39 (4), 202.

[117] R Core Team., 2013. R: A Language and Environment for Statistical Computing.

[118] Reinhardt JM, Ding K, Cao K, Christensen GE, Hoffman EA and Bodas SV., 2008. Registration-based estimates of local lung tissue expansion compared to xenon CT measures of specific ventilation. *Med Image Anal* 12 (6), 752-763.

[119] Robinson PJ and Kreel L., 1979. Pulmonary tissue attenuation with computed tomography: comparison of inspiration and expiration scans. *J Comput Assist Tomogr* 3 (6), 740-748.

[120] Roca J, Burgos F, Barbera J, Sunyer J, Rodriguez-Roisin R, Castellsague J, Sanchis J, Antoo J, Casan P and Clausen J., 1998. Prediction equations for plethysmographic lung volumes. *Respir Med* 92 (3), 454-460.

[121] Salome CM, King GG and Berend N., 2010. Physiology of obesity and effects on lung function. *J Appl Physiol* 108 (1), 206-211.

[122] Schroeder JD, McKenzie AS, Zach JA, Wilson CG, Curran-Everett D, Stinson DS, Newell Jr JD and Lynch DA., 2013. Relationships Between Airflow Obstruction and Quantitative CT Measurements of Emphysema, Air Trapping, and Airways in Subjects With and Without Chronic Obstructive Pulmonary Disease. *Am J Roentgenol* 201 (3), W460-W470.

[123] Sieren JP, Hoffman EA, Guo J, Lynch DA, Newell J, Judy PFN and COPDGene Investigators., 2011. A Phantom For Characterizing Trachea Air Ct Numbers In A Multi-Center Quantitative Ct Lung Study. *Am J Respir Crit Care Med* 183 A5206.

[124] Smith JC and Stamenovic D., 1986. Surface forces in lungs. I. Alveolar surface tension-lung volume relationships. *J Appl Physiol* 60 (4), 1341-1350.

[125] Sorkness RL, Bleecker ER, Busse WW, Calhoun WJ, Castro M, Chung KF, Curran-Everett D, Erzurum SC, Gaston BM, Israel E, Jarjour NN, Moore WC, Peters SP, Teague WG, Wenzel SE and National Heart, Lung and Blood Institute's Severe Asthma Research Program., 2008. Lung function in adults with stable but severe asthma: air trapping and incomplete reversal of obstruction with bronchodilation. *J Appl Physiol* 104 (2), 394-403.

[126] Steimle KL, Mogensen ML, Karbing DS, Bernardino de la Serna, Jorge and Andreassen S., 2011. A model of ventilation of the healthy human lung. *Comput Methods Programs Biomed* 101 (2), 144-155.

[127] Sterk P and Bel E., 1989. Bronchial hyperresponsiveness: the need for a distinction between hypersensitivity and excessive airway narrowing. *Eur Respir J* 2 (3), 267-274.

[128] Sterk PJ, Fabbri LM, Quanjer PH, Cockcroft DW, O'Byrne PM, Anderson SD, Juniper EF and Malo JL., 1993. Airway responsiveness. Standardized challenge testing with pharmacological, physical and sensitizing stimuli in adults. Report Working Party Standardization of Lung Function Tests, European Community for Steel and Coal. Official Statement of the European Respiratory Society. *Eur Respir J Suppl* 16 53-83.

[129] Stocks J and Quanjer PH., 1995. Reference values for residual volume, functional residual capacity and total lung capacity. *Eur Respir J* 8 (3), 492-506.

[130] Svenningsen S, Kirby M, Starr D, Coxson HO, Paterson NA, McCormack DG and Parraga G., 2014. What are ventilation defects in asthma? *Thorax* 69 63-71.

[131] Tawhai MH, Pullan AJ and Hunter PJ., 2000. Generation of an anatomically based three-dimensional model of the conducting airways. *Ann Biomed Eng* 28 (7), 793-802.

[132] Tawhai MH, Hunter P, Tschirren J, Reinhardt J, McLennan G and Hoffman EA., 2004. CT-based geometry analysis and finite element models of the human and ovine bronchial tree. *J Appl Physiol* 97 (6), 2310-2321.

[133] Tschirren J, Hoffman EA, McLennan G and Sonka M., 2005. Intrathoracic airway trees: segmentation and airway morphology analysis from low-dose CT scans. *IEEE Trans Med Imag* 24 (12), 1529-1539.

[134] Tzeng Y, Hoffman E, Cook-Granroth J, Gereige J, Mansour J, Washko G, Cho M, Stepp E, Lutchen K and Albert M., 2008. Investigation of hyperpolarized 3He magnetic resonance imaging utility in examining human airway diameter behavior in asthma through comparison with high-resolution computed tomography. *Acad Radiol* 15 (6), 799.

[135] Venegas JG, Schroeder T, Harris S, Winkler RT and Melo MF., 2005. The distribution of ventilation during bronchoconstriction is patchy and bimodal: a PET imaging study. *Respir Physiol Neurobiol* 148 (1-2), 57-64.

[136] Venegas JG, Winkler T, Musch G, Vidal Melo MF, Layfield D, Tgavalekos N, Fischman AJ, Callahan RJ, Bellani G and Harris RS., 2005. Self-organized patchiness in asthma as a prelude to catastrophic shifts. *Nature* 434 (7034), 777-782.

[137] Vreman A., 2004. An eddy-viscosity subgrid-scale model for turbulent shear flow: Algebraic theory and applications. *Phys Fluids* 16 (10), 3670-3681.

[138] Wadell H., 1933. Sphericity and roundness of rock particles. *J Geol* 41 (3), 310-331.

[139] Walker C, Gupta S, Hartley R and Brightling CE., 2012. Computed tomography scans in severe asthma: utility and clinical implications. *Curr Opin Pulm Med* 18 (1), 42-47.

[140] Wanger J, Clausen J, Coates A, Pedersen O, Brusasco V, Burgos F, Casaburi R, Crapo R, Enright P and Van Der Grinten C., 2005. Standardisation of the measurement of lung volumes. *Eur Respir J* 26 511-522.

[141] Washko G, Parraga G and Coxson H., 2012. Quantitative pulmonary imaging using computed tomography and magnetic resonance imaging. *Respirology* 17 (3), 432-444.

[142] Watson RA and Pride NB., 2005. Postural changes in lung volumes and respiratory resistance in subjects with obesity. *J Appl Physiol* 98 (2), 512-517.

[143] Wenzel SE, Busse WW and National Heart, Lung, and Blood Institute's Severe Asthma Research Program., 2007. Severe asthma: lessons from the severe asthma research program. *J Allergy Clin Immunol* 119 (1), 14-21.

[144] West JB., 2008. *Respiratory physiology: the essentials.* 8th, Lippincott Williams & Wilkins, Baltimore.

[145] White FM., 2011. *Fluid Mechanics.* 5th, McGraw-Hill, New York.

[146] Wongviriyawong C, Harris RS, Greenblatt E, Winkler T and Venegas JG., 2013. Peripheral resistance: a link between global airflow obstruction and regional ventilation distribution. *J Appl Physiol* 114 (4), 504-514.

[147] Wongviriyawong C, Harris RS, Zheng H, Kone M, Winkler T and Venegas JG., 2012. Functional effect of longitudinal heterogeneity in constricted airways before and after lung expansion. *J Appl Physiol* 112 (1), 237-245.

[148] World Health Organization., 2007. prevention and control of chronic respiratory diseases: a comprehensive approach. *Global surveillance* .

[149] Xia G, Tawhai MH, Hoffman EA and Lin C., 2010. Airway wall stiffening increases peak wall shear stress: a fluid–structure interaction study in rigid and compliant airways. *Ann Biomed Eng* 38 (5), 1836-1853.

[150] Yin Y, Choi J, Hoffman EA, Tawhai MH and Lin CL., 2010. Simulation of pulmonary air flow with a subject-specific boundary condition. *J Biomech* 43 (11), 2159-2163.

[151] Yin Y, Hoffman EA and Lin CL., 2009. Local tissue-weight-based nonrigid registration of lung images with application to regional ventilation. *Proc of SPIE* 7262 72620C.

[152] Yin Y, Hoffman EA and Lin CL., 2009. Mass preserving nonrigid registration of CT lung images using cubic B-spline. *Med Phys* 36 (9), 4213-4222.

[153] Yin Y, Hoffman EA and Lin CL., 2010. Lung lobar slippage assessed with the aid of image registration. *MICCAI* 6362 578-585.

[154] Yin Y, Choi J, Hoffman EA, Tawhai MH and Lin CL., 2012. A multiscale MDCT image-based breathing lung model with time-varying regional ventilation. *J Comput Phys* 244 168-192.

[155] Zach JA, Newell JD,Jr, Schroeder J, Murphy JR, Curran-Everett D, Hoffman EA, Westgate PM, Han MK, Silverman EK, Crapo JD, Lynch DA and COPDGene Investigators., 2012. Quantitative computed tomography of the lungs and airways in healthy nonsmoking adults. *Invest Radiol* 47 (10), 596-602.

[156] Zapke M, Topf HG, Zenker M, Kuth R, Deimling M, Kreisler P, Rauh M, Chefd'hotel C, Geiger B and Rupprecht T., 2006. Magnetic resonance lung function– a breakthrough for lung imaging and functional assessment? A phantom study and clinical trial. *Respir Res* 6 (7), 106.

[157] Zhang Z, Kleinstreuer C and Kim CS., 2009. Comparison of analytical and CFD models with regard to micron particle deposition in a human 16-generation tracheobronchial airway model. *J Aerosol Sci* 40 (1), 16-28.

[158] Zhang H and Papadakis G., 2010. Computational analysis of flow structure and particle deposition in a single asthmatic human airway bifurcation. *J Biomech* 43 (13), 2453.